# Lorentz-Covariant SU(3)³ Lattice Model for Particles and Spacetime

By Bryant Villeponteau

*Triad Institute*
*San Diego, CA   USA*

**Preface.**
This work develops a **lattice effective-field theory (EFT)** based on **SU(3)³** in which common substructures assemble quarks, leptons, and gauge bosons and admit a Lorentz-covariant continuum limit consistent with the Standard Model and General Relativity. The emphasis is **phenomenology**: we provide a (3+1)D Lagrangian, a 3D lattice Hamiltonian reduction, and **testable targets** in B-physics and axion searches. The framework is **speculative but internally consistent** and is submitted as a conceptual unification equipped with concrete pass/fail criteria.

**Abstract:**
We present a Lorentz-covariant lattice framework on **SU(3)³** in which twelve axion-like modes assemble **four SU(3) octets** that act as common building blocks for quarks, dyad bosons (γ, W, Z), lepton triads, and a discrete spacetime lattice of lepton-triad dimers. We present a (3+1)D continuum Lagrangian and a 3D lattice Hamiltonian; the continuum limit **recovers SM gauge invariance and Lorentz symmetry**, with leading $k^6$(dimension-6, even-in-$k$) dispersion corrections. Gravity enters via conformal–torsional distortions (Einstein–Cartan–compatible). **Phenomenology:** (i) two **narrow dimuon** resonances in $B \to KX$, $X \to \mu^+\mu^-$at $\sim 0.6$ and $\sim$ 7 GeV with $\mathrm{Br} \sim 10^{-7} - 10^{-8}$; (ii) **axion–photon coupling** $g_{a\gamma\gamma} \sim 10^{-12} - 10^{-11}\ \mathrm{GeV}^{-1}$ within reach of LSW/helioscope experiments; (iii) **Planck-suppressed** Lorentz-violation scaling $|\ \Delta v\ |/c \sim (a/\lambda)^4$. The construction is **speculative but testable** and remains consistent with current bounds.

**Keywords:** lattice EFT; **SU(3)³**; axion-like particles; B-physics rare decays; dimuon resonances; axion–photon coupling; confinement/flux tubes; emergent Lorentz symmetry; dimension-6 dispersion; Einstein–Cartan torsion; discrete spacetime; lattice dragging in a Kerr ergosphere; Hubble constant inferred from early-time CMB vs distance ladder

# Contents

## 1.0 Introduction

Since the birth of modern physics, quantum field theory (QFT) and general relativity (GR) have stood as two pillars of our understanding of nature. Yet despite their immense successes—subatomic scattering on one side, spacetime curvature on the other—these frameworks remain stubbornly ununified. Attempts at a single synthesis (string theory, loop quantum gravity, and others) have yielded deep mathematics but, so far, no universally accepted, background-independent account with clear, decisive empirical support.

A second, closely related puzzle concerns the *internal* structure of the quanta. In the Standard Model (SM), gauge bosons, quarks, and leptons are treated as point-like excitations (or effective fields); in string theory, as extended objects. By contrast, in chemistry and biology, three-dimensional geometry is often the key to how building blocks interact. This has motivated periodic returns to structural/composite ideas. Early "preon" models [1,2] fell short, but more recent work suggests that higher-symmetry and exceptional-algebra structures might underlie both the SM and aspects of GR [3–5, 7].

This manuscript develops that direction into a concrete proposal. We introduce the **Triad Model**, in which twelve light axion-like modes (each carrying energy $\hbar\omega$) assemble, in groups of order $\alpha^{-1}$, into eight-gluon **Octons** governed by octahedral geometry and SU(3) color. Using $\mathbf{3\times 3}$ **Jordan–octonion matrices** together with **octonion vector diagrams**, we show how these Octons self-organize—by orthogonal intersections and three-color coupling—into (i) **quarks** (as single Octons), (ii) **Dyads** of two Octons (photons and the W/Z weak bosons with chiral selection), and (iii) **Triads** of three Octons (the charged leptons and neutrinos). Color confinement appears as **Gluet** flux-tube substructures built from the same eight-gluon units, giving a single architectural origin for hadrons and their strings.

The reach of the model extends to spacetime itself. The same Octon Triads tile space as **Stellated Rhombic Dodecahedra**, assembling into an alternating, charged **dimer lattice** with manifest $\mathrm{SU}(3)\times\mathrm{SU}(3)\times\mathrm{SU}(3)$ and discrete octahedral symmetries. In this lattice we propose **Higgs-like scalar dimers** (electron-, muon-, tau-flavor) as *vacuum excitations*; we treat the association of the $\sim$125 GeV Higgs with a particular dimer as a **phenomenological hypothesis**. Gravity is modeled as axion-driven, conformal changes of lattice spacing (with an Einstein–Cartan–type torsion response in rotating regimes), while a pervasive "axion sea" provides a minimal dark-matter agent. Heavier Higgs-flavor dimers act as environment-dependent vacuum pressure, suggesting an effective $\Lambda_{\mathrm{eff}}$ that varies with local dimer composition.

Our contribution is twofold: a **unified substructure** for SM matter/forces **and a discrete, background-independent medium** for spacetime—both built from the same axion–gluon units. Technically, we (i) formulate a $(3+1)\mathrm{D}$ **Lagrangian** with a **3D lattice reduction** (§3.6–3.7), (ii) derive static and time-dependent Hamiltonians with **locking terms** that select lepton and neutrino modes (§3.5, 6.1–6.4), (iii) construct Dyads/Triads and Gluet flux tubes consistent with color saturation (§4–7), and (iv) assemble a **falsifiable test program** spanning colliders, precision photonics, gravitational-wave ringdowns, and black-hole shadow systematics (§9.8). Where claims reach beyond established theory (an adaptable discrete spacetime lattice, variable $\Lambda_{\rm eff}$, torsion cores), we present them explicitly as **testable hypotheses** tied to measurable signatures.

If even part of this architecture mirrors reality, the Triad Model offers a symmetry-driven route toward reconciling QFT with gravitational dynamics, replacing a fixed continuum with a finite, $SU(3)^3$ lattice woven from a single set of twelve axion/gluon building blocks.

**Scope & assumptions.** We assume a physical 3D lattice of axion oscillators with octahedral unit cells, and treat SU(3) × SU(3) × SU(3) as a global organizing symmetry spontaneously reduced to $SU(3)_C \times SU(2)_L \times U(1)_Y$, yielding **12 Goldstone-like axion modes**. Within this framework we derive (i) Octon (8-gluon) substructure for quarks/leptons/bosons, (ii) a Lorentz-covariant continuum limit with even-in-k, dimension-6 suppressed LV, and (iii) a conformal-torsion effective description of gravity from lattice distortions. We label as **hypotheses** (to be tested) the dynamical spacetime lattice, variable $\Lambda_{\{\rm\ eff\}}$ from dimer composition, and torsion-regulated black-hole interiors; we provide specific pass/fail experimental criteria in §9.8.

## 2.0 Searching for the putative structure of the spacetime quantum

It is increasingly plausible that spacetime is not a perfectly smooth continuum but has a microscopic, quantized substructure. Many approaches have pursued this idea from different angles—gravitons on fixed backgrounds, string/brane excitations, and loop-quantized spin networks. While each has yielded valuable insights, none has produced a broadly accepted, background-independent micro-model of spacetime that also meshes cleanly with low-energy quantum field theory (QFT).

Two empirical pressures guide our search. First, "empty" space behaves like an active medium: quantum fluctuations, vacuum polarization, and axion-like mixing all suggest a dynamical substrate. Second, naive QFT estimates of vacuum energy overshoot observations by $\sim 10^{120}$, indicating that a realistic microstructure must both support field propagation and regulate vacuum energy.

To be viable within the Triad Model, a candidate **3D spacetime subunit** should satisfy four minimal criteria:

1. **High symmetry and isotropy.** No preferred direction at large scales; at minimum a full octahedral symmetry $O_h$ for rotations/reflections, and the capacity to host internal $\mathrm{SU}(3) \times \mathrm{SU}(3) \times \mathrm{SU}(3)$ labels used by the particle substructure.
2. **Space-filling tessellation.** It must tile $\mathbb{R}^3$ homogeneously and isometrically.
3. **Efficient connectivity.** Local deformations should transmit uniformly to neighbors, enabling long-range, approximately isotropic curvature/field propagation.

4. **Conformal flexibility.** The subunit must change size smoothly when exchanging axion energy with matter/bosons, preserving background independence.

Among canonical space-filling polyhedra, the **rhombic dodecahedron** stands out for uniform neighbor contact (Voronoi cell of the FCC lattice). We adopt its **stellated** variant (a rhombic dodecahedron with congruent triangular stellations) as our working subunit because it preserves $O_h$ symmetry while providing interlocking "nodes" that enhance mechanical and field-like coupling across the lattice (Figs. 1–2). In what follows we refer to this unit as the **Triad cell**.

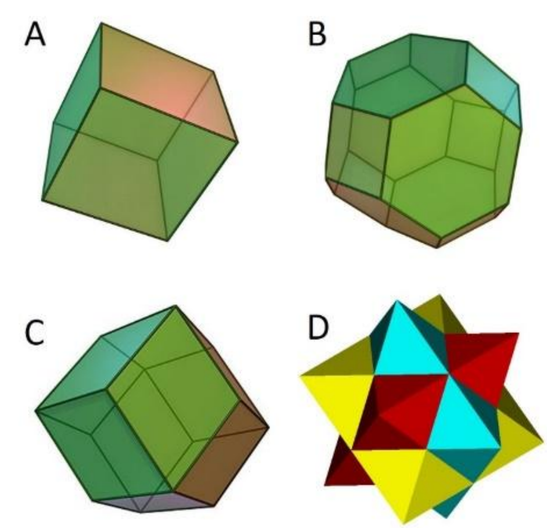


**Figure 1: Examples of symmetric space-filling polyhedra: A.** Cube. **B.** Truncated octahedron. **C.** Rhombic dodecahedron. **D.** Stellated Rhombic Dodecahedron **SRD**). These are known symmetrical 3D solids that generate a homogeneous isometric space-filling lattice. The stellated rhombic dodecahedron in D was created by Tom Ruen under public domain.

**Figure 2: The SRD tessellates $\mathbb{R}^3$.** Each cell connects to eight neighbors via triads of triangular faces, yielding uniform, high-connectivity contact. Each subunit uses 6 of 48 equal triangular faces to tightly bind each of 8 neighboring subunits. Each subunit is symmetrically surrounded by its subunit neighbors in the lattice.

## The Stellated Rhombic Dodecahedron as a Triad of Orthogonal Octons

Criterion 4 (conformal flexibility) is central: the spacetime quantum must be able to **rescale** under axion exchange so that curvature arises from local microphysics rather than a prescribed background metric. Geometrically, the SRD admits a convenient decomposition that makes this flexibility explicit: it can be represented as the **orthogonal interpenetration (⊥) of three octahedra**, which we call **Octons**,

$$\mathrm{T} = \Phi_{\mathrm{x}} \perp \Phi_{\mathrm{y}} \perp \Phi_{\mathrm{z}} \tag{1}$$

each aligned with one of the x, y, z axes (Fig. 3). In the Triad Model these Octons are the same eight-gluon assemblies that appear as quark subunits elsewhere in the paper.

Crucially, each Octon is **slightly anisotropic**: one axis is shorter than the other two by the factor

$$\frac{L'}{L} = \frac{1}{\sqrt{2}} \Rightarrow 1 - \frac{L'}{L} = = 0.29289 \ \ (29.289\%).$$

matching the energetic argument in § 4.0 (doubling of color-force quanta along one axis and the resulting box-eigenvalue rescaling). This common anisotropy across $\Phi_x \perp \Phi_y \perp \Phi_z$ both preserves overall $O_h$ symmetry of the SRD tiling and furnishes a **controlled conformal degree of freedom**: when local axion occupation changes (via the Lagrangian in § 3.6 and drive terms in § 3.7), the Octons rescale coherently, shrinking or expanding the Triad cell.

Physically:

- **Background independence.** Curvature is encoded as spatially varying Octon/Triad scale factors driven by axion exchange with matter/radiation, not imposed externally.
- **Compatibility with particle substructure.** Because each $\Phi$ is the same eight-gluon Octon used to build quarks, leptons (Triads), and bosons (Dyads), the **space lattice** and the **particle spectrum** share a single set of microscopic building blocks.
- **Propagation and rigidity.** The SRD's eight-neighbor contact transmits conformal changes efficiently, while the shared $SU(3) \times SU(3) \times SU(3)$ labeling maintains consistent coupling rules across cells.

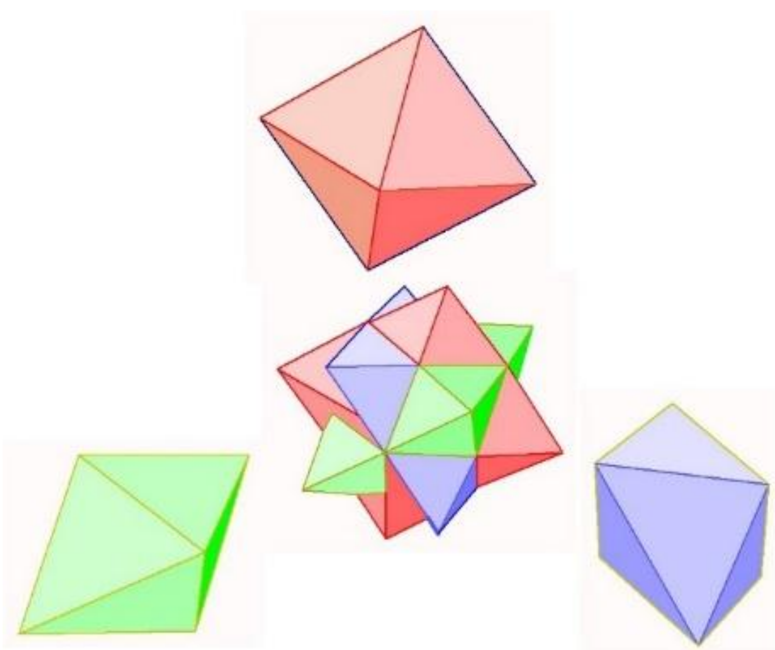

**Figure 3. Three mutually orthogonal Octons**

$\Phi_x \perp \Phi_y \perp \Phi_z$ – each an octahedron with one axis shortened by 29.289% - interpenetrate to form a Triad cell $T = \Phi_x \perp \Phi_y \perp \Phi_z$. This same Triad geometry underlies both the spacetime lattice (§8) and the leptonic Triads (§6).

While the Triad lattice is introduced as a working hypothesis, this is no more speculative than the use of local quantum field theories (e.g., QED or the Standard Model) that are themselves effective theories below a certain scale. In this view, the lattice plays a dual role: it encodes physical substructure and regulates ultraviolet divergences, much like Wilsonian lattice field theory does. A derivation from a deeper UV-complete model (e.g., via asymptotic safety or modified nonlocal QFT) remains an open avenue for latter work.

Most of the manuscript is devoted to deriving quarks (§3 - §4), flex tube linked protons and neutrons (§5), leptons (§6), bosons (§7) and the space lattice (§8) substructures using self-assembly via the strong color forces in the gluons.

## 3.0 Matched Sets of Axions/Gluons Self-Assemble into Octon Quarks

In the Standard Model (SM) and quantum field theory (QFT), quarks and gluons are treated as point-like, structureless particles [11]. In contrast, the Triad Model proposes that quarks have an **internal substructure**: matched sets of eight gluons that exhibit SU(3) group symmetry and self-assemble into an **Octon quark**.

An Octon quark is modeled geometrically as an octahedron composed of eight irregular tetrahedrons. A regular tetrahedron has 24 symmetries (12 rotational, 12 reflectional), but in the Octon quark each tetrahedron has one short axis aligned with one face of the surrounding octahedron.

The eight gluons of QCD are already established as the SM bosons mediating the strong force [12, 13], confining quarks inside hadrons (two- and three-quark systems). In the Triad Model, each gluon has a matching axion partner. Large numbers of axions of the same type can interpenetrate to generate the corresponding strong-force gluon, which then self-assembles into the eight tetrahedrons of the Octon quark.

The gluon substructure underlying strong-force confinement is treated in detail in §5, after the axion, gluon, and Octon quark constructions are introduced in §3–§4.

### 3.1 Axion/gluons form *3 x 3 Jordan octonion matrices*

In the Triad Model, each axion/gluon carries two of the three low-energy ($< 10^{-15}$ eV · s) color forces (b = blue, g = green r = red), which are modeled as spinor operators using the Pauli $2 \times 2$ matrices as shown in Eqs. (2). We use the charge–monopole notation: where $E^+$ = positive charge, $E^-$ = negative charge, $B^N$ = Magnetic North monopole, $B^S$ = Magnetic South monopole.

$$\text{b} = \begin{pmatrix} 0 & E^{+} \\ B^{N} & 0 \end{pmatrix} \sim \begin{pmatrix} 0 & 1 \\ 1 & 0 \end{pmatrix} \quad \begin{matrix}\text{Positive Charge} \\ \text{Magnetic North}\end{matrix}$$

$$\text{g} = \begin{pmatrix} 0 & -i \\ i & 0 \end{pmatrix} = \begin{pmatrix} 0 & -i \\ i & 0 \end{pmatrix} \quad \begin{matrix}\text{Neutral Charge} \\ \text{Magnetic Neutral}\end{matrix} \qquad (2)$$

$$\text{r} = \begin{pmatrix} B^{S} & 0 \\ 0 & E^{-} \end{pmatrix} \sim \begin{pmatrix} 1 & 0 \\ 0 & -1 \end{pmatrix} \quad \begin{matrix}\text{Magnetic South} \\ \text{Negative Charge}\end{matrix}$$

**Pauli- Matrix Properties**

The Pauli matrices in Eqs. (2) have the key properties of being **Hermitian**, **involutory**, and **unitary**, making them complex analogues of symmetric matrices [11]. When squared, each generates the identity matrix $I$, and each is its own inverse:

$$b^2 = g^2 = r^2 = \begin{pmatrix} 1 & 0 \\ 0 & 1 \end{pmatrix} = I \qquad (3)$$

These balanced internal symmetries form the algebraic basis for SU(2), allow quaternion construction, and permit many interpenetrating copies of Pauli-matrix quaternions to occupy the same Hilbert space. This is the foundation for the gluon and quark constructions described in §3.3.

**From Pauli Quaternions to 12 Axion/Gluons**

Using these Pauli-matrix color-force operators, we construct **12 symmetric quaternions** $A_1 \ldots A_{12}$ that represent the axion/gluons (Eqs. 4). Each axion contains two color forces and their two anti-colors in a balanced configurations. Substituting Eqs. (2) into Eqs. (4) yields Eqs. (5)–(6), generating SU(3) symmetry.

The Pauli 2 × 2 matrices also satisfy the Lie algebra antisymmetry property $[X,Y] = -[Y,X]$ and the Jacobi identity [X, [Y, Z]] + $[Y, [Z, X]] + [Z, [X, Y]] = 0$, which are both necessary conditions for SU(2) symmetry. The Pauli matrices form a subset of the Hermitian SU(3) Gell-Mann matrices.

**Relation to Gell-Mann and QCD**

The $A_1 \ldots A_9$ axions correspond closely to the eight Gell-Mann matrices of QCD [14,15], which describe gluons and quarks in the strong force. The full $A_1 \ldots A_{12}$ set can generate **four independent sets of 3 × 3 Jordan–octonion matrices**. These matrices are Hermitian, non-associative, and self-adjoint, with octonion entries. ***The extra three axions $A_{10} \ldots A_{12}$ extend beyond the Gell-Mann basis, providing the structural degrees of freedom needed to unify gluon substructure for hadrons, bosons, and leptons. S*ee section 3.7.4 where 12 Axions" ≅ 12-Dimensional Coset of** $SU(3)^3 \to SU(3) \times SU(2) \times U(1)$.

| | | | | |
|---|---|---|---|---|
| Twelve | 1. $-i(r\bar{g} - g\bar{r})/\sqrt{2}$ | 5. $(r\bar{b} + b\bar{r})/\sqrt{2}$ | 9. $(b\bar{b} - g\bar{g})/\sqrt{2}$ | |
| Stable | 2. $(r\bar{r} - b\bar{b})/\sqrt{2}$ | 6. $(b\bar{g} + g\bar{b})/\sqrt{2}$ | 10. $(b\bar{b} - r\bar{r})/\sqrt{2}$ | (4) |
| Axions | 3. $-i(g\bar{b} - b\bar{g})/\sqrt{2}$ | 7. $(r\bar{g} + g\bar{r})/\sqrt{2}$ | 11. $(g\bar{g} - r\bar{r})/\sqrt{2}$ | |
| **A1-12** | 4. $-i(r\bar{b} - b\bar{r})/\sqrt{2}$ | 8. $(r\bar{r} - g\bar{g})/\sqrt{2}$ | 12. $(\bar{g}g - \bar{b}b)/\sqrt{2}$ | |

**Collapse to Nonzero Axions**

To form a Jordan–octonion matrix with nonzero axion content, the **off-diagonal** axion operators must be "collapsed." As it turns out, 9 of the 12 available axions vanish to zero in the symmetric limit (Eqs 5), while 3 axions give non-zero axions (Eqs 6):

$$A_2 = A_5 = A_6 = A_7 = A_8 = A_9 = A_{10} = A_{11} = A_{12} = 0 \tag{5}$$

and $$A_1 = -\frac{2b}{\sqrt{2}},\ A_3 = -\frac{2r}{\sqrt{2}},\ A_4 = \frac{2g}{\sqrt{2}}, \tag{6}$$

The eigenvalues of these matrices (or more precisely, of the associated color operators) are ±1. Choosing the +1 eigenvalue for *b, r, g* gives:

$$A_1 = -\sqrt{2}\,, \quad A_3 = -\sqrt{2}\,, \quad A_4 = \sqrt{2}\,, \tag{7}$$

**Example: Down Quark and Anti-Down Quarks**

In the Jordan–octonion representation, the three nonzero axions occupy the diagonal entries, with the other six axions vanishing on the diagonal but retaining defined positions off-diagonal (see Fig. 5).

Down quark:

$$D = \{A_1, A_2, A_6, A_5, A_3, A_7, A_9, A_8, A_4\} \tag{8}$$

$$D = \mathrm{diag}(-\sqrt{2}, -\sqrt{2}, \sqrt{2}) \tag{9}$$

Anti-down quark:

$$\overline{D} = \{A_1, A_6, A_9, A_{10}, A_3, A_8, A_7, A_5, A_4\} \tag{10}$$

$$\overline{D} = \mathrm{diag}(-\sqrt{2}, -\sqrt{2}, \sqrt{2})$$

The shared diagonal form reflects quark–antiquark color symmetry despite opposite charges and small mass differences from stability energy shifts.

**Example: Up and Anti-Up Quarks**

Up quark:

$$U = \{A_4, A_9, A_7, A_6, A_3, A_{10}, A_{11}, A_5, A_1\} \tag{11}$$

$$U = \mathrm{diag}(\sqrt{2}, -\sqrt{2}, -\sqrt{2})$$

Anti-up quark:

$$\overline{U} = \{A_4, A_8, A_6, A_7, A_3, A_5, A_{12}, A_2, A_1\} \tag{12}$$

$$\overline{U} = \mathrm{diag}(\sqrt{2}, -\sqrt{2}, -\sqrt{2})$$

**Diagonal Symmetry and Flavor Assignment**

Both down/up and anti-down/anti-up share fixed diagonal patterns:

$$D = \mathrm{diag}(-\sqrt{2}, -\sqrt{2}, \sqrt{2}), \quad U = \mathrm{diag}(\sqrt{2}, -\sqrt{2}, -\sqrt{2}) \tag{13}$$

Flavor and charge are determined by **off-diagonal axions**:

---

- The set $\{A_2, A_8, A_9, A_{10}, A_{11}, A_{12}\}$ carries the distinct charge–flavor assignments
- The set $\{A_1, A_3, A_4, A_5, A_6, A_7\}$ is net-neutral and appears in all four flavor states.

---

**Structural Role**

Embedding these $3 \times 3$ Jordan–octonion kernels into two-quark (dyad) or three-quark (triad) composites captures both **gauge** and **matter** substructures algebraically. Even without the full octonion-vector diagrams or ladder-operator dynamics, this representation already encodes the essential $SU(3)^3$ symmetry and axion–gluon substructure. Further details appear in Table 3 (§9.7).

## 3.2 Formation of leptons and photons

---

Using the diagonal Jordan–octonion matrices *D* and *U* from Fig. 13, and noting that $\overline{D} = D$, $\overline{U} = U$ from §3.1, we compute the composite states as follows.

**Electron Triad:** $D \times U \times D$

**Step 1.1.** Compute

$$D \times U = \mathrm{diag}\left[(-\sqrt{2})\ (\sqrt{2}), (-\sqrt{2})(-\sqrt{2}), (\sqrt{2})(-\sqrt{2})\right].$$

$$D \times U = \mathrm{diag}(-2,\ 2,\ -2)$$

**Step 1.2.** Multiply by the second down quark:

$$(D \times U) \times D = \mathrm{diag}(-2,\ 2,\ -2) \times \mathrm{diag}(-\sqrt{2},\ -\sqrt{2}, \sqrt{2}).$$

$$T_e = (D \times U \times D) = \mathrm{diag}(2\sqrt{2},\ -2\sqrt{2},\ -2\sqrt{2}). \tag{14e-}$$

**Positron Triad** $U \times D \times U$

**Step 2.1. Multiply the first two quarks**:

$$U \times D = diag\left[(\sqrt{2})\ (-\sqrt{2}), (-\sqrt{2})(-\sqrt{2}), (-\sqrt{2})(\sqrt{2})\right].$$

$$U \times D = \mathrm{diag}\ (-2, 2, -2).$$

**Step 2.2**. **Multiply by the second up quark:**

$$(U \times D) \times U = \mathrm{diag}\ (-2, 2, -2) \times \mathrm{diag}\ (\sqrt{2}, -\sqrt{2}, -\sqrt{2})$$

Thus, the positron triad is:

$$T_{pos} = T_{e+} = \mathrm{diag}(-2\sqrt{2},\ -2\ \sqrt{2},\ 2\sqrt{2}) \tag{14e+}$$

---

**Photon Structures:** $\boldsymbol{D \times \overline{D}}$ and $\boldsymbol{U \times \overline{U}}$

Since $\boldsymbol{D = \overline{D}}$ and $\boldsymbol{U = \overline{U}}$ , both products reduce to perfect squares of the diagonal entries:

$$D \times \overline{D} = \mathrm{diag}\left[(-\sqrt{2}\ )^2, (-\sqrt{2}\ )^2, (\sqrt{2}\ )^2\right] = \mathrm{diag}(2, 2, 2)$$

(15)

$$U \times \overline{U} = \mathrm{diag}\left[(\sqrt{2}\ )^2, (-\sqrt{2}\ )^2, (-\sqrt{2}\ )^2\right] = \mathrm{diag}(2, 2, 2)$$

Both photon structures yield the fully symmetric diag(2, 2, 2) corresponding to a **color-neutral gauge boson**. The contrasting diagonal patterns of the electron/positron triads versus the perfectly symmetric photon states reveal how the Triad Model's algebra encodes charge conjugation and color neutrality directly in the matrix structure—a symmetry analysis developed in detail in the next section.

---

## 3.3. Analysis and Symmetry

### Electron vs. Positron:

$$T_e = \mathrm{diag}(2\sqrt{2}, -2\sqrt{2}, -2\sqrt{2}), \qquad T_{e+} = \mathrm{diag}(-2\sqrt{2}, -2\sqrt{2}, 2\sqrt{2}) \quad (16)$$

The two are mirrored in sign pattern, encoding charge-conjugation symmetry: the two negative entries (from the two down quarks) and one positive entry (from the up quark) swap between particle and antiparticle. This relative sign change captures particle–antiparticle symmetry while the asymmetry in the diagonal entries reflects the different contributions of the two down quarks (or anti–down quarks) versus the one up quark, reproducing the correct quantum numbers for electrons and positrons.

### Photon Structures:

The products $D \times \overline{D}$ and $U \times \overline{U}$ both yield:

$$\mathrm{diag}(2, 2, 2). \quad (17)$$

This form is completely symmetric, confirming that quark–antiquark pairs form a color-neutral gauge boson. The mixed signs in *D x U* (or *U x D*) show that order and relative phase matter. The nontrivial diagonals of the lepton triads reflect the internal structure of leptons, while the symmetric photon diagonals reflect complete color cancellation.

These results demonstrate how algebraic products of the 3 × 3 Hermitian Jordan–octonion matrices of quarks naturally encode both the internal symmetries of charged leptons and the neutrality of photons in the Triad Model's unified framework.

---

### Product Structures Produced Using Gell-Mann Matrix Generators

In Gell-Mann Matrix calculations, as seen below, only the $D \times \overline{D}$ combination yields a singlet diag(2 ,2 , 2) while mixed products like D × U × D remain "colored" and thus cannot serve as viable lepton or photon states without additional projection operators or ad-hoc linear combinations:

| Product | Result | Color State | Strong Force | Lepton Viability |
|---|---|---|---|---|
| $\mathrm{D} \times \overline{D}$ | $-2I$ | Singlet (1) | Blocked | No |
| $\mathrm{U} \times \overline{U}$ | $\mathrm{diag}(-2, -2, 0)$ | Non-singlet | Allowed | No |
| $\mathrm{D} \times \mathrm{U} \times \mathrm{D}$ | $\mathrm{diag}(-2\sqrt{2}, -2\sqrt{2}, 0)$ | Non-singlet | Allowed | No |
| $\mathrm{U} \times \mathrm{D} \times \mathrm{U}$ | $\mathrm{diag}(-2\sqrt{2}, -2\sqrt{2}, 0)$ | Non-singlet | Allowed | No |

## Why Jordan–Octonion Matrices Are Preferable to Gell-Mann Generators:

Although the eight Gell-Mann matrices form a complete basis for the Lie algebra of SU(3), they do not naturally produce the orthogonal intersections required to generate both color-neutral leptons and gauge bosons from the same quark–antiquark building blocks:

- **Singlet construction**

  In the Gell-Mann matrices, only the $\mathrm{D} \times \overline{D}$ product collapses to the color singlet diag(2, 2, 2); mixed products like $\mathrm{D} \times \mathrm{U} \times \mathrm{D}$ remain colored and need extra projection operators or engineered linear combinations to force singlet behavior. In contrast, Jordan–octonion matrices enforce orthogonality through their octonionic multiplication rules, giving Photon states ($\mathrm{D} \times \overline{D}$ or $\mathrm{U} \times \overline{U}$) automatically yield color-neutral diag(2, 2 ,2), while lepton triads ($\mathrm{D} \times \mathrm{U} \times \mathrm{D}$, $\mathrm{U} \times \mathrm{D} \times \mathrm{U}$) produce nontrivial diagonals that are largely color-neutral.

- **Extended gluon/axion spectrum**

  Gell-Mann constructions are limited to one set of eight gluon generators. In contrast, four sets of 3 x 3 Hermitian Jordan–octonion matrices are naturally generated from a symmetric set of **twelve** axion–gluon quanta, which decompose into four distinct SU(3) octets. This richer spectrum provides the correct multiplicity and structural stability for the four sets of stable ($D$, $U$, $\overline{D}$, and $\overline{U}$) quark subunits that are required throughout the Triad Model to generate all substructures in the SM.

- **Organic charge assignments**

Only Jordan–octonion constructions organically attach both electric and magnetic charges to each axion/gluon subunit (as viewed in our octonion vector diagrams), and hence to the composite quarks themselves. In the Gell-Mann framework, one must append extra U(1) operators or craft ad-hoc linear combinations to impose the correct charge assignments—an external patch rather than an emergent feature of the quark.

In sum, Jordan–octonion matrices realize the same SU(3) symmetry as the Gell-Mann matrices but do so with built-in geometric intersections and an expanded particle spectrum that together yield self-contained, charge-consistent, quark constructions of gauge bosons and leptons, as well as the known SM hadrons. This direct mapping from octonionic algebra to physical quark composites makes them the superior choice for the unified, substructure-based Triad Model. Moreover, these algebraic structures, grounded in Jordan algebras and octonions, are being investigated for their potential role in understanding the origins and properties of the Cabibbo-Kobayashi-Maskawa (CKM) matrix and quark mixing [10].

In the next section, we build on this algebraic foundation by showing how the same twelve axion–gluon subunits that define quark and lepton structure also generate an emergent electromagnetic field. This leads naturally to the axion–electrodynamics framework in §3.4, where the color-axion mapping to electric and magnetic components is made explicit.

## 3.4 Axion Electrodynamics and the Emergent Electromagnetic Field

In the Triad Model the same twelve low-energy “color” axions that self-assemble into gluons and quarks also form an **axion field** whose collective oscillations reproduce Maxwell-like electromagnetic waves. Concretely:

1. **Color-Charge ↔ EM-Charge Mapping**
   - **Red/anti-red** forces carry a net negative electric monopole charge (E−) and a magnetic south monopole ($B_S$)
   - **Blue/anti-blue** forces carry a net positive electric monopole charge (E+) and a magnetic north monopole ($B_N$).
   - **Green/anti-green** forces are electrically neutral and serve as a complex “modulator” of the red/blue vectors.
2. **Quantization via $\hbar$**

   As in the photoelectric effect, electromagnetic energy is quantized by

   $$E_\gamma = h f,$$

   with $h$ Planck’s constant and $f$ the wave frequency. Introducing $\hbar = \mathrm{h} / 2\pi$ makes $\hbar$ the natural quantum of angular momentum in both atomic physics and field theory.

Likewise, each axion oscillator carries energy on the order of $\alpha\,\hbar\,\omega$ (see §3.5) and satisfies Heisenberg's bound $\Delta x\,\Delta p \geq \hbar/2$.

3. **Visinelli (2014) and Axion-Photon Duality**

   Luca Visinelli [8] demonstrated that adding a light, pseudoscalar "axion-like" field to Maxwell's equations preserves the electric–magnetic duality. This means that the field equations remain symmetric under interchange of *E* and *B*. In particular, Visinelli showed that electromagnetic waves can carry coherent axion oscillations without spoiling Maxwell's form, implying that an axion field can propagate alongside a photon field as a unified "axion–EM wave.

   **Triad Model Proposal**

   We identify the twelve color-axions with the pseudoscalar field $a(x)$. In the Triad lattice, each axion executes quantized oscillations along specific tetrahedral symmetry axes. These oscillations are represented mathematically by **dual sets of harmonic-oscillator ladder operators** (introduced in §3.5), with each set acting along one of two orthogonal spatial directions. Collectively, these ladder-operator modes map directly onto electric and magnetic field components that satisfy Maxwell's equations in the classical limit. Simultaneously, these $\hbar$-sized axions neutralize the QCD $\theta$-term (solving the strong CP problem) by balancing the gluonic field inside quarks.

4. **Why this Matters**

   - **Unified Origin:** The same quantum subunits yield both strong color forces (gluonic forces with large numbers of axions of the same type) and electromagnetic forces.
   - **Natural Quantization:** $\hbar$ enters as the fundamental action quantum in both sectors.
   - **Predictive Framework:** Axion electrodynamics carries concrete signatures (e.g. vacuum birefringence) that can be tested [9].

In the following section (§3.5), we formalize this picture by introducing the **dual ladder-operator framework** for the twelve axion types. These operators define the quantized excitation modes along the tetrahedral lattice axes, providing the algebraic structure that will later enter the Lagrangian and Hamiltonian formulations of the Triad Model.

## 3.5 Dual Ladder Operators

A cornerstone of the Triad Model is that each of the twelve axion types is quantized by **two** independent sets of harmonic-oscillator ladder operators acting along orthogonal spatial axes. For a single 1D oscillator, we define

$$\hat{a} = \sqrt{\frac{m\omega}{2\hbar}} \left(\hat{x} + \frac{i}{m\omega}\hat{p}\right), \quad \hat{a}^\dagger = \sqrt{\frac{m\omega}{2\hbar}} \left(\hat{x} - \frac{i}{m\omega}\hat{p}\right) \tag{18}$$

with the canonical commutation relation

$$[\hat{a}^\dagger \hat{a}] = 1$$

Each axion type $i$ carries one pair of $\{\hat{a}^\dagger \hat{a}\}$ along two of the three orthogonal axes x, y, z, as determined by the lattice geometry. The special 8th tetrahedron carries four independent pairs of $\{\hat{a}^\dagger \hat{a}\}$ oriented along four distinct symmetry axes, reflecting its unique role in lattice asymmetry and excitation pathways.

These ladder operators generate a three-dimensional tetrahedral oscillator space within each of the eight tetrahedra. Excitations may populate levels up to a cutoff $N_{max}$; in our preliminary treatment we set $N_{max} = 8$ for concreteness, with "ejection" processes corresponding to transitions near that upper bound. More generally one could identify:

$$N_{max} = \frac{1}{\alpha} \approx 137$$

so that an axion is emitted whenever the oscillator reaches its 137th quantum of energy. This hypothesis's energetic viability depends on the chosen value of $\hbar\omega$ and is left for future phenomenological study.

**Methodological Note.**
Some approaches to "quantum tetrahedra" employ SU(2) spin-network ladder operators, as in loop quantum gravity, closing four face-area vectors into a singlet. While elegant for deriving area and volume spectra, that formalism does not naturally yield the twelve independent energy levels, octonionic intersections, or direct number-operator counting ($\sum_i N_i = 1 / \alpha$ with $\alpha$ = Fine Structure Constant) for each $N_i = \hat{a}^\dagger \hat{a}^\dagger$ that our axion–oscillator framework provides. The dual harmonic-oscillator ladders instead give an immediate mapping to $SU(3)^3$ symmetry, energy quantization, and both static and dynamical Hamiltonians in one self-contained algebraic system.

Importantly, the ladder operators defined here are the **quantum building blocks** for the Lagrangian and Hamiltonian densities introduced in §3.6 and §3.7, where they are assembled into field-theoretic form to describe both the static structure and driven dynamics of the Triad lattice.

## 3.6 Lagrangian Density for the Axion-Oscillator System

We introduce real scalar fields $\varphi_i(t, x)$ (one per oscillator site in the axion–gluon chain).

### (A) Relativistic (3+1)D Lagrangian — *Continuum Field*

$$\mathcal{L}^{(3+1)D}_{Triad} = \sum_{i=1}^{N} \left[\tfrac{1}{2}(\dot{\phi}_i^2 - \tfrac{1}{2}|\nabla\phi_i|^2 - \tfrac{1}{2}\omega_i^2\,\phi_i^2\ \right] - V_{drive}(t,\{\phi_i\}), \qquad (19)$$

with $|\nabla\phi_i|^2 = (\partial_x\phi_i)^2 + (\partial_y\phi_i)^2 + (\partial_z\phi_i)^2$.

The driving potential encodes asymmetric excitations; we take the **potential-energy** convention

$$\mathrm{V}_{\mathrm{drive}}(t,\{\phi_i\}) = -\frac{1}{\alpha}\, f(t)\, D(\{\phi_i\})$$

where *f(t)* is a real modulation function and *D({ϕij})* is the field-space operator selecting asymmetry-sensitive oscillator sites. Appears "- V " in $\mathcal{L}$ and "+ V " in $\mathcal{H}$ below.

### (B) Nonrelativistic 3D Lattice Reduction— *Discrete Network*

On the axion–gluon lattice, continuous gradients are replaced by nearest-neighbor couplings $K_{ij}$:

$$\mathcal{L}^{(3D)}_{Lattice} = \sum_{i=1}^{N}\left[\tfrac{1}{2}\,\dot{\phi}_i^2 - \tfrac{1}{2}\,\omega_i^2\,\phi_i^2\right] - \tfrac{1}{2}\sum_{\{\langle i,j\rangle\}} K_{ij}(\phi_i - \phi_j)^2 - V_{drive}(t,\{\phi_i\}). \qquad (20)$$

Here $K_{ij}$ defines the coupling strength between neighboring sites (isotropic if all $K_{ij} = \kappa$, anisotropic if direction-dependent).

**Methodological Note — Continuous Field vs. Lattice Network:**
Equation (19) is the standard continuum field-theory form; Eq. (20) is its lattice reduction. In the long-wavelength limit they agree (with $|\nabla\phi|^2 \leftrightarrow \sum K_{ij}(\phi_i-\phi_j)^2$), but the lattice network is more natural for quark and gluon self-assembly.

## 3.7 Static and Dynamic Hamiltonian Formulations

### (A) General Relativistic (3+1)D Hamiltonian— *Continuum Field*

The canonical momentum is $\pi_i(t,x) = \partial\mathcal{L}/\partial\dot{\phi}_i = \dot{\phi}_I$. The Hamiltonian density and total Hamiltonian are

$$\mathcal{H}^{(3+1D)}(t,x) = \sum_{i=1}^{N}\left[\tfrac{1}{2}\pi_i^2(t,x) + \tfrac{1}{2}|\nabla\phi_i|^2 + \tfrac{1}{2}\omega_i^2\phi_i^2\right] + V_{drive}(t,\{\phi i\}), \qquad (21A)$$

$$\mathcal{H}^{(3+1D)}_{Total} = \int d^3x\,\mathcal{H}^{(3+1D)}(t,\boldsymbol{x}).$$

Here $|\nabla\phi_i|^2 = (\partial_x\phi_i)^2 + (\partial_y\phi_i)^2 + (\partial_z\phi_i)^2$ is the **continuous** spatial gradient energy.

## (B) Nonrelativistic 3D Lattice Hamiltonian — *Discrete Network*

On the axion–gluon lattice, spatial couplings are **discrete**. Replace the gradient energy by a **nearest-neighbor** term with couplings $K_{ij}$ (isotropic: $K_{ij} = \kappa$ for neighbors, 0 otherwise; anisotropy uses direction-dependent $K_{ij}$):

$$\mathcal{H}_{Lattice}^{(3D)} = \sum_{i=1}^{N}\left[\frac{1}{2}\pi_i^2 + \frac{1}{2}\omega_i{}^2\phi_i{}^2\right] + \frac{1}{2}\sum_{\{\langle i,j\rangle\}} K_{ij}\,(\phi_i - \phi_j)^2 + V_{drive}(t,\{\phi_i\}) \tag{21B}$$

This is a **total** lattice Hamiltonian (sum over sites and bonds), not a density. The discrete coupling term $\frac{1}{2}\sum_{\{\langle i,j\rangle\}} K_{ij}\,(\phi_i - \phi_j)^2$ is the lattice analogue of the continuum $\frac{1}{2}|\nabla\phi_i|^2$; they are different operators but both penalize spatial variation.

## (C) Quantization and Static Energy Levels

In the quantized lattice, each mode is a harmonic oscillator with ladder operators $\hat{a}_i{}^\dagger\hat{a}_i$ and number operator $\hat{N}_i = \hat{a}_i{}^\dagger\hat{a}_i$ and α = Fine Structure Constant.

### Static quark:

$$\hat{H}_{\text{quark}} = \sum_{i=1}^{9}\alpha\hbar\omega\,\hat{N}_i,\quad \sum_{i=1}^{9}\hat{N}i = \frac{1}{2\alpha}, \tag{22}$$

### Static Photon:

$$\hat{H}_{\text{photon}} = \sum_{i=1}^{18}\alpha\hbar\omega\,\hat{N}_i,\quad \sum_{i=1}^{18}\hat{N}i = \frac{1}{\alpha}. \tag{23}$$

## (D) Time-Dependent Hamiltonian

To account for axion flux modulation, we include the driving term explicitly. The total time-dependent Hamiltonian for a photon becomes

$$\hat{H}\gamma(t) = \hat{H}_{static} + \hat{H}_{drive}(\mathrm{t}) = \sum_{i=1}^{18}\alpha\hbar\omega\,\hat{N}_i + \frac{1}{\alpha}f(t)\,\hat{D} \tag{24}$$

where $\hat{D}$ is the operator acting on asymmetric axion modes and $f(\mathrm{t})$ modulates the strength of the axion injection/ejection process over time.

Time evolution follows the Schrödinger equation:

$$\mathrm{i}\hbar \frac{\partial}{\partial t}\Psi(t) = \hat{H}\gamma(t)\,\Psi(t).$$

### 3.7.1 Lorentz symmetry (lattice → Continuum)

**Set-up. For one axion field on a cubic lattice of spacing $a$ with nearest-neighbor couplings K, the discrete action is**

$$\textbf{(L1)}\quad S_a = \int dt \ \sum_{n\in Z^3} \left[ \tfrac{1}{2}\,\dot{\phi}_n^{\,2} - \tfrac{K}{2}\, a^{-2} \sum_{j=1}^{3} ( \phi_{n+\hat{e}_j} - \phi_n)^2 - \tfrac{1}{2}\,\mathrm{m}^2\,\phi_n^{\,2}\right].$$

**(A) Lorentz-covariant continuum limit with dimension-6, even-in-k corrections**

Fourier expanding $\phi_n(t) = \int (d^3k)/(2\pi)^3\, e^{ik\cdot an}\, \phi_k(t)$ gives the exact lattice dispersion

$$\textbf{(L2)}\quad \omega^2(\mathbf{k}) = \mathrm{m}^2 + 4\mathrm{K}\, a^{-2} \sum_{j=1}^{3} sin^2\left(\tfrac{1}{2}a\mathrm{k}_j\right).$$

For $|\mathbf{k}|a \ll 1$, leading $\mathcal{O}(a^2\,\mathrm{k}^4)$, next $\mathcal{O}(a^4\,\mathrm{k}^6)$

$$\textbf{(L3)}\quad \omega^2(\mathbf{k}) = \mathrm{m}^2 + \mathrm{c}^2\mathbf{k}^2 - \tfrac{1}{12}\mathrm{c}^2\, a^2 \sum_j k_j^{\,4} + \mathcal{O}(a^4\,\mathrm{k}^6), \quad c^2 \equiv K.$$

so the first Lorentz-violating (LV) term is **quartic in momentum** (dimension-6) and **even in k.**

**Group-velocity correction (ultra-relativistic, isotropic).**
With $\sum_j k_j^4 \to k^4$,

$$\omega \simeq \mathrm{ck}\,[1 - (a^2k^2)/24], \quad \mathcal{V}_g \equiv \frac{\partial\omega}{\partial k} \simeq \mathrm{c}\left[1 - \tfrac{1}{8}\, a^2k^2\right].$$

**Time-of-flight bound.**
For a photon of energy $E = \hbar\omega$ over distance $L$,

$$\Delta\mathrm{t} \simeq \frac{\mathrm{L}}{8\mathrm{c}}\, a^2\left(\frac{E}{\hbar c}\right)^2 = \frac{\mathrm{L}}{8\mathrm{c}}\left(\frac{E}{\Lambda}\right)^2, \qquad \Lambda \equiv \hbar\mathrm{c}/a\,.$$

Thus any Lorentz-violation is even in k and **dimension-6 suppressed** $\propto( (E/\Lambda)^2$ .

$$\textbf{(L4)}\quad \omega^2 = m^2 + c^2\boldsymbol{k}^2,$$

with Lorentz-violating leading corrections suppressed by $\mathcal{O}(a^4\,\mathrm{k}^6)$

*Takeaway:* microscopic discreteness only induces $\mathcal{O}(a^2)$even-in-momentum deviations; for wavelengths $\gg a$ the kinematics are Lorentz invariant with limiting speed $c^2 \equiv K$.

### (B) Lattice "boosts" à la Baxter (1+1D slices) and rapidity

Along any 1D slice (hold y, z fixed), the axion sector admits an integrable discretization aligned with the eight-vertex model. With row transfer matrix $T(u)$ (elliptic "rapidity" $u$) and corner transfer matrix $C(u)$, the **lattice boost operator** ($\mathcal{B}$) is

$$\text{(L5)}\quad \mathcal{B} \equiv \frac{\mathrm{d}}{\mathrm{d}u} \ln T(u)\big|u{=}u_0 \;\Rightarrow\; [\mathcal{B}, H] = iP,\;\; [\mathcal{B}, P] = iH/\mathrm{c}^2,\;\; \mathrm{c}^2 \equiv K.$$

(in the integrable limit and appropriate units), realizing the $1+1$ Lorentz algebra on the lattice. In the $a \to 0$ limit this reproduces the Lorentz structure of massive Thirring/sine-Gordon.

*Takeaway:* Corner transfer matrix as lattice boost; eight-vertex↔sine-Gordon/Thirring in the continuum. A continuous **lattice boost** exists already at finite $a$; *the Octon's "8" dovetails with the eight-vertex construction [22]*.

### (C) Local Lorentz covariance (curved effective metric)

Allow the Triad to "breathe" via a conformal field $\sigma(x)$ that rescales local time/space coefficients. The coarse-grained action is

$$\text{(L6)}\qquad \mathrm{S}_{\mathrm{eff}} = \frac{1}{2}\int \mathrm{d}^4\mathrm{x}\,\sqrt{-\mathrm{g}}\;\left[\mathrm{g}^{\mu\nu}(\mathrm{x})\,\partial_\mu\phi\,\partial_\nu\phi - \mathrm{m}^2\phi^2\right],$$

$$\mathrm{g}_{\mu\nu}(\mathrm{x}) = \mathrm{e}^{2\sigma(\mathrm{x})}\eta_{\mu\nu} + \mathcal{O}(\partial 2\sigma).$$

To leading order the scalar curvature is

$$\text{(L7)}\qquad \mathrm{R} = -6\,\mathrm{e}^{-2\sigma}\left((\Box\sigma + (\partial\sigma)^2\right),\quad \sigma \simeq \Phi_{\mathrm{N}}/\mathrm{c}^2,$$

$$\nabla^2\Phi_{\mathrm{N}} \simeq 4\pi\mathrm{G}\;\left(\rho_{\mathrm{matter}} + \rho_{axion}^{eff}\right),$$

so geodesics bend as in GR in the weak-field limit. Matching (L6) to (L1) fixes the local light-cone via $\mathrm{c}^2(\mathrm{x}) = \mathrm{K}(\mathrm{x})/\mathrm{Z}_t^2(\mathrm{x})$; lattice adaptivity enforces $\mathrm{K}/\mathrm{Z}_t^2 \approx$ const, preserving **local** Lorentz invariance.

*Takeaway:* the same lattice that yields emergent Lorentz symmetry in flat space uplifts to a manifestly covariant effective action with metric $\mathrm{g}_{\mu\nu} = \mathrm{e}^{2\sigma}\eta_{\mu\nu} + \cdots$.

### (D) Size and form of possible violations

From (L3), the leading deviation is

$$\textbf{(L8)}\quad \omega^2 - (\mathrm{m}^2 + \mathrm{c}^2\mathbf{k}^2) = -\tfrac{1}{12}\,\mathrm{c}^2\, a^2 \textstyle\sum_{j} k_j^{\,4} + \mathcal{O}(a^4 k^6),\ \mathrm{c}^2 = K$$

**Lorentz Takeaways.**

- **Even-in-*k***: leading LV terms are parity/T-even; there are **no** CPT-odd, linear-in-$k$ (dimension-5) effects.
- **Rotationally symmetric** to this order if the coupling $K_{ij}$ is isotropic.
- **Dimension-6 suppression**: all observable LV scales as $\mathcal{O}((\mathrm{E}/\Lambda)^2)$
- **IR Lorentz restoration**: as $a \to 0$ (or $\mathrm{E} \ll \Lambda$), the algebra closes exactly and $\omega^2 - (\mathrm{m}^2 + \mathrm{c}^2\mathbf{k}^2)$.
- **Baxter/rapidity link**: the corner-transfer matrix acts as a lattice boost; elliptic rapidities map to continuum rapidity, matching the Lorentz-invariant sine-Gordon/Thirring limit.

**Net result.** With $a$ tied to the axion cutoff (taken near/below the Planck scale), the Triad lattice is **effectively Lorentz-invariant** at accessible energies: LV is **rotationally symmetric, even-in-$k$, and dimension-6 suppressed**, rendering time-of-flight and dispersion constraints naturally satisfied.

---

### 3.7.2 Axion Sector (Consistency with Existing Bounds)

We describe each of the twelve light axion modes $a_\ell$ ($\ell = 1,\dots,12$) by the standard ALP effective terms

$$\mathcal{L}_{\text{axion}} = -\frac{1}{4}\, g^{(\ell)}_{a\gamma\gamma}\, a_\ell\, F_{\mu\nu}\tilde{F}^{\mu\nu} - \frac{1}{2}(\partial a_\ell)^2 - \frac{1}{2}\,\mathrm{m}_\ell^2\, a_\ell^2 + g^{(\ell)}_{ae}(\partial_\mu a_\ell)\bar{e}\gamma^\mu\gamma_5 e + \cdots,$$

with the usual mapping $g^{(\ell)}_{a\gamma\gamma} = \alpha C^{(\ell)}_{a\gamma}/2\pi\, f^{(\ell)}_a$.

(Here $f_a$ is the axion "decay constant"; to avoid confusion with the drive function ***f(t)*** used in §3.6–3.7, we sometimes write $F_a$ for the decay constant in text.)

In an external magnetic field $B$ over length $L$, photon–axion conversion obeys

$$P_{a\leftrightarrow\gamma} \simeq \left(\frac{1}{2} g_{a\gamma\gamma} B\, L\right)^2 \mathrm{sinc}^2\left(\frac{\Delta k\, L}{2}\right),\quad \mathrm{sinc}\,x \equiv \frac{\sin x}{x},\quad \Delta k = \frac{1}{2E}\,|\mathrm{m}_a^2 - \mathrm{m}_\gamma^2|,$$

which is the basis for CAST/helioscope and "light-shining-through-walls" constraints with sinc.

**Placement within the Triad framework.**
In our construction, the axion modes are the quantized oscillators of the axion–gluon chain (§3.6–

3.7). Their couplings $g_{a\gamma\gamma}$ arise from overlap integrals between Octon/lattice modes and the electromagnetic field in the axion-electrodynamics limit; the continuum 3+1D formulation preserves **Lorentz invariance** at leading order, with even-in-momentum corrections suppressed by $a^2k^4$ (dimension-6), consistent with §3.7.1 (Lorentz-symmetry), which shows leading Lorentz invariance and dimension-6, even-in-$k$ corrections.

**Conservative parameter choice consistent with current bounds.**
A model-independent way to stay within CAST/stellar limits while remaining interesting for haloscopes is:

$$f_a \gtrsim 10^9\text{–}10^{10}\ \text{GeV}, \qquad C_{a\gamma} = \mathcal{O}(1) \implies g_{a\gamma\gamma} \lesssim 10^{-12}\text{–}10^{-11}\ \text{GeV}^{-1},$$

and suppress tree-level electron couplings ($g_{ae} \approx 0$ at leading order, with only loop-level/geometry-suppressed contributions). This keeps us within **helioscope** and **stellar-cooling** bounds, while allowing **haloscope** sensitivity in the $\mu eV$ mass band for a QCD-like axion (and broader masses for generic ALPs). Birefringence searches (e.g., PVLAS/OVAL) further bound $g_{a\gamma\gamma}$ ; our preferred range is safely below current rotation/ellipticity sensitivities.

**QCD-axion mapping.**
If one of the twelve modes is identified with the QCD axion, we use

$$m_a\, f_a \simeq m_\pi\, f_\pi \sqrt{z}\,/(1+z)\,, \qquad z = m_u/m_d\,,$$

and the same $g_{a\gamma\gamma}$ normalization above; the remaining modes behave as generic ALPs with independent $(m_\ell,\ f_\ell,\ C_{a\gamma}^{(\ell)})$. This keeps the axion sector **anchored to standard EFT** while preserving the Triad-specific origin (Octon/lattice oscillators) and the Lorentz-symmetric continuum limit already established in §3.7.1.

---

### 3.7.3 Masses and CKM from Octon-Bond Laplacians

**Set-up (one quark family).**
Model each Octon as a weighted graph on the 8 (or 9) axion/gluon "addresses." Let the **weighted Laplacian** $L_q$ encode bonds for family $q$:

- For $i \neq j$: $(L_q)_{ij} = -w_{ij}$ if sites $i, j$ are bonded, else 0.
- Diagonal: $(L_q)_{ii} = \sum_{j\neq i} w_{ij}$.
- **Strong 3-color bond:** $w_{ij} = s$.
- **Weak 2-color bond (from a swap):** $w_{ij} = s(1-\varepsilon)$ with_ $0 < \varepsilon \ll 1$.

Define the **effective static Hamiltonian**

$$H_q = \mu_q \mathrm{I} + \kappa_q L_q,$$

where $\mu_q$ is a common offset (baseline occupation energy) and $\kappa_q$ sets the stiffness/scale.

**Mass from the Laplacian.**
Let $\lambda_{\min}(\mathrm{L_q})$ be the **lowest nonzero** eigenvalue of $\mathrm{L_q}$ Identify the stabilization energy (quark "mass") via

$$\mathrm{m_q c^2} \simeq \mu + \kappa_\mathrm{q}\, \lambda_{\min}(\mathrm{L_q}).$$

---

**Boxed Eq. (CKM1) — Single-bond mass uplift (first order).**
Weakening a single bond $(i—j)$ is the rank-2 update
$\Delta L = \varepsilon_s (e_i—e_j)(e_i—e_j)^\top$ .
For the lowest nonzero mode $\nu^{(\min)}$ of the parent (all-strong) Laplacian:

$$\delta_{\mathrm{mq}} \mathrm{c}^2 \approx \kappa_\mathrm{q}\, \varepsilon_\mathrm{s} \left( \nu_\mathrm{i}^{(\min)} - \nu_\mathrm{j}^{(\min)}\right)^2. \qquad \textbf{(CKM-1)}$$

*Implications:* the mass shift grows with (i) how many bonds are weakened (linearly), and (ii) **where** they are weakened (through the mode shape factor $(\nu_\mathrm{i} - \nu_\mathrm{j})^2$).

---

**CKM from relative diagonalizations.**
Build **family Hamiltonians**

$$H_u = \mu_u \mathbf{I} + \kappa_u L_u, \qquad H_d = \mu_d \mathbf{I} + \kappa_d L_d.$$

Diagonalize

$$U_u^\dagger H_u U_u = \mathrm{diag(m_u,m_c,m_t)}, \qquad U_d^\dagger H_d U_d = \mathrm{diag(m_d,m_s,m_b)}.$$

Then the **CKM matrix** is the **relative rotation**

$$\mathrm{V_{CKM}} = U_u^\dagger U_d. \qquad \textbf{(CKM-2)}$$

For a **single** weak bond in (say) $L_d$ and none in $L_u$, the leading mixing between the two lightest modes obeys a Cabibbo-type estimate

$$\theta_{12} \approx \langle \nu^{(1)} | \Delta \mathrm{L} | \nu^{(2)} \rangle / (\lambda_2^{(0)} — \lambda_1^{(0)}) = \frac{\varepsilon \mathrm{s}}{\Delta\lambda} ( \nu_\mathrm{i}^{(1)} - \nu_\mathrm{j}^{(1)})( \nu_\mathrm{i}^{(2)} - \nu_\mathrm{j}^{(2)})$$

Leading mixing angle (two-mode estimate).

$$\theta_{12} \approx \frac{\varepsilon s}{\Delta\lambda}\left( \nu_i^{(1)} - \nu_j^{(1)}\right)\left( \nu_i^{(2)} - \nu_j^{(2)}\right)$$

with $\Delta\lambda = \lambda_2^{(0)} - \lambda_1^{(0)}$ from the unperturbed all-strong Laplacian.

**CP violation from loop phases.**

Allow tiny **orientation phases** on bonds, $w_{ij} \to w_{ij}\, e^{i\theta_{ij}}$ with $\theta_{ij} = -\theta_{ji}$. Gauge-invariant **cycle phases** (sum of $\theta$ around closed Octon loops) produce a physical complex phase in $V_{CKM} = U_u^\dagger U_d$. The Jarlskog $J$ is then proportional (to leading order) to **differences of loop phases** between the up- and down-sector Laplacians, times products of the small mixing angles.

**Six-step recipe (practical fit):**

1. **Fix the base graph.** Choose the 8 (or 9) addresses and the 12 strong bonds; compute $L^{(0)}$, its eigenvalues $\lambda_n^{(0)}$ and modes $\nu^{(n)}$.
2. **Encode flavors.** For each $q \in \{u,c,t\}$ and $\{d,s,b\}$, set which bonds are weak and by how much $\varepsilon_q$ (your swaps). This defines $L_q$.
3. **Masses.** Choose $(\mu_u,\kappa_u)$, $(\mu_d,\kappa_d)$ once; adjust the few $\varepsilon_q$ to fit $(m_u, m_c, m_t)$ and $(m_d, m_s, m_b)$. Use (M1) for guidance; confirm by diagonalization.
4. **Mixing.** Compute $U_u, U_d$, then $V_{CKM} = U_u^\dagger U_d$ single weak bond mainly feeds $\theta_C$; additional weak bonds feed $\theta_{23}, \theta_{13}$.
5. **CP phase.** Turn on minimal loop phases $\theta_{ij}$ on selected bonds; fit $\delta_{CKM}$ (and Jarlskog $J$) with **small** phase differences across up vs. down cycles.
6. **Predictions.** Once masses are set, the model **correlates** mixing angles and the CP phase with **which specific bonds** are weakened and by **how much**—a falsifiable structural claim.

**Takeaways.**

• Quark masses arise as Rayleigh-quotient eigenvalues of a **graph Laplacian**; "bond rearrangement" → **rank-2 updates** with analytic mass shifts.
• CKM = relative eigenbasis of two Laplacians (up vs. down).
• CP violation = **loop phases** on Octon cycles.

All operators are Hermitian and finite-dimensional; the construction is standard linear algebra tied directly to named bonds.

### 3.7.4 "12 Axions" ≅ 12-Dimensional Coset of $SU(3)^3 \to SU(3) \times SU(2) \times U(1)$

**Methodological Note (MN) on Parent Symmetry.** Take the minimal trinification group

$$G = SU(3)_C \times SU(3)_L \times SU(3)_R\,,\ \dim G = 8 + 8 + 8 = 24 \qquad \text{(MN-1)}$$

Unbroken subgroup matching the SM.

$$H = SU(3)_C \times SU(2)_L \times U(1)_Y\,,\quad \dim H = 8 + 3 + 1 = 12 \qquad \text{(MN-2)}$$

**Coset dimensionality (the "12"):**
The broken directions are the coset *G / H* with

$$\dim(G/H) = \dim G - \dim H = 24 - 12 = 12 \qquad \text{(MN-3)}$$

Identify the twelve axion modes $\{A_a(x)\}_{a=1}^{12}$ with the coordinates $\xi^a(x)$ on this coset.

**Nonlinear sigma model (CCWZ) realization.**
Let $X_a$ be the 12 broken generators and define

$$U(x) = \exp\left(\tfrac{i}{f}\,\xi^a(x)\,X_a\right) \qquad \text{(MN-4)}$$

A gauge-covariant low-energy Lagrangian for the axion sector is

$$\mathcal{L}_{ax} = (f^2/4)\mathrm{Tr}[(D_\mu U)(D^\mu U)^\dagger] - V(\xi),\ \ D_\mu U = \partial_\mu U - iA_\mu U + iUB_\mu, \quad \text{(MN-5)}$$

where $\mathcal{A}_\mu, \mathcal{B}_\mu$ embed the relevant gauge connections. When the full $G$ is gauged, the 12 Goldstones are "eaten" by the 12 broken gauge fields (Stückelberg/Higgs mechanism), leaving exactly the **12 unbroken generators of the SM** massless (gluons 8 + $SU(2)_L$ 3 + $U(1)_Y$ 1) prior to electroweak breaking.

**Explicit breaking and light pseudo-NGB masses.**
Lattice anisotropies or couplings to other sectors generate

$$V(\xi) = \frac{1}{2}\,\xi^a\,\mu^2_{ab}\,\xi^b + \cdots\,,\quad (M^2_{axion})_{ab} = (\partial^2 V)/(\partial\xi^a\,\partial\xi^b)|_{\xi=0}, \quad \text{(MN-6)}$$

so the twelve modes can remain light pseudo-Nambu–Goldstones rather than being entirely eaten, consistent with our axion phenomenology.

**Mapping the "12 ↔ 12".**

- **Triad:** twelve axion modes $\{\xi^a\}$ parameterize *G / H*.
- **SM:** twelve unbroken generators $\mathrm{su}(3)_C \oplus \mathrm{su}(2)_L \oplus \mathrm{u}(1)_Y$.

This yields a crisp, model-independent 12 dimensional coset:

$$\text{Triad's 12 axions } \{\xi^a\}_{a=1}^{12} \Leftrightarrow SU(3)^3/(SU(3)_C \times SU(2)_L \times U(1)_Y)\,,$$

MN-1 and MN-2 give MN-3 as $\dim(G/H) = \dim G - \dim H = 24 - 12 = 12$.

## 3.8 The Triad Model and the Heisenberg uncertainty equation

Each axion oscillator (along $\hat{x}$, $\hat{y}$, or $\hat{z}$) satisfies the standard quantum harmonic–oscillator commutation relations. For one axis (say x):

$$\hat{a} = \sqrt{\frac{m\omega}{2\hbar}} \cdot \hat{x} + \frac{i}{\sqrt{2m\hbar\omega}} \cdot \hat{p}\,, \qquad \hat{a}^\dagger = \sqrt{\frac{m\omega}{2\hbar}} \cdot \hat{x} - \frac{i}{\sqrt{2m\hbar\omega}} \cdot \hat{p}$$

obeying $[\hat{a}_i^\dagger, \hat{a}_i] = 1$. From these definitions one recovers the canonical commutator for position and momentum operators along each axis:

$$[\hat{x}, \hat{p}] = i\hbar.$$

The Heisenberg uncertainty principle then follows in the usual way. Defining the standard deviations

$$\Delta x = \sqrt{\langle \hat{x}^2 \rangle - \langle \hat{x} \rangle^2}, \quad \Delta p = \sqrt{\langle \hat{p}^2 \rangle - \langle \hat{p} \rangle^2},$$

Then the Robertson inequality yields

$$\Delta x \, \Delta p \geq \frac{1}{2} \left|\langle [\hat{x}, \hat{p}] \rangle\right| = \frac{\hbar}{2}\,.$$

Thus, the Triad Model provides a robust and mathematically consistent quantum substructure through the dual ladder operator mechanism and the fractional energy quantization of axions.

### Interpretation in the Triad Model

- **Per–axis uncertainty:** Since each axion oscillator along the x, y, and z axes obeys the same commutator, the inequalities

  $$\Delta x \, \Delta p_x \geq \hbar/2, \;\; \Delta y \, \Delta p_y \geq \hbar/2, \;\; \Delta z \, \Delta p_z \geq \hbar/2$$

  hold independently for each tetrahedral direction.

- **Ground–state minimal uncertainty**

  In the axion ground state $|0\rangle$ (Fock vacuum), $\langle \widehat{N} \rangle = 0$, so

  $$\Delta x \, \Delta p = \frac{\hbar}{2} \left(2 \langle \widehat{N} \rangle + 1\right) \longrightarrow \frac{\hbar}{2}$$

This minimal uncertainty underpins the inherent 'fuzziness' of axion/gluon positions and momenta. When assembled across all 18 sites of a photon or across the 9 sites of a quark, these uncertainties combine to produce the extended, wave-like character of Triad Model fields.

- **Triad (lepton) structure:**

  When three octahedral quarks interpenetrate into a Stellated Rhombic Dodecahedron, the combined uncertainties remain bounded by the same $\hbar/2$ per axis. However, correlated fluctuations among the individual $(\hat{x}_i, \hat{p}_i)$ modes can arise. In particular, the driving terms $\frac{1}{\alpha}$ $f(t)\ D$ can redistribute axions between modes in a way that respects the uncertainty limit but induces the net momentum and spin that characterize particle states.

  Thus, the fundamental Heisenberg relation

$$\Delta x\ \Delta p \geq \frac{\hbar}{2}$$

  is built directly into the Triad Model's use of ladder operators and carries through from single–axion oscillators up to the full quark and lepton structures.

## 3.9 From Weak-Color Axions to Strong-Color Gluons

1. **Wave-to-Particle Crossover**

Individual axions behave as low–energy, wave–like oscillators with characteristic energy:

$$E_{axion} \approx \alpha\, \hbar\, \omega$$

When approximately

$$N_c = \alpha^{-1} \approx 137$$

axions occupy a single axion/gluon site, they undergo a collective transition into a strongly coupled gluon mode. Thus, below the critical threshold $N_c$, axions remain delocalized waves; above it, they condense into gauge–boson (gluon) states.

2. **Equilibrium Flow**

Under steady conditions, axions flow into and out of each site at balanced rates. For each completed unit of Nc axions, the site frequency increases discretely,

$$f_n = n\, f_0\,, \qquad n \in Z^+,$$

where $f_0$ corresponds to the base frequency associated with one quantum of gluon occupancy.

**3. Gluon Octet Formation**

Once all eight axion/gluon "addresses" in a quark octahedron each reach the threshold $N_c$, they self–assemble into a coherent gluon octet. The symmetry is slightly broken at the special **eighth address**, which accepts *two distinct axion types* at threshold, thereby supplying all three color charges simultaneously. This intrinsic asymmetry underpins quark spin orientation and directional momentum transfer.

**4. Large, Ubiquitous Axion Fields**

Even low–frequency photons eject enormous axion fluxes. For example:

• VLF radio waves ($f \approx 3 \times 10^4$ Hz) eject $\approx 1.9 \times 10^5$ axions/s
• X–rays ($f \approx 3 \times 10^{18}$ Hz) eject $\approx 1.9 \times 10^{19}$ axions/s
• Gamma rays ($f \approx 3 \times 10^{20}$ Hz) eject $\approx 1.9 \times 10^{21}$ axions/s

Thermal and blackbody emission likewise generate vast axion backgrounds:
• Earth radiates $\approx 1.22 \times 10^{17}$ W
• The Sun radiates $\approx 3.8 \times 10^{26}$ W

Even "empty" space, with vacuum energy density $\rho_{vac} \approx 0.6$ eV/cm³, implies a dense sea of background axions.

**5. Minimum of 137 Axions**

At the Planck base frequency $f = 1$ Hz, the threshold flux per gluon is:

$$A_t(f) = \alpha^{-1} f \approx 137\, f \quad \textit{(axions per site per second)}$$

Scaling with f ensures that photon excitations respect local U(1) gauge invariance, consistent with quantum electrodynamics..

**6. Dynamic Balance plus gauge symmetry**

If one gluon site falls below threshold, its effective size expands, raising its capture cross–section until equilibrium is restored. Conversely, an over–occupied gluon contracts, reducing its capture rate. This negative–feedback process can be represented schematically as:

$$\Delta N_i \to -\kappa\, \Delta N_i\,, \quad \kappa > 0$$

which enforces stability across the eight sites and preserves the octahedral (Octon) symmetry of quarks.

**Methodological Note — Critical Occupancy and Symmetry**

The identification of $N_c = \alpha^{-1}$ as the axion–to–gluon transition threshold reflects the fine–structure constant's role in fractional energy quantization (§3.7). This is analogous to critical density thresholds in other collective phenomena (e.g., Bose–Einstein condensation), where wave–like quanta lock into a coherent state once the particle number exceeds a well–defined limit. The Triad lattice's auto–resizing feedback provides a self–stabilizing mechanism absent from conventional QCD, ensuring robust preservation of octahedral symmetry.

## 4.0 Gluon Octets and the Self-Assembly of Stable Quarks

In the Triad Model there are exactly four distinct gluon-octet configurations that self-assemble into the stable down ($D$ and $\overline{D}$) and stable up ($U$ and $\overline{U}$) quarks. Each octet consists of eight axion/gluon "addresses" (tetrahedral sites) whose collective three-color couplings yield an octahedral (Octon) quark. Only two gluon addresses — #2 and #8 — vary among the four possible octets (Eq. 25).

The 8th address is special: it supports **two distinct axion types**, predicted to eject axion flux in orthogonal directions. One flux stream is directed outward; the second is expelled rearward, generating both **intrinsic spin** and **forward propulsion** of the quark.

Because gluons carry explicit color couplings, they are the natural building blocks of quarks, while axions remain free to modulate the surrounding color-field environment. To maintain octahedral balance and stability, the background axion field enforces nearly equal populations at each of the eight gluon addresses

$$
\begin{array}{cc}
\begin{array}{ll}
\multicolumn{2}{c}{\mathbf{G_d}} \\
1.\ -i(r\bar{g} - g\bar{r})/\sqrt{2} & 5.\ (r\bar{b} + b\bar{r})/\sqrt{2} \\
2.\ (r\bar{r} - b\bar{b})/\sqrt{2} & 6.\ (b\bar{g} + g\bar{b})/\sqrt{2} \\
3.\ -i(g\bar{b} - b\bar{g})/\sqrt{2} & 7.\ (r\bar{g} + g\bar{r})/\sqrt{2} \\
4.\ -i(r\bar{b} - b\bar{r})/\sqrt{2} & 8.\ (r\bar{r} + b\bar{b} - 2g\bar{g})/\sqrt{6}
\end{array}
&
\begin{array}{ll}
\multicolumn{2}{c}{\mathbf{G_{\bar{d}}}} \\
1.\ -i(r\bar{g} - g\bar{r})/\sqrt{2} & 5.\ (r\bar{b} + b\bar{r})/\sqrt{2} \\
2.\ (b\bar{b} - r\bar{r})/\sqrt{2} & 6.\ (b\bar{g} + g\bar{b})/\sqrt{2} \\
3.\ -i(g\bar{b} - b\bar{g})/\sqrt{2} & 7.\ (r\bar{g} + g\bar{r})/\sqrt{2} \\
4.\ -i(r\bar{b} - b\bar{r})/\sqrt{2} & 8.\ (r\bar{r} + b\bar{b} - 2g\bar{g})/\sqrt{6}
\end{array}
\\
\begin{array}{ll}
\multicolumn{2}{c}{\mathbf{G_u}} \\
1.\ -i(r\bar{g} - g\bar{r})/\sqrt{2} & 5.\ (r\bar{b} + b\bar{r})/\sqrt{2} \\
2.\ (b\bar{b} - g\bar{g})/\sqrt{2} & 6.\ (b\bar{g} + g\bar{b})/\sqrt{2} \\
3.\ -i(g\bar{b} - b\bar{g})/\sqrt{2} & 7.\ (r\bar{g} + g\bar{r})/\sqrt{2} \\
4.\ -i(r\bar{b} - b\bar{r})/\sqrt{2} & 8.\ (b\bar{b} + g\bar{g} - 2r\bar{r})/\sqrt{6}
\end{array}
&
\begin{array}{ll}
\multicolumn{2}{c}{\mathbf{G_{\bar{u}}}} \\
1.\ -i(r\bar{g} - g\bar{r})/\sqrt{2} & 5.\ (r\bar{b} + b\bar{r})/\sqrt{2} \\
2.\ (r\bar{r} - g\bar{g})/\sqrt{2} & 6.\ (b\bar{g} + g\bar{b})/\sqrt{2} \\
3.\ -i(g\bar{b} - b\bar{g})/\sqrt{2} & 7.\ (r\bar{g} + g\bar{r})/\sqrt{2} \\
4.\ -i(r\bar{b} - b\bar{r})/\sqrt{2} & 8.\ (r\bar{r} + g\bar{g} - 2b\bar{b})/\sqrt{6}
\end{array}
\end{array}
\tag{25}
$$

**Figure 4** illustrates the octonion vector diagram for the $G_d$ (down) quark in Eq. (25). The octonion structure encodes SU(3) symmetries across addresses 1–7, with the dual structure at address 8 ensuring closure of the color geometry. The diagram depicts eight nodes and 36 force vectors, with address 8 carrying all three colors simultaneously.

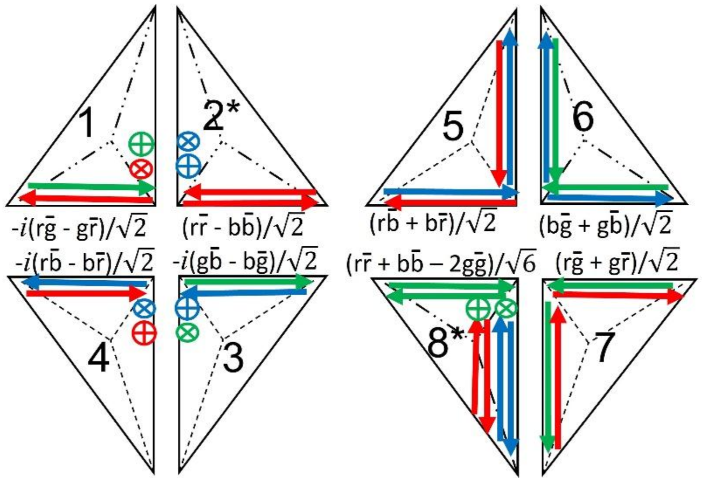


**Figure 4. The octonion vector diagram for the first $G_d$ set of gluons in Eqs (25) is reformatted using vector diagrams for each gluon.** The 8th gluon tetrahedron with all 3 color forces and 8 color force vectors is expressed as a simple SU(3) symmetry group using the Vector diagram with 8 nodes denoting the 8 tetrahedral addresses with 36 vector forces.

### Geometric Consistency from Color-Force Concentration

The Triad Model further predicts that quark octahedra adopt an **irregular geometry**: one axis of the octahedron is shortened by precisely 29.289%. This arises naturally from the distribution of color-force vectors.

In the Octon quark, the X-axis hosts 16 force vectors, while the Y and Z axes host only 8 each (plus four asymmetric vectors at the 8* site). Treating the quark interior heuristically as a one-dimensional confinement "box," the energy spectrum is

$$E_n = (n^2 \pi^2 \hbar^2)/(2\, m\, L^2)\ .$$

Doubling the number of force vectors along the X-axis is modeled as doubling the confinement energy scale along X. To restore the same eigenvalue, the axis length must shrink by

$$\frac{L'}{L} = \frac{1}{\sqrt{2}}\ ,$$

so that

$$1 - \frac{L'}{L} = 1 - \frac{1}{\sqrt{2}} = 0.29289 \ \ (29.289\%).$$

This precise 29.289% axis reduction matches exactly the irregular octahedral geometry required for interpenetration into the Stellated Rhombic Dodecahedron of Fig. 3.

**Methodological Note — Energy vs. Geometry.**

The last 3 equations apply the simple "particle in a box" analogy to model quark confinement. While the mapping of **force-vector multiplicity → confinement energy scaling** is heuristic, the resulting 29.289% axis reduction coincides exactly with the geometric requirement of the Triad lattice. This striking agreement provides strong circumstantial evidence that the color-force distribution and lattice geometry are mutually consistent.

## 4.1 Structural Models of the Stable Up/Down Quarks and Their Antiquarks

The Standard Model (SM) includes three generations of "up-type" quarks (*u, c, t*) and three of "down-type" quarks (*d, s, b*), each with its corresponding antiquarks. The Triad Model provides a unified way to represent all six up- and down-type flavors (plus antiquarks) and offers insight into why there are exactly three generations.

Table 1 summarizes SM quark data and their Triad-Model symbols. Stable quarks (*u, d*) are light, while higher generations (*c, s, t, b*) are heavier and unstable.

**Table 1.** Quark Data (Standard Model, with Triad symbols)

| Flavor | Mass (MeV) | Charge | Standard Symbol | Triad Symbol |
|---|---|---|---|---|
| up | ≈ 2.2 | +2/3 e | u | $\Phi_u$ |
| anti-up | ≈ 2.2 | −2/3 e | ū | $\Phi_{\bar{u}}$ |
| down | ≈ 4.7 | −1/3 e | d | $\Phi_d$ |
| anti-down | ≈ 4.7 | +1/3 e | d̄ | $\Phi_{\bar{d}}$ |
| charm | ≈ 1280 | +2/3 e | c | $\Phi_c$ |
| anti-charm | ≈ 1280 | −2/3 e | c̄ | $\Phi_{\bar{c}}$ |
| strange | ≈ 96 | −1/3 e | s | $\Phi_s$ |
| anti-strange | ≈ 96 | +1/3 e | s̄ | $\Phi_{\bar{s}}$ |
| top | ≈ 173100 | +2/3 e | t | $\Phi_t$ |
| anti-top | ≈ 173100 | −2/3 e | t̄ | $\Phi_{\bar{t}}$ |
| bottom | ≈ 4180 | −1/3 e | b | $\Phi_b$ |
| anti-bottom | ≈ 4180 | +1/3 e | b̄ | $\Phi_{\bar{b}}$ |

## 4.2 Octon Structure of the Down Quark ($\Phi_d$)

Figure 5 shows the proposed 3D "Octon" (octahedral) structure for the down quark $\Phi_d$. Each of the eight tetrahedral sites is occupied by a gluon, itself a bound state of ≥ 137 axions. In octonion vector diagrams, sites 1–7 correspond to single axion addresses, while the special site 8 carries a dual axion node.

**Visualization of the Octon structure (Fig. 5):**

- The octahedron splits into two halves: addresses 1–4 (left) and 5–8 (right).
- Color vectors project along the ±X, ±Y, and ±Z directions. Z-axis vectors are denoted as "in" (⊗) or "out" (⊕).
- To render the full 3D structure, the right half (5–8) is shifted onto the left half (1–4).

**Charge assignment:**

Quark charges arise from the axion choices at the adjustable sites {A2, A8, A9, A10, A11, A12}. Stable quarks result when these combine as:

- Down quark (d): charge = (4e− from A2) + (0 from A8, A9) = −1/3 e
- Anti-down ($\bar{d}$): charge = (4e+ from A10) + (0 from A8, A9) = +1/3 e
- Up quark (u): charge = (2e+ from A9) + (6e+ from A9, A11) = +2/3 e
- Anti-up ($\bar{u}$): charge = (2e− from A8) + (6e− from A2, A12) = −2/3 e

**Special Address 2* and 8*:**

• Address 2* carries A2 in the down quark, or A9 in the up quark.

• Address 8* carries a dual axion pair (A8 + A9 for d; A10 + A11 for u).

• These star positions determine quark flavor and charge.

### Stability and Dynamics

• All 12 nearest-neighbor gluon pairs couple via strong three-color bonds: (1–4), (1–2), (2–3), (3–4), (5–8), (5–6), (6–7), (7–8), (1–5), (2–6), (3–7), (4–8).

• This complete coupling ensures maximal stabilization.

• Address 8* is asymmetric: dual axion ejection produces net forward propulsion and a likely counterclockwise spin, consistent with conservation of momentum and angular momentum.

Thus, the Octon structure of Φd both reproduces the correct −1/3 electric charge and exhibits a natural mechanism for quark stability, motion, and spin. Figure 5 illustrates the octonion vector diagram for this construction.

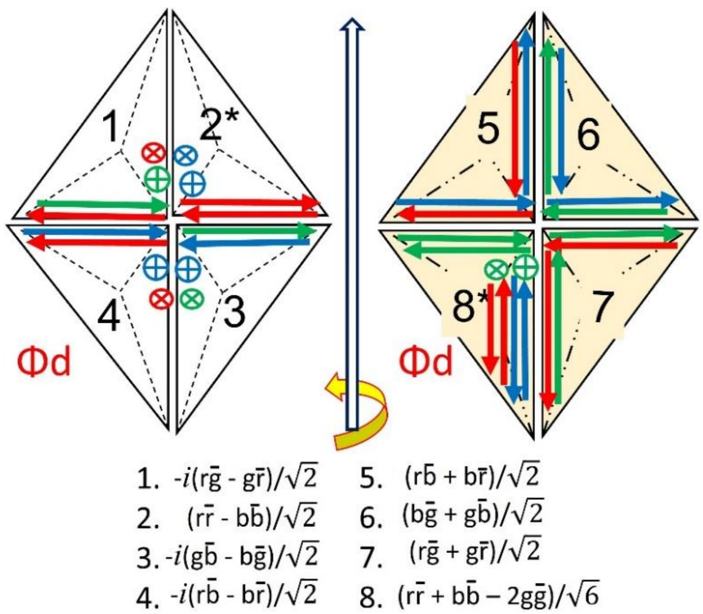


**Figure 5 shows the octonion vector diagram of 8 tetrahedrons that Octon down quark octahedron.** The octahedron is split into two halves (addresses 1–4 on the left, 5–8 on the right). Each tetrahedral address is labeled with its axion type(s). *Note that tetrahedrons gluon addresses 2* and 8* change axion type depending on the quark*. *For the down quark, tetrahedron gluon address 2* = A2 axions and 8* = A8 + A9 axions.* Given the known -1/3 charge for the down (d) quark, this Octon structure is a viable candidate for the down quark $\Phi_d$.

## 4.3 Octon Structure for the Up Octon Quark $\Phi_u$

Figure 6 shows a candidate octahedral ("Octon") structure for the up quark Φu, which carries charge +2/3 e. As with the down quark (Φd), the Octon comprises eight gluon sites, each built from ≥137 interpenetrating axions. The special sites 2* and 8* now host axion types A9 and A10 + A11, respectively, while the remaining six sites are unchanged from Φd.).

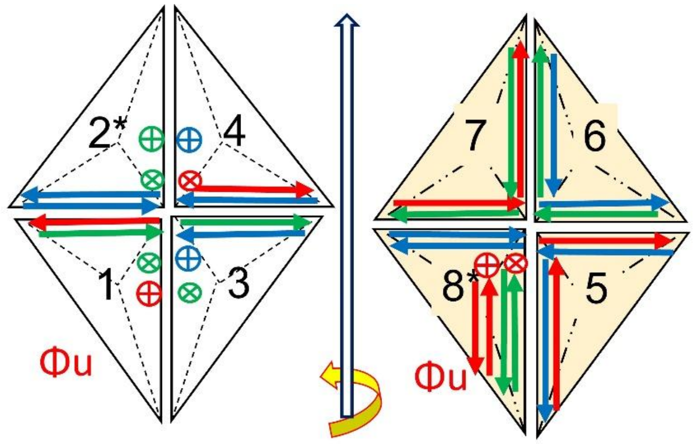


1. $-i(r\bar{g} - g\bar{r})/\sqrt{2}$
2. $(b\bar{b} - g\bar{g})/\sqrt{2}$
3. $-i(g\bar{b} - b\bar{g})/\sqrt{2}$
4. $-i(r\bar{b} - b\bar{r})/\sqrt{2}$
5. $(r\bar{b} + b\bar{r})/\sqrt{2}$
6. $(b\bar{g} + g\bar{b})/\sqrt{2}$
7. $(r\bar{g} + g\bar{r})/\sqrt{2}$
8. $(b\bar{b} + g\bar{g} - 2\bar{r}r)/\sqrt{6}$

**Figure 6. Octonion vector diagram of the up quark** has an independent gluon octet. Tetrahedron gluon addresses 2* and 8* change axion type depending on the quark. For the up quark, tetrahedron gluon address 2* = A9 and 8* = A10 + A11. The Octon has a net charge of +2/3 volt (see section 4.22), which makes it a viable candidate for the up quark Φu.

This minimal reassignment of two axion addresses explains the close kinship between u and d quarks: both retain complete 3-color strong coupling at all twelve gluon–gluon bonds, ensuring maximal stability. The structural asymmetry at address 8* again drives both propulsion and spin, mirroring the mechanism proposed for Φd.

Because u and d differ only in axion assignments at 2* and 8*, they are the lightest and most stable quark flavors. Together they form the proton (*u d u*) and, when bound in atomic nuclei, the neutron (*d u d*).

## 4.4 Octon structures for the anti-down ($\Phi\bar{d}$) and anti-up ($\Phi\bar{u}$)

Figures 7 and 8 show the corresponding antiparticles of Φd and Φu. Their Octon geometries remain identical; only the axion assignments at 2* and/or 8* are altered, flipping the sign of electric charge.

- **Anti-down ($\Phi\bar{d}$):**
  Address 2* changes to A10, while 8* remains A8 + A9. This yields charge +1/3 e. All twelve gluon–gluon pairs remain strongly coupled, preserving structural stability.
- **Anti-up ($\Phi\bar{u}$):**
  Both special sites change (2* = A8, 8* = A2 + A12), giving charge −2/3 e. As with Φu, all twelve bonds are stabilized by 3-color couplings.

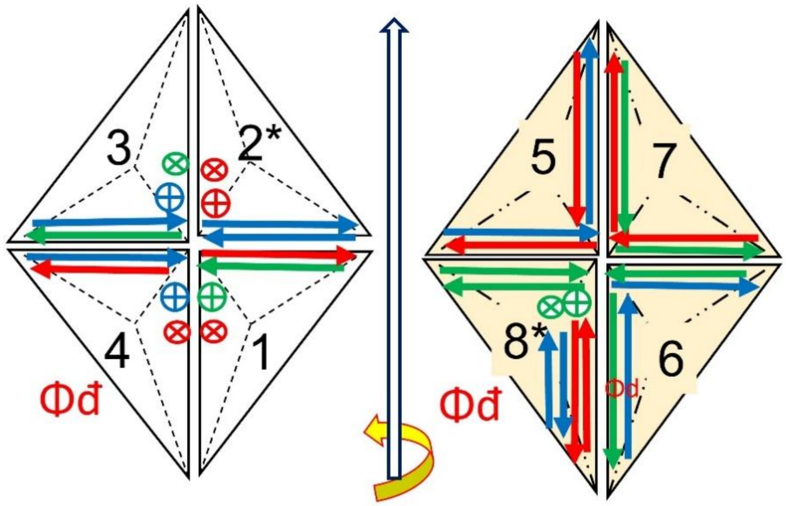


1. $-i(r\bar{g} - g\bar{r})/\sqrt{2}$
2. $(b\bar{b} - r\bar{r})/\sqrt{2}$
3. $-i(g\bar{b} - b\bar{g})/\sqrt{2}$
4. $-i(r\bar{b} - b\bar{r})/\sqrt{2}$
5. $(r\bar{b} + b\bar{r})/\sqrt{2}$
6. $(b\bar{g} + g\bar{b})/\sqrt{2}$
7. $(r\bar{g} + g\bar{r})/\sqrt{2}$
8. $(r\bar{r} + b\bar{b} - 2g\bar{g})/\sqrt{6}$

**Figure 7. Octonion vector diagram of the anti-down quark**. Only 2* gluon in the gluon octet is changed (2* = A10), while (8* = A8 + A9) remains the same compared to the down quark. Octon structural stability has 3-color strong coupling constants at all the 12 gluon pairings (4-3), (3-2), (2-1), (1-4), (8-5), (5-7), (7-6), (6-8), (5-3), (7-2), (8-4), (6-1). The anti-down Octon has a net charge of +1/3 e.

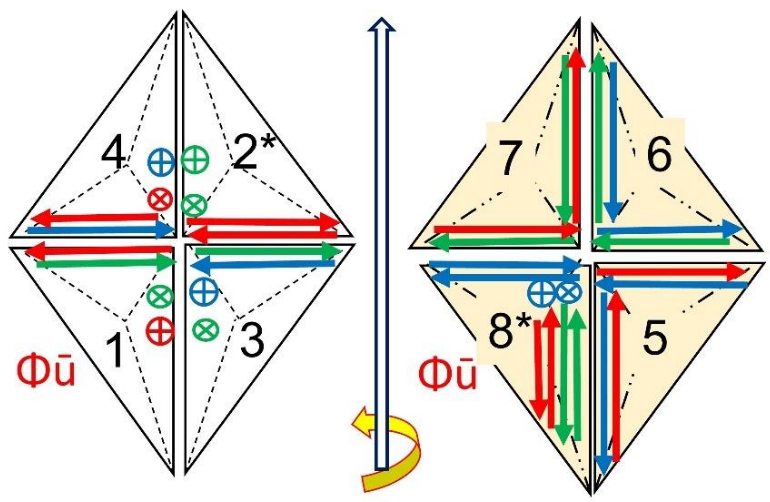


1. $-i(r\bar{g} - g\bar{r})/\sqrt{2}$
2. $(r\bar{r} - g\bar{g})/\sqrt{2}$
3. $-i(g\bar{b} - b\bar{g})/\sqrt{2}$
4. $-i(r\bar{b} - b\bar{r})/\sqrt{2}$
5. $(r\bar{b} + b\bar{r})/\sqrt{2}$
6. $(b\bar{g} + g\bar{b})/\sqrt{2}$
7. $(r\bar{g} + g\bar{r})/\sqrt{2}$
8. $(r\bar{r} + g\bar{g} - 2b\bar{b})/\sqrt{6}$

**Figure 8. Octonion vector diagram of the anti-up quark.** Both 2* and 8* gluons in the gluon octet are changed (2* = A8 and 8* = A2 + A12). The net effect on Octon structural stability is the same with 3-color strong coupling constants to stabilize the gluon generated Octon structure at all possible 12 gluon pairs (1-4), (4-2), (2-3), (3-1), (8-7), (7-6), (6-5), (5-8), (4-7), (2-6), (1-8), (3-5). The anti-up Octon has a net charge of -2/3 e.

Thus, $\Phi\bar{d}$ and $\Phi\bar{u}$ are as stable as their particle counterparts. These four configurations ($\Phi$d, $\Phi$u, $\Phi\bar{d}$, $\Phi\bar{u}$) exhaust the possible independent 8-gluon octets with full 3-color stabilization. Additional quark flavors must therefore emerge from perturbations of these core octets.

## 4.5 Second-Generation Quarks: Strange and Charm

The strange (s) and charm (c) quarks arise as minimal perturbations of the stable Φd and Φu structures. Because no new independent gluon-octets are available, the Triad Model determines that the **least disruptive** way to produce the second-generation flavors is by a single pairwise swap of gluon sites within the existing Octon geometry.

- **Strange (Φs) Fig 9:**

  Derived from Φd by *swapping gluons at addresses 5 and 6*. Eleven of twelve bonds remain strongly coupled; only the (2–5) pairing weakens to a 2-color bond. The net charge remains −1/3 e, identical to Φd.

- **Charm (Φc) Fig 10:**

  Derived from Φu by *swapping sites 6 and 7*. Again, eleven strong couplings persist, with a single weakened bond between addresses 2 and 6. The net charge remains +2/3 e, identical to Φu.

These "single-swap" modifications reduce structural stability, consistent with the higher masses and shorter lifetimes of s and c quarks relative to their first-generation counterparts.

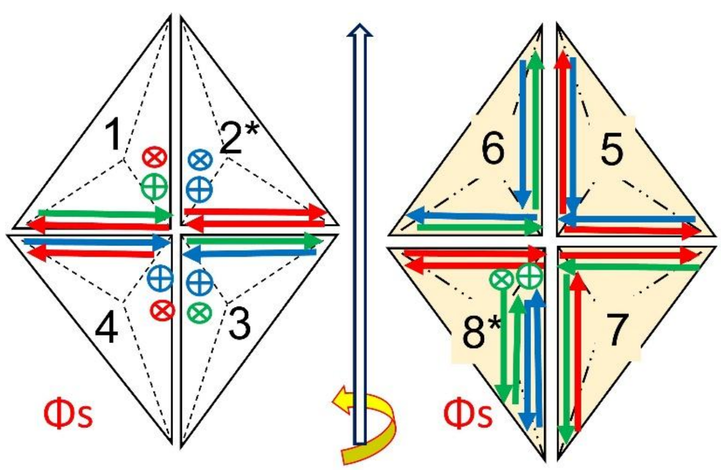


1. $-i(r\bar{g} - g\bar{r})/\sqrt{2}$
2. $(r\bar{r} - b\bar{b})/\sqrt{2}$
3. $-i(g\bar{b} - b\bar{g})/\sqrt{2}$
4. $-i(r\bar{b} - b\bar{r})/\sqrt{2}$
5. $(r\bar{b} + b\bar{r})/\sqrt{2}$
6. $(b\bar{g} + g\bar{b})/\sqrt{2}$
7. $(r\bar{g} + g\bar{r})/\sqrt{2}$
8. $(r\bar{r} + b\bar{b} - 2g\bar{g})/\sqrt{6}$

**Figure 9. Octonion vector diagram of the strange (s) quark** using the same independent gluon octet used for the down quark (Fig 5). Swap gluons at addresses 5 and 6. The only broken strong-coupling bond is now between that new #5 and #2 pair: addresses 2 and 5 share only a weak 2-color bond. All other gluon assignments remain identical except for the weak 2-color coupling at the coupling of #2 with #5 gluons (1-4), (1-2), (2-3), (3-4), (8-6), (6-5), (5-7), (7-8), (1-6), (~~2-5~~), (4-8), (3-7). The strange quark Octon has the same net charge of -1/3 e as the down quark, as its axions are identical.

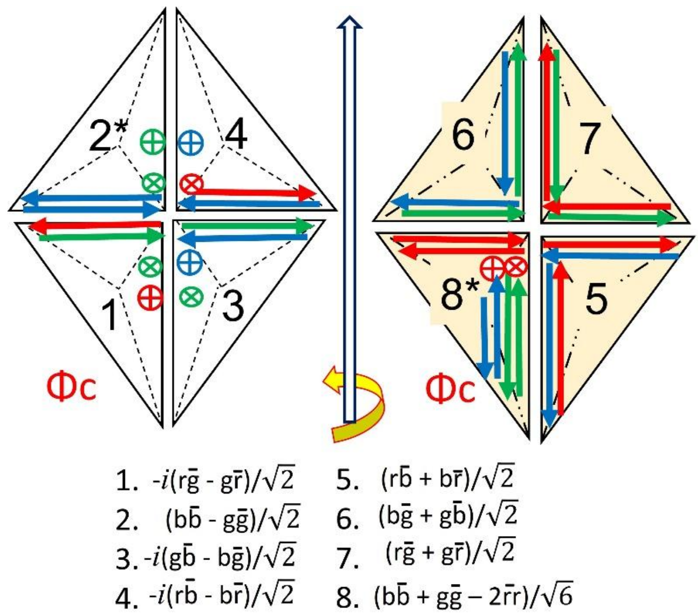


**Figure 10. Octonion vector diagrams of the charm (c) quark**. Using the gluon octet in the up quark (Fig 6), the Octon charm quark structure is generated by a simple switch in position of the #6 gluon with the #7 gluon within the 8 Octon slots. The charm quark Octon has 11 of 12 possible gluon pairs (1-2), (2-4), (4-3), (3-1), (6-7), (7-5), (5-8), (8-6), (~~2-6)~~, (4-6), (1-8), (3-5) that have 3-color strong coupling constants to stabilize the gluon generated Octon quark structure but includes one weak coupling between the #2 and #6 gluons. The charm Octon has a net charge of +2/3 e like the up quark, as its axions are identical.

**Methodological Note**

In the Triad Model, second-generation quarks arise from the most economical modification of stable first-generation octets. A single gluon swap preserves 11 of 12 strong couplings, with one bond downgraded to a weaker 2-color interaction. This rule explains both the reduced stability of s and c quarks and their retention of the same fractional charges as d and u, respectively.

---

## 4.6 Lagrangian → Hamiltonian Descriptions for Strange and Charm Quarks

The lattice-oscillator framework of §3.6–3.7 extends to second-generation quarks. Both strange (s) and charm (c) are modeled as perturbed nine-site octahedra; destabilization is encoded via quadratic number-operator penalties. Throughout, $\widehat{N}_i = \hat{a}_i^{\dagger}\hat{a}_i$ .

### 1. Strange-quark ($\Phi_s$)

Starting from the down quark lattice, swapping gluon sites 5 ↔ 6 introduces a weak two-color bond between sites 2 and 5. The effective Lagrangian is:

$$\mathcal{L}_s = \sum_{i=1}^{9}\left[ \frac{1}{2}\dot{\phi}_i^{\,2} - \frac{1}{2}|\nabla\phi_i|^2 - \frac{1}{2}\omega^2\phi_i^2 \right]$$

$$-\left[ \alpha\hbar\omega\sum_{i=1}^{9}\widehat{N}_i + \epsilon_s\,(\widehat{N}_2 - \widehat{N}_5)^2 \right] - \frac{1}{\alpha} f_s(t)\,\widehat{D}_s \qquad (26L)$$

**(A) Canonical field Hamiltonian** (from the Lagrangian via Legendre transform; includes kinetic, spatial, and on-site terms). Conjugate momenta are $\pi_i = \dot{\phi}_I$. The Hamiltonian becomes:

$$\hat{H}_s(t) = \sum_{i=1}^{9}\left[ \frac{1}{2}\hat{\pi}_i^{\,2} + \frac{1}{2}|\nabla\hat{\phi}_i|^2 + \frac{1}{2}\omega^2\hat{\phi}_i^{\,2} \right] + \alpha\hbar\omega\sum_{i=1}^{9}\widehat{N}_i$$

$$+\,\epsilon_s\,(\widehat{N}_2 - \widehat{N}_5)^2 + \frac{1}{\alpha} f_s(t)\,\widehat{D}_s \qquad (26H)$$

(On the discrete nine-site lattice, replace $|\nabla\hat{\phi}_i|^2$ by $\frac{1}{2}\sum_{\langle i,j\rangle}\boldsymbol{K}_{ij}(\hat{\phi}_i - \hat{\phi}_j)^2$, with $K_{ij}=K_{ji}>0$ for nearest neighbors and zero otherwise; the factor $\frac{1}{2}$ avoids double counting of bonds $\langle i, j\rangle$.)

**(B) Mode-reduced number-operator Hamiltonian** (effective, after projecting onto on-site normal modes and absorbing the lattice couplings into a renormalized $\overline{\omega}$; off-diagonal hopping and constants suppressed).

$$\hat{H}_s^{eff} = \alpha\hbar\overline{\omega}\sum_{i=1}^{9}\widehat{N}_i + \epsilon_s\,(\widehat{N}_2 - \widehat{N}_5)^2 + \frac{1}{\alpha} f_s(t)\,\widehat{D}_s \qquad (27Hm)$$

with $\overline{\omega}_s$ the **renormalized on-site frequency** after integrating out gradient/bond terms to leading order and dropping additive constants (e.g. $\sum_i \frac{1}{2}\hbar\overline{\omega}$). The perturbative term $\Delta\hat{H}_s = \epsilon_s\,(\widehat{N}_2 - \widehat{N}_5)^2$ encodes the loss of one strong 3-color bond.

**2. Charm Quark ($\Phi_c$)**

Relative to the up quark, swapping sites 6 ↔ 7 introduces a weak bond between sites 2 and 6. The effective Lagrangian is

$$\mathcal{L}_c = \sum_{i=1}^{9}\left[ \frac{1}{2}\dot{\phi}_i^{\,2} - \frac{1}{2}|\nabla\phi_i|^2 - \frac{1}{2}\omega^2\phi_i^2 \right]$$

$$-\left[ \alpha\hbar\omega\sum_{i=1}^{9}\widehat{N}_i + \epsilon_c\,(\widehat{N}_2 - \widehat{N}_6)^2 \right] - \frac{1}{\alpha} f_c(t)\,\widehat{D}_c \qquad (28L)$$

The **Mode-reduced number-operator Hamiltonian** is

$$\hat{H}_c(t) = \alpha\hbar\overline{\omega}\sum_{i=1}^{9}\widehat{N}_i + \epsilon_c\,(\widehat{N}_2 - \widehat{N}_6)^2 + \frac{1}{\alpha} f_c(t)\,\widehat{D}_c \qquad (28Hm)$$

$\overline{\omega}_c$ is a flavor-dependent renormalized on-site frequency; $\varepsilon_c$ encodes the weak-bond penalty from the specific gluon swap; $f_q(t)\,\widehat{D}_q$ is the same drive operator form as in §3.7. The perturbation $\Delta\hat{H}c = \varepsilon_c\,(\hat{N}_2 - \hat{N}_6)^2$ reflects a single weak bond. The corresponding stabilization energy is ~ 695 × larger than for Φu, accounting for the charm quark's much higher mass.

**3. General Framework**

For any higher-generation quark q ∈ {s, c, b, t } , the additional mass contribution is represented by a quadratic penalty term:

$$\Delta\hat{H}_q = \varepsilon_q\,(\hat{N}_i - \hat{N}_j)^2,$$

applied to the base Hamiltonian of §3.7. This compact prescription preserves the SU(3) ladder structure while distinguishing flavors by their weak-bond asymmetries.

## 4.7 Bottom and Top Quarks: Loss of Strong-Coupling Sites

The third generation of quarks—the bottom (b) and top (t)—arise within the Triad Model through the same *minimal-swap principle* applied in §4.5–4.6. Each structure derives from its first-generation analog (down or up) but with additional gluon rearrangements that progressively weaken color couplings.

**Bottom Quark (Φb):**

As shown in Fig. 11, Φb is obtained by swapping gluons #6 and #7 in the down-quark Octon. The resulting structure preserves 11 of the 12 original three-color couplings, with only the (3–6) bond reduced to a weaker two-color interaction. This introduces a measurable destabilization while maintaining the overall quark topology.

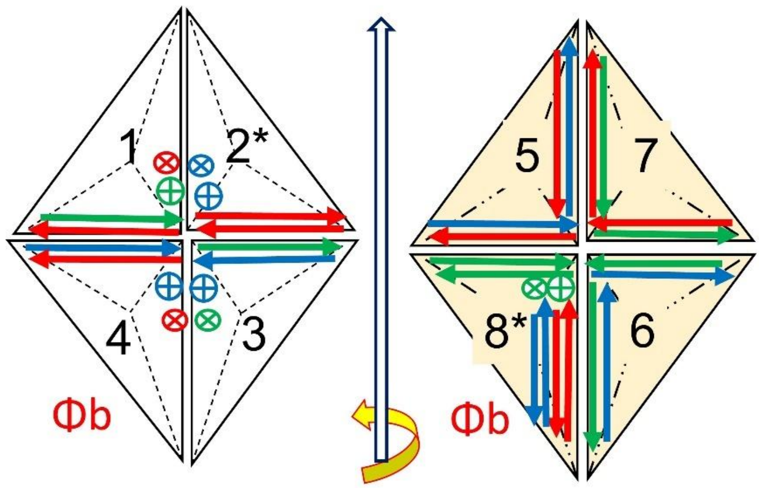


1. $-i(r\bar{g} - g\bar{r})/\sqrt{2}$
2. $(r\bar{r} - b\bar{b})/\sqrt{2}$
3. $-i(g\bar{b} - b\bar{g})/\sqrt{2}$
4. $-i(r\bar{b} - b\bar{r})/\sqrt{2}$
5. $(r\bar{b} + b\bar{r})/\sqrt{2}$
6. $(b\bar{g} + g\bar{b})/\sqrt{2}$
7. $(r\bar{g} + g\bar{r})/\sqrt{2}$
8. $(r\bar{r} + b\bar{b} - 2g\bar{g})/\sqrt{6}$

**Figure 11. Octonion vector diagrams of the bottom (b) quark** using the same independent gluon octet used for the down quark**.** The bottom quark Octon structure is generated by a simple switch in position of the #6 gluon with the #7 gluon within the Octon. The bottom quark Octon has 11 of 12 possible gluon pairs (4-1), (1-2), (2-3), (3-4), (8-5), (5-7), (7-6), (6-8~~)~~, (1-5), (2-7), (4-8), (~~3-6)~~ that have 3-color strong coupling constants to stabilize the gluon generated Octon quark structure. One gluon coupling at site (3-6) has weak 2 color couplings.

**Top Quark (Φt):**

As shown in Fig. 12, Φt arises by swapping gluons #5 and #6 in the up-quark Octon. This modification creates *two* weak two-color bonds—between (4–5) and (3–6)—leaving only 10 strong couplings intact. Consequently, Φt is the most destabilized and energetically demanding of all six flavors.

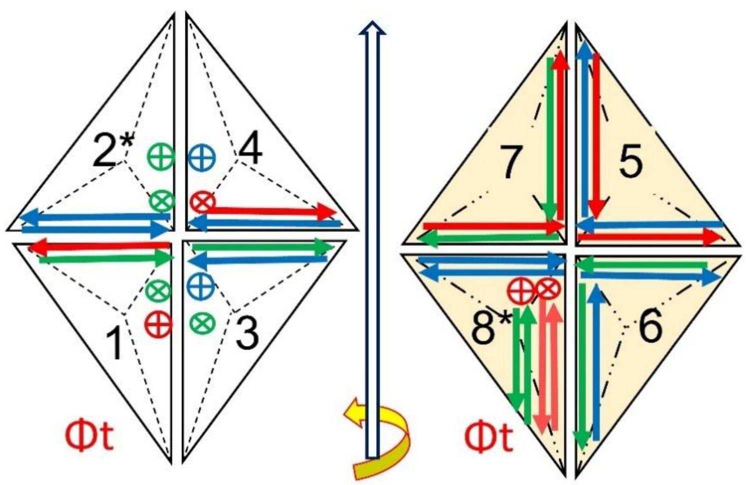


1. $-i(r\bar{g} - g\bar{r})/\sqrt{2}$
2. $(b\bar{b} - g\bar{g})/\sqrt{2}$
3. $-i(g\bar{b} - b\bar{g})/\sqrt{2}$
4. $-i(r\bar{b} - b\bar{r})/\sqrt{2}$
5. $(r\bar{b} + b\bar{r})/\sqrt{2}$
6. $(b\bar{g} + g\bar{b})/\sqrt{2}$
7. $(r\bar{g} + g\bar{r})/\sqrt{2}$
8. $(b\bar{b} + g\bar{g} - 2\bar{r}r)/\sqrt{6}$

**Figure 12. Octonion vector diagrams of the Top (t) quark** using the same gluon octet in the up quark**.** The top quark Octon structure is generated by a simple switch in position of the #5 gluon with the #6 gluon within the 8 Octon slots. The top quark Octon has 10 of 12 strong 3-color coupling constants at the same gluon pairs (1-2), (2-4), (4-3), (3-1), (8-7), (7-5), (5-6), (6-8), (2-7), (~~4-5)~~, (1-8), (~~3-6~~), but has 2 weak gluon coupling sites at 4-5 and 3-6.

The pattern is consistent with observed quark masses:

- First generation: u ≈ 2.2 MeV, d ≈ 4.7 MeV
- Second generation: s ≈ 96 MeV, c ≈ 1280 MeV
- Third generation: b ≈ 4180 MeV, t ≈ 173,100 MeV

Thus, the progressive loss of strong bonds (0 → 1 → 2) correlates directly with the steep rise in mass and the decreasing stability of higher-generation quarks. The extraordinary mass of Φt reflects the vast number of additional axions required to offset two weakened bonds.

## 4.8 Lagrangian → Hamiltonian Descriptions for Bottom and Top Quarks

The third-generation quarks (bottom b and top t) are modeled as minimal-swap perturbations of the first-generation down and up octets, respectively. As in §4.6, we use a nine-site oscillator lattice with one (bottom) or two (top) weak two-color bonds encoded by quadratic number-operator penalties. Throughout, $\widehat{N}_I = \hat{a}_i^{\dagger}\hat{a}_i$ .

---

**Bottom Quark Φ*b*– Perturbation of Φ*d***

Swapping gluons #6 and #7 (relative to Φd ) weakens the (3-6) bond. The Lagrangian and Hamiltonian of Φb are

$$\mathcal{L}_{\mathrm{b}} = \sum_{i=1}^{9}\left[\, \tfrac{1}{2}\dot{\phi}_i^{\,2} - \tfrac{1}{2}|\nabla\phi_i|^2 - \tfrac{1}{2}\omega^2\phi_i^2 \,\right]$$

$$-\left[\, \alpha\hbar\omega\sum_{i=1}^{9}\widehat{N}_i + \epsilon_{\mathrm{b}}\,(\widehat{N}_3 - \widehat{N}_6)^2 \,\right] - \frac{1}{\alpha} f_{\mathrm{b}}(t)\,\widehat{D}_{\mathrm{b}}$$

Conjugate momenta are $\pi_i = \dot{\phi}_I$. The **Mode-reduced number-operator Hamiltonian** becomes:

$$\hat{H}_{\mathrm{b}}(t) = \alpha\hbar\overline{\omega}\sum_{i=1}^{9}\widehat{N}_i + \epsilon_{\mathrm{b}}\,(\widehat{N}_3 - \widehat{N}_6)^2 + \frac{1}{\alpha} f_{\mathrm{b}}(t)\,\widehat{D}_{\mathrm{b}}$$

$\overline{\omega}_b$ is a flavor-dependent renormalized on-site frequency; $\varepsilon_b$ encodes the weak-bond penalty from the specific gluon swap. Choosing $\varepsilon_b$ to match phenomenology yields $E_{b,static} \approx 890\, E_{d,static}$ . The electric charge remains −1/3 e.

**Top Quark Φt: perturbation of Φu**

Swapping gluons #5 and #6 (relative to Φu) weakens two bonds, (4-5) and (3-6). The Lagrangian and Hamiltonian of Φt are:

$$\mathcal{L}_t = \sum_{i=1}^{9}\left[ \frac{1}{2}\dot{\phi}_i^{\,2} - \frac{1}{2}|\nabla\phi_i|^2 - \frac{1}{2}\omega^2\,\phi_i^2 \right]$$

$$-\left[ \alpha\hbar\omega \sum_{i=1}^{9}\hat{N}_i + \epsilon_t\left((\hat{N}_4 - \hat{N}_5)^2 + \epsilon_t\,(\hat{N}_3 - \hat{N}_6)^2\right)\right] - \frac{1}{\alpha} f_t(t)\,\hat{D}_t$$

The **Mode-reduced number-operator Hamiltonian** is

$$\hat{H}_t(t) = \alpha\hbar\overline{\omega} \sum_{i=1}^{9}\hat{N}_i + \epsilon_t\left((\hat{N}_4 - \hat{N}_5)^2 + \epsilon_t\,(\hat{N}_3 - \hat{N}_6)^2\right) + \frac{1}{\alpha} f_t(t)\,\hat{D}_t$$

$\overline{\omega}_t$ is a flavor-dependent renormalized on-site frequency; $\varepsilon_t$ encodes the weak-bond penalty from the specific gluon swaps. Calibrating $\boldsymbol{\varepsilon_t}$ gives $E_{t,static} \approx 7.99 \times 10^4\, E_{t,static}$, reflecting two weakened bonds and the top's extreme mass. The electric charge remains +2/3 e.

**Methodological Note — Calibration of $\boldsymbol{\varepsilon_b}$ *and* $\boldsymbol{\varepsilon_t}$**

$\boldsymbol{\varepsilon_b}$ ***and*** $\boldsymbol{\varepsilon_t}$ are effective penalty coefficients that encode weak-bond asymmetries introduced by the swaps. They are not free in principle: once a microscopic map between bond strength and $(\hat{N}_i - \hat{N}_j)^2$ is specified, $\varepsilon_q$ follows. Here we set them phenomenologically to reproduce the observed stabilization-energy (mass) hierarchy while keeping the operator structure identical to §4.6.

## 4.9 Octon Quark Structures Explain the Three Generations

**Claim.** In the Triad Model, the observed three generations of up/down–type quarks arise from a single structural rule: start from the two fully stabilized first-generation octets (Φd, Φu) and introduce **minimal gluon swaps** that convert one or two 3-color bonds into weaker 2-color bonds. The number of weakened bonds correlates with increased stabilization energy (mass) and reduced lifetime.

### (i) First generation (d, u): fully saturated strong-coupling topology

- Φd and Φu have **all 12** neighbor pairs in **3-color strong coupling** (no weak bonds).
- Static Hamiltonian contains only the base term $\alpha\hbar\omega\,\Sigma_i\,\hat{N}_i$ (cf. §3.7, §4.6).
- Result: **lightest masses, longest lifetimes** (d ≈ 4.7 MeV, u ≈ 2.2 MeV).

### (ii) Second generation (s, c): one weakened bond via a single swap

• $\Phi$s (from $\Phi$d) and $\Phi$c (from $\Phi$u) each lose exactly one 3-color bond, replaced by a 2-color bond.

• Perturbation: $\Delta\hat{H}_q = \varepsilon_q\,(\hat{N}_i - \hat{N}_j)^2$ added to the base Hamiltonian (Eqs. (26)–(28)).

• Result: heavier, shorter-lived: s ≈ 96 MeV, c ≈ 1280 MeV.

### (iii) Third generation (b, t): one vs. two weakened bonds

• $\Phi$b (from $\Phi$d): one weak bond (different pair than s) → $E_{b,static}$ } ≈ 890 × $E_{d,static}$ .

• $\Phi$t (from $\Phi$u): two weak bonds → $E_{t,static} \approx 7.99 \times 10^4 \times E_{u,static}$ .

• Result: much heavier, least stable, with t the most destabilized (b ≈ 4180 MeV, t ≈ 173 100 MeV).

**Compact summary (model-level, approximate):**

| Generation | Quark | Weak bonds | ΔĤ (perturbation) | Relative stabilization energy | Charge |
|---|---|---|---|---|---|
| 1st | d | 0 | – | baseline $\propto \Sigma\,\hat{N}_i$ | −1/3 e |
| 1st | u | 0 | – | baseline $\propto \Sigma\,\hat{N}_i$ | +2/3 e |
| 2nd | s (from d) | 1 | $\varepsilon_s\,(\hat{N}_5 - \hat{N}_6)^2$ | ≈ 19.8 × Ed | −1/3 e |
| 2nd | c (from u) | 1 | $\varepsilon_c\,(\hat{N}_2 - \hat{N}_6)^2$ | ≈ 6.95 × $10^2$ × Eu | +2/3 e |
| 3rd | b (from d) | 1 | $\varepsilon_b\,(\hat{N}_3 - \hat{N}_6)^2$ | ≈ 8.90 × $10^2$ × Ed | −1/3 e |
| 3rd | t (from u) | 2 | $\varepsilon_t\,[\,(\hat{N}_4 - \hat{N}_5)^2 + (\hat{N}_3 - \hat{N}_6)^2\,]$ | ≈ 7.99 × $10^4$ × Eu | +2/3 e |

*($\epsilon_q$ are effective penalties calibrated to the observed hierarchy)*

## Why exactly three generations?

• **Finite octet basis**. The model admits four independent 8-gluon octets ($\Phi$d, $\Phi$u, $\Phi\bar{d}$, $\Phi\bar{u}$).

• **Flavor construction rule**. All quark flavors (and antiquarks) arise by **rearrangements** within these fixed octets; no additional independent octet exists to seed a fourth generation.

• **Prediction**. The spectrum closes with the six quarks (and six antiquarks). A fourth generation would require a new independent octet beyond the model's construction.

**Quantum-mechanical consistency**

• **Hermitian, bounded Hamiltonians**. The static $\hat{H}_0 = \alpha\hbar\omega\, \Sigma_i\, \hat{N}_i$ and perturbations $\Delta\hat{H} = \varepsilon_q$ $(\hat{N}_i - \hat{N}_j)^2$ are **Hermitian** and **bounded below**, yielding a well-defined, discrete spectrum.

• **Perturbation theory intuition**. Each weakened bond raises the ground-state energy; **more** weakened bonds ⇒ **larger** mass shift, matching the observed hierarchy.

• **Dynamics and coherence**. The drive term $\alpha^{-1}$ $f(t)\, \hat{D}$ enables coherent axion-flux processes (cf. §3.6–§3.7) without altering the flavor-counting logic above.

**Summary**

The Triad Model's Octon-plus-perturbation framework explains **why three generations exist** and **why their masses/lifetimes scale as observed**: the generational ladder tracks the **count and placement of weakened color bonds** within a finite set of gluon octets. This yields a discrete, closed flavor spectrum with testable stabilization-energy ratios tied to specific bond rearrangements.

## 5.0 Gluons also generate strong force flux-tube substructures

In QCD, pulling quarks apart collimates color fields into string-like **flux tubes** (linear potential $V(R) \sim \sigma\, R$). In the Triad Model, the same eight-gluon octets that self-assemble into Octon quarks can reconfigure into extended, electrically neutral **Gluet** modules that tile into flux tubes. Concretely:

• A **Gluet** is a neutral **16-gluon** repeat unit formed by pairing a quark-type gluon octet with its conjugate octet:

– down-type: $G_d - G_{\bar{d}}$

– up-type: $G_u - G_{\bar{u}}$

• Each internal gluon–gluon contact remains **a perfect 3-color coupling**, making the module both axially stiff and hard to compress—exactly the traits needed for confinement.

• Coarse-graining the lattice Hamiltonian (§3.6–3.7) over one neutral module of axial length $\ell_{sub}$ defines an **effective string tension**:

$$\sigma_{eff} \equiv E_{sub} / \ell_{sub}$$

where $E_{sub}$ is the static energy of a neutral Gluet. Long tubes are then modeled by $V(R) \approx \sigma_{eff} R + V_0$, consistent with linear confinement.

**Methodological Note — QCD strings vs. Gluets.**
QCD treats flux tubes as field configurations of the gluon field; the Triad Model furnishes a microscopic, SU(3)-consistent tiling by neutral 16-gluon modules. In the long-wavelength limit the two views coincide (same linear potential), while at short scales the Triad construction predicts discrete vibrational/torsional modes tied to the module.

## 5.1 From Down/anti-down Octets → Down-Type Gluet ($Gd$-$G\bar{d}$)

**Construction.** Pair the down-type gluon octet $Gd$ with the anti-down octet $G\bar{d}$ to make a neutral 16-gluon unit. Because all internal bonds are 3-color couplings, the unit is **maximally rigid**.

**Geometry & twist.** Addresses 1–4 carry secondary color vectors on the $\hat{z}$ axis; concatenating modules with consistent address alignment naturally yields a **gentle tetrahedral helix** (a geometric twist) without breaking color symmetry.

**Tiling.** The neutral repeat unit can start/end on either end-address pair (Fig. 13) that preserves 3-color matching (e.g., start at #4 on $Gd$ end at #3 on $G\bar{d}$; **or** start at #1 on $Gd$, end at #4 on $G\bar{d}$). Repeating the unit produces long flux tubes suitable for d-type attachments. The individual $Gd$ and $G\bar{d}$ octets inherit the down/anti-down charge assignments within the Triad axion framework, but the **paired Gluet unit is *neutral***.

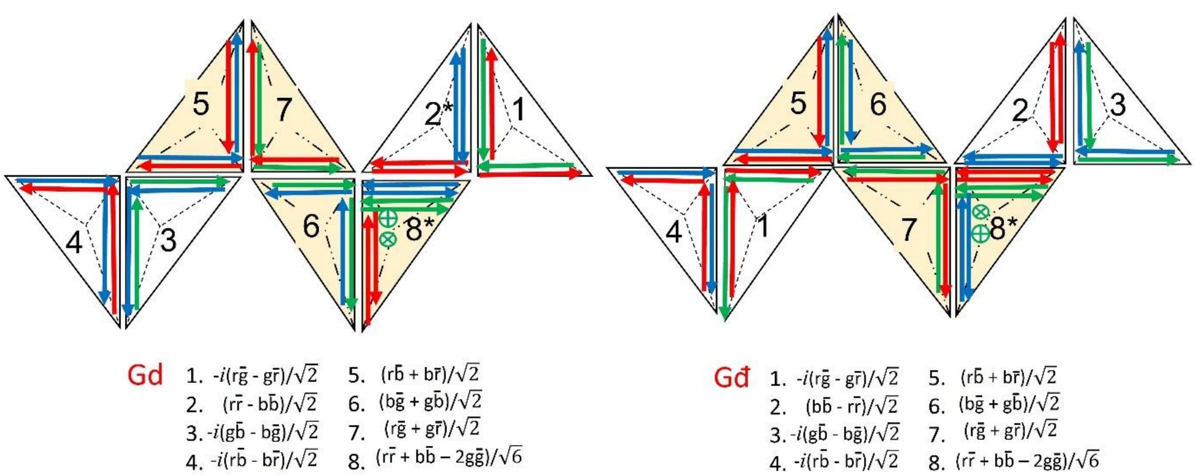


**Figure 13. The Gluet octonion vector diagrams for the down (Gd) and anti-down ($G\bar{d}$) gluon octets.** All the gluon subunits are bound together by perfect 3 color strong coupling to form the zig-zag shown (starts at #4 on $Gd$ end at #3 on $G\bar{d}$; or start at #1 on $Gd$, end at #4 on $G\bar{d}$).

## 5.2 From anti-up/up octets → up-type Gluet $G_{\bar{u}} - G_u$

**Construction**. Analogous to §5.1, pair $G_{\bar{u}} - G_u$ to yield a neutral 16-gluon $G_{\bar{u}} - G_u$ module.

**Charge & neutrality**. The isolated $G_{\bar{u}}$ (−2/3 e) and $G_u$ (+2/3 e) cancel in the paired module, making it the **preferred** repeat unit for up-type tubes.

**End-address order.** The permissible start/end addresses contain two options (e.g., Start at #1 on $G_{\bar{u}}$, end at #4 on $G_u$, **or** start at #3 on $G_{\bar{u}}$, end at #1 on $G_u$). This preserves 3-color matching and supports long, uncharged tubes for u-type attachments.

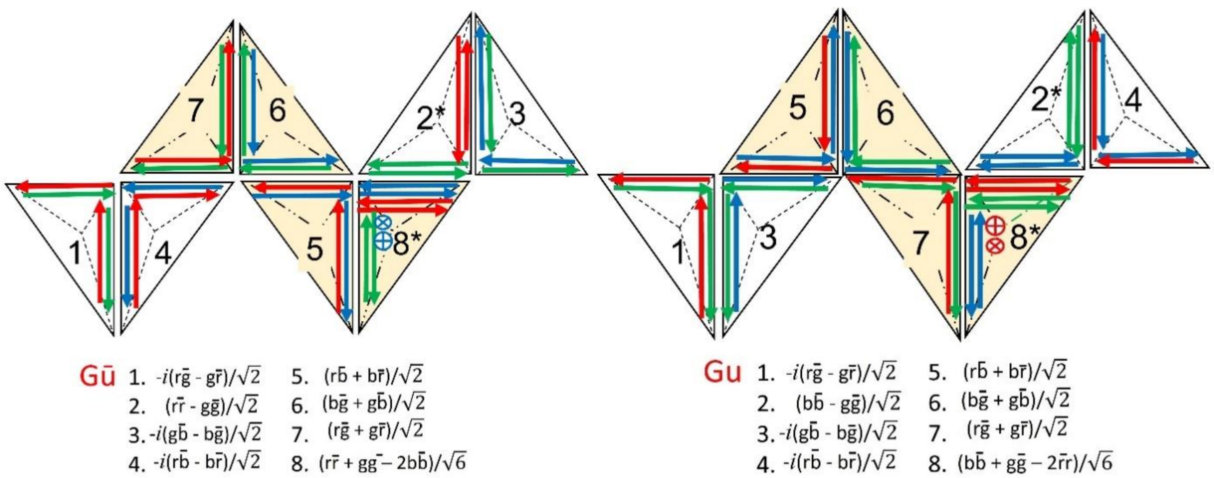


**Figure 14. The Gluet octonion vector diagrams for the anti-up (Gū) and up (Gu) gluon octets.** Start at #1 on $G_{\bar{u}}$, end at #4 on $G_u$, **or** start at #3 on $G_{\bar{u}}$, end at #1 on $G_u$

## 5.3 Coupling of Gluet Flux Tubes to the Octon Quarks

**Figure 15 (see below). Gluet coupling to Octon quarks.** These Gluet structures use the 4 to 1 $G_d$ - $G_{\bar{d}}$ Gluet to bind to the #1 gluon in the down Octon quark and the 1 to 4 $G_{\bar{u}} - G_u$ Gluet to bind at 90 degrees angle to the #4 gluon in the same down Octon Quark. The Gluets ae likely to extend for over 100 Gluet modules to end up coupling to two more up or down Octon Quarks.

**Port-matching rule.** Each Octon quark exposes **addressed ports** (the eight gluon sites). A Gluet module connects by **like-to-like address interpenetration** at the endpoints, ensuring 3-color continuity:

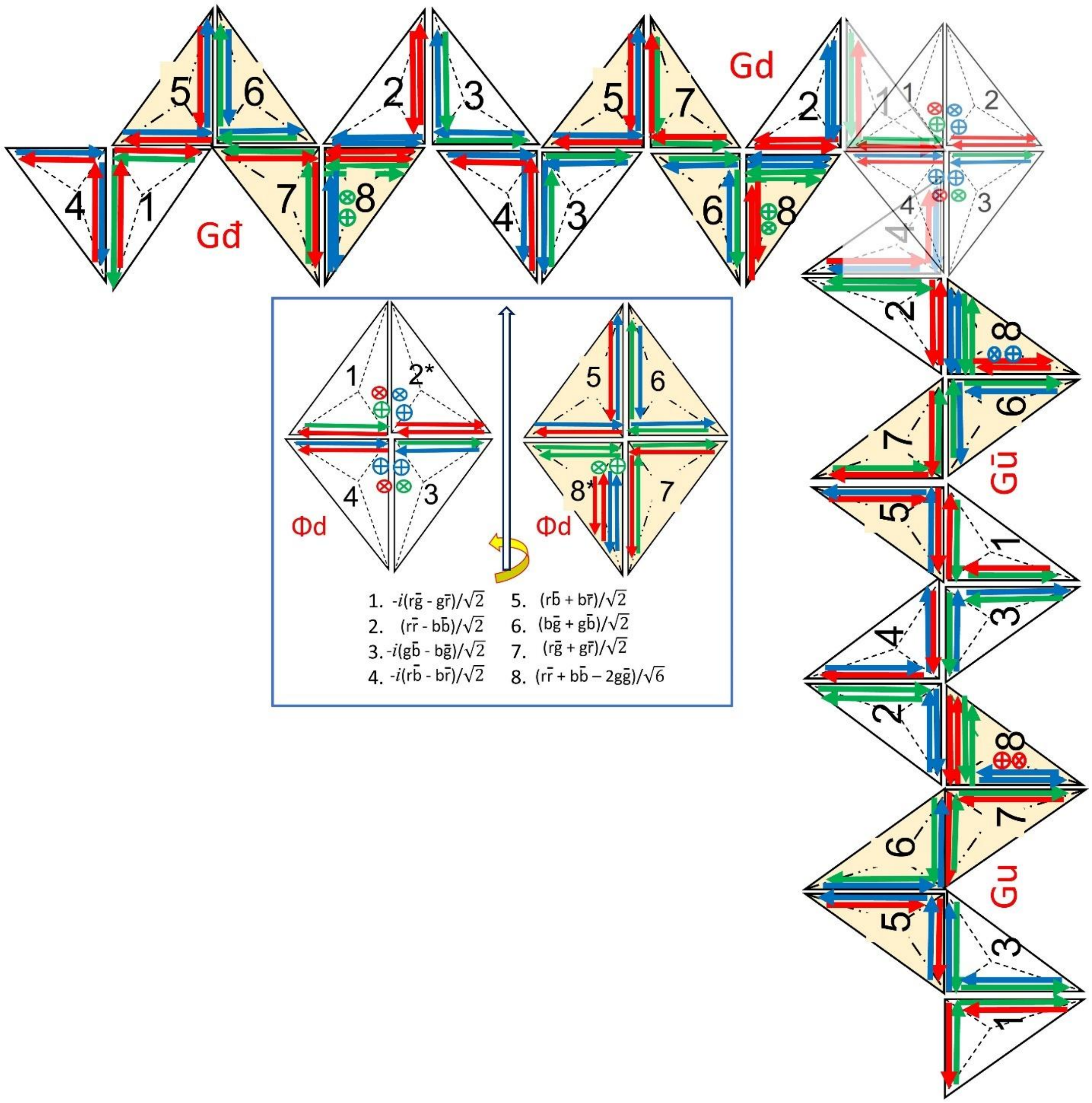


- **Example (down quark):** a $G_d$ - $G_{\bar{d}}$ Gluet can couple at port #1 on a Φd Octon, while a $G_u$ – $G_{\bar{u}}$ Gluet can couple at port #4 orthogonally (with its axis along $\hat{z}$ ). The orthogonality arises from the underlying tetrahedral vector layout, not from broken symmetry.
- **Selection rules.** Valid attachments are those for which the endpoint address of the Gluet's terminal tetrahedron matches the target Octon's port address and orientation (X/Y/Z projection), guaranteeing perfect 3-color coupling at the junction.
- **Mechanics.** Coarse-grained, the tube contributes a linear potential $V(R) \approx \sigma_{eff} R$. Torsional and transverse excitations correspond to discrete module modes (twist/zig-zag) rather than a

continuum, offering potential spectroscopic signatures distinct from a purely continuum string.

## Phenomenological implications:

1. **Confinement & string breaking**. As R grows, energy stored ~ $\sigma_{\text{eff}} R$ can nucleate a neutral Gluet pair that "snaps" the Gluet tube—Triad's discrete version of string breaking—seeding quark–antiquark production via axion influx at star addresses (cf. §3.9).
2. **Mode spectrum**. The helical/zig-zag module geometry predicts quantized vibrational bands; lattice-scale spacing $\ell$ subsets the band gap.
3. **End-port specificity**. Baryon vs. meson assembly depends on which ports are occupied (e.g., triads vs. dimers), giving selection rules for hadron topologies.

## 5.4 Strong Force Containment of Quarks Inside Baryons

With Gluet–to–Octon **port matching** (§5.3), the Triad Model supplies a microscopic confinement mechanism for hadrons. In baryons, neutral Gluet modules tile into short **string segments** that attach to each quark's addressed port, producing a piecewise-linear network with effective tension $\sigma_{\text{eff}}$ (defined in §5.0).

- **Baryon geometry (proton/neutron).**
  A proton (uud) or neutron (udd) is confined by a network that minimizes total Gluet length. In the coarse-grained limit this is equivalent to a **Y-like Steiner tree**: three Gluet branches meeting at a junction that adjusts to minimize

$$V_0 \approx \sigma_{\text{eff}}\, L_{\min} + V_0$$

where $L_{\min}$ is the minimal total length of the three branches.

In the Triad construction, **discrete port orientations** (e.g., ports aligned along $\hat{x}, \hat{y}, \hat{z}$) quantize the allowed junction configurations and small oscillations (torsion/zig-zag) arise from the **module** degrees of freedom rather than a continuum string.

- **Stretch vs. approach.**
  When quarks are pulled apart, branches **lengthen**, increasing $V$ linearly (restoring force ~ $\sigma_{\text{eff}}$). When quarks approach, the network **reconfigures** by shortening/redirecting segments; there is no "compression spring" per se—energy is reduced by decreasing total length. Perhaps it is best interpreted as **geometric rerouting** required by discrete port matching while preserving 3-color continuity.

- **Mesons vs. baryons.**
  Mesons ($q\bar{q}$) require a **single** neutral Gluet chain between two ports; baryons require **three**

branches meeting at a junction. Both cases use the same $\sigma_{\text{eff}}$ defined by the neutral 16-gluon modules.

- **Inter-nucleon (residual) force.**
  Within nucleons, confinement is the Gluet network above. Between nucleons, the Triad Model predicts a **residual interaction** that can be viewed as exchange of short Gluet **linklets** or effective mesonic modes; in the long-wavelength limit this matches the standard meson-exchange picture of nuclear forces.
-

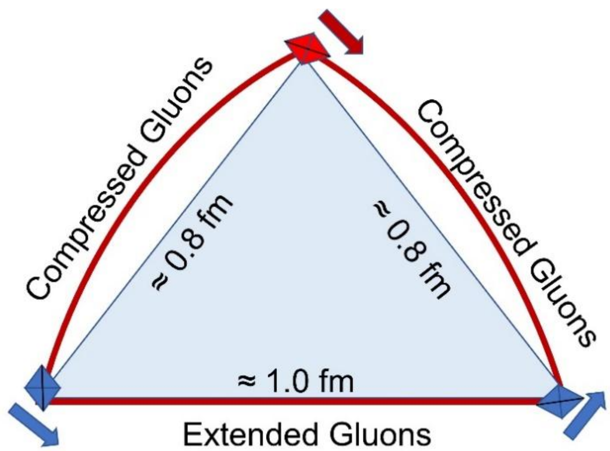


**Figure 16. Gluet strong force confinement of Octon quarks inside the proton.** The proton has two charged (+2/3 e) up Octon quarks (blue diamonds) and one charged (-1/3 e) down Octon quark (red diamond) that are confined within the proton. The Triad Model proposes that the Gluet flux tubes shown in Figs 13-14 act to **keep the two up quarks from flying apart** by increasing V linearly (restoring force ~ $\sigma_{\text{eff}}$). The opposite charged particles are retrained from approaching each other by the Gluet **geometric rerouting** to resist Gluet compression. This combined attraction-repulsion strong nuclear force of the Gluet structures acts like the SM mechanism to confine quarks inside hadrons. The neutron structure would also look similar except that the red diamond would be an up Octon quark and the 2 blue diamonds would be down Octon quarks.

## 5.5 Summary (Gluets and confinement)

Gluons in **eight-member octets** are the **same building blocks** that: (i) self-assemble into Octon quarks and (ii) tile into **neutral 16-gluon Gluet modules**. By port-matching these modules to quark addresses, the Triad Model yields a **finite, flavor-insensitive** confinement mechanism with an effective tension $\sigma_{\text{eff}}$ common to u/d (and, by attachment, to s/c/b/t). In the continuum limit, baryon/meson potentials reduce to familiar linear forms, while at short scales the model predicts **discrete vibrational/torsional bands** (module modes) and **quantized junction geometries**—providing concrete, testable signatures beyond a purely continuum string description.

## 6.0 Leptons as Triads of Orthogonal Octon Quarks

In the Standard Model, leptons are treated as point-like fermions. In the **Triad Model**, every lepton is a single quantum **Triad**: three Octon quarks (Φ's) inserted **orthogonally** along $\hat{x}, \hat{y}, \hat{z}$ and interpenetrating to form a **Stellated Rhombic Dodecahedron (SRD)** core (Fig. 3). The triad is compact: its three Octons share ports internally and leave **no external ports** for Gluet attachment—so leptons are **blind to the strong force**, consistent with observation.

**Why quark subunits?**

- In §3–5 we showed how eight-gluon **Octon quarks** self-assemble via perfect 3-color couplings.
- The same SU(3) geometry that binds quarks in hadrons also permits **three Octons to lock orthogonally** into one rigid SRD—yielding a lepton without external flux tubes.

**Leptons vs. baryons/mesons**

- **Baryons/mesons:** independent Octons linked by **Gluet** flux tubes (linear tension $\sigma_{\text{eff}}$; §5).
- **Leptons:** a **single** Octon–Octon–Octon SRD; **no Gluets** are possible because all ports are internally saturated by the orthogonal triad.

**Chirality (handedness)**

The triad admits both right- and left-handed embeddings. **Cyclic order** of the three Octons around $\hat{x} \to \hat{y} \to \hat{z}$ defines chirality; inversion flips it. Charged leptons possess both chiralities (Dirac fermions). For neutrals, only the SM-allowed chiralities couple to $W / Z$.

**Table 2. Standard Model Leptons and Proposed Structures** show SM data for the Leptons and the putative Triad Model structures for all the leptons. R stands for right-handed, and L stands for left-handed. The symbol ⊥ denotes **orthogonal interpenetration (⊥)** along distinct axes.

| Flavor | Name | Symbol | Mass (MeV) | Charge | Triad Structure |
|---|---|---|---|---|---|
| *e* | electron | $e^-$ | ≈ 0.511 | -1 | $\Phi\bar{u} \perp \Phi\bar{d} \perp \Phi\bar{u}$ |
| ***e*** | positron | $e^+$ | ≈ 0.511 | +1 | $\Phi u \perp \Phi d \perp \Phi u$ |
| ***e*** | L-neutrino | $\nu_e$ | < 2.2 eV | 0 | $\Phi u \perp \Phi d \perp \Phi d$ |
| ***e*** | R-antineutrino | $\bar{\nu}_e$ | <2.2 eV | 0 | $\Phi\bar{d} \perp \Phi\bar{d} \perp \Phi\bar{u}$ |
| *μ* | muon | $\mu^-$ | ≈ 105.66 | -1 | $\Phi\bar{u} \perp \Phi\bar{s} \perp \Phi\bar{u}$ |
| *μ* | antimuon | $\mu^+$ | ≈ 105.66 | +1 | $\Phi u \perp \Phi s \perp \Phi u$ |
| *μ* | muon L-neutrino | $\nu_\mu$ | <0.17 | 0 | $\Phi u \perp \Phi d \perp \Phi s$ |
| *μ* | muon R-antineutrino | $\bar{\nu}_\mu$ | <0.17 | 0 | $\Phi d \perp \Phi s \perp \Phi u$ |
| *τ* | tau | $\tau^-$ | ≈ 1776.8 | -1 | $\Phi\bar{u} \perp \Phi\bar{b} \perp \Phi\bar{u}$ |
| *τ* | antitau | $\bar{\tau}^+$ | ≈ 1776.8 | +1 | $\Phi u \perp \Phi b \perp \Phi u$ |
| *τ* | tau L-neutrino | $\nu_\tau$ | <18.2 | 0 | $\Phi u \perp \Phi d \perp \Phi b$ |
| *τ* | tau R-antineutrino | $\bar{\nu}_\tau$ | <18.2 | 0 | $\Phi\bar{d} \perp \Phi\bar{b} \perp \Phi\bar{u}$ |

**How the quantum numbers arise**.

The diagonal Jordan–octonion entries of each $\Phi$ (cf. §3.1–3.3) set the core symmetry, while off-diagonal axion choices (from {$A_2$, $A_8$, $A_9$, $A_{10}$, $A_{11}$, $A_{12}$} determine electric charge In the triad, the three $\Phi$'s are arranged so that all color ports are internally saturated; net charge (0, ±1) follows directly from the combined off-diagonal content of the three constituents, whereas no external color remains—explaining why leptons do not participate in the strong interaction**.**

## 6.1 Triad Structures for the -1-charge Leptons

Each charged lepton $\ell \in \{ e, \mu, \tau\}$ is modeled as an orthogonal Triad of three antiquark Octons:

$$\Phi_{\bar{u}} \perp \Phi_{\bar{q}} \perp \Phi_{\bar{u}}, \quad \text{with} \quad \bar{q} \in \{\bar{d}, \bar{s}, \bar{b}\}$$

arranged along $\hat{x}, \hat{y}, \hat{z}$**.** All internal color "ports" are saturated (no external Gluet attachments).

**(A) Effective 3D lattice Lagrangian for a lepton Triad**

Let $S = A \cup B \cup C$ denote the $3 \times 9$ oscillator sites of the three Octons (left A = $\Phi_{\bar{u}}$, center B = $\Phi_{\bar{q}}$, right C = $\Phi_{\bar{u}}$). With intra–Octon couplings $K_{st}$ and large "locking" terms that enforce port matching between Octons, a nonrelativistic 3D lattice Lagrangian is:

$$\mathcal{L}_\ell^{(3DLat)} = \sum_{s\in S} \left[\frac{1}{2} \dot{\phi}_s^{\,2} - \frac{1}{2} \omega_s^2 \, \phi_s^2 \right] - \frac{1}{2} \sum_{(s,t)\in \text{Intra-Octon}} K_{st} \, (\phi_s - \phi_t)^2$$

$$- V_{lock}^{(A,B,C)} - V_{\text{flavor}} \, (\bar{q}) - V_{\text{drive}}(t)$$

with

- $V_{lock}^{(A,B,C)} = \kappa_{\text{lock}} \sum_{p\in M_{AB}} (\phi_p^{\,A} - \phi_{p'}^{\,B})^2 + \kappa_{\text{lock}} \sum_{p\in M_{BC}} (\phi_{p''}^{\,B} - \phi_{p'''}^{\,C})^2$ (large $\kappa_{\text{lock}}$ **saturates** the internal color ports, i.e., no external flux tubes);
- $V_{flavor}^{\;(\bar{q})}$ $\;$ *encodes the* **weak – bond** *perturbation inside the* **central** *Octon* $B = \bar{q}$ *(see below)*;
- $V_{\text{drive}}(t) = -\,\frac{1}{\alpha} f_\ell\,(t)\,\widehat{D}_\ell\,(\{\phi_s\})$ is the Triad drive term, as in §3.6–3.7.

Large $K_{\text{lock}}$ saturates the internal color ports (i.e., enforces equal amplitudes across matched ports and forbids external flux tubes). A continuum (3+1)D form follows by replacing $(\phi_s - \phi_t)^2$ with $|\nabla \phi_{\text{i}}|^2$; we use the lattice form (Eq. 20) because the Triad is a discrete interpenetrating assembly.

**(B) Hamiltonian and number-operator form**

Canonical momenta: $\pi_s = \partial L / \partial \dot{\phi}_s = \dot{\phi}_s$. The static lattice Hamiltonian (classical) is

$$\hat{H}_{\ell}^{Static} = \sum_{s\in S} [\tfrac{1}{2}\pi_s^2 + \tfrac{1}{2}\omega_s^2 \phi_s^2] + \tfrac{1}{2}\sum_{(s,t)\epsilon intra-Octon} K_{st}(\phi_s - \phi_t)^2$$

$$+ \hat{H}_{\text{Lock}} + \Delta\hat{H}_{\text{flavor}}(\bar{q}),$$

Upon quantization $(\phi_s, \pi_s \longrightarrow \hat{\phi}_s, \hat{\pi}_s)$ and projection to on-site normal modes with $\hat{N}_s = \hat{a}_s^{\dagger}\hat{a}_s$ ,

$$\hat{H}_{\ell}^{Static} = \alpha\hbar\omega \sum_{s\in S} \hat{N}_s + \hat{H}_{\text{Lock}} + \Delta\hat{H}_{flavor}^{(\bar{q})}$$

where ω is the base on-site frequency (renormalized by intra-Octon couplings). The full time-dependent Triad Hamiltonian is

$$\hat{H}_{\ell}(t) = \hat{H}_{\ell}^{Static} + \hat{H}_{\text{drive}}(\text{t}), \quad \hat{H}_{\text{drive}}(t) = \frac{1}{\alpha} f_{\ell}(t)\, \hat{D}_{\ell}$$

governing the Schrödinger equation $i\hbar\, \partial_t\, \Psi(t) = \hat{H}_{\ell}(t)\, \Psi(t).$

## (C) Specialization to *e, μ, τ* (central antiquark controls the generation)

- **Electron** ($\bar{q} = \bar{d}$): no weak-bond perturbation in the central Octon,

$$\Delta\hat{H}_{Flavor}^{\bar{d}} = 0$$

- **Muon** ($\bar{q} = \bar{s}$): one weak 2-color bond from the strange-sector swap (sites 2 and 5), matching § 4.6,

$$\Delta\hat{H}_{Flavor}^{\bar{s}} = \varepsilon_s\, (\hat{N}_2^B - \hat{N}_5^B)^2,$$ with $\varepsilon_s$ calibrated so that $E_\mu / E_e \approx 206.768.$

- **Tau** ($\bar{q} = \bar{b}$) one weak 2-color bond at (sites 3 and 6), matching § 4.8,

$$\Delta\hat{H}_{Flavor}^{\bar{b}} = \varepsilon_b\, (\hat{N}_3^B - \hat{N}_6^B)^2,$$ with $\varepsilon_b$ calibrated so that so that $E_\tau / E_e \approx 3477.$

**Consistency with § 4.6–4.8.** The index pairs (2 ,5) for s and (3,6) for b are the same weak-bond locations used in the quark sector; here they are embedded inside the central antiquark B = $\bar{q}$ of the lepton Triad while the outer $\bar{u}$ Octons are locked to it.

**Interpretation.** The electron needs only base occupancy plus locking (no weak bond). The muon and tau require extra stabilization energy to compensate for a single weakened 2-color bond inside the central antiquark; holding $\kappa_{lock}$ and ω fixed across the family, the empirical ratios

$E_\mu / E_e$ and $E_\tau / E_e$ fix $\varepsilon_s$ and $\varepsilon_b$ (up to small mode–mixing corrections). The drive term $\frac{1}{\alpha} f_\ell(t)\, \widehat{D}_\ell$ permits coherent axion flux through the Triad without opening external color ports—consistent with leptons' insensitivity to the strong force.

## 6.2 Vector Diagrams for Charged Leptons (Electron & Positron)

**Concept.** A charged lepton is a compact Triad: three orthogonally interpenetrating Octon quarks (Φ's) forming a Stellated Rhombic Dodecahedron (SRD). For the electron and positron the Triads are:

- $e^-$: $\Phi_{\bar{u}} \perp \Phi_{\bar{d}} \perp \Phi_{\bar{u}}$
- $e^+$: $\Phi_u \perp \Phi_d \perp \Phi_u$

**We visualize these 3-D overlaps in 2-D projections from the X, Y, and Z axes:**

1. **X-axis view (Fig. 17a):**
   – Momentum arrow points upward (Y-direction).
   – Sixteen color-force vectors align along X; four asymmetric vectors (the "8*" sites) provide propulsion/spin.
   – The top four tetrahedra project into the page; the bottom four project out of the page.
2. **Y-axis view (Fig. 17b):**
   – The middle Octon (anti-down quark) is flipped onto its Y-axis, so its momentum arrow points left (left-handed chirality).
3. **Z-axis view (Fig. 17c):**
   – The third Octon (anti-up quark) is rotated so its vectors project along Z.
4. **Net electric charge:**
   – $e^-$: off-diagonal axions across the three Φ's sum to −1
   – $e^+$: off-diagonal axions across the three Φ's sum to +1

By superimposing these three projections - merging their top halves and bottom halves - we reconstruct the full 3-D Triad. In the left-handed electron (Fig. 17), every tetrahedral address contains all three colors, yielding maximum coupling.

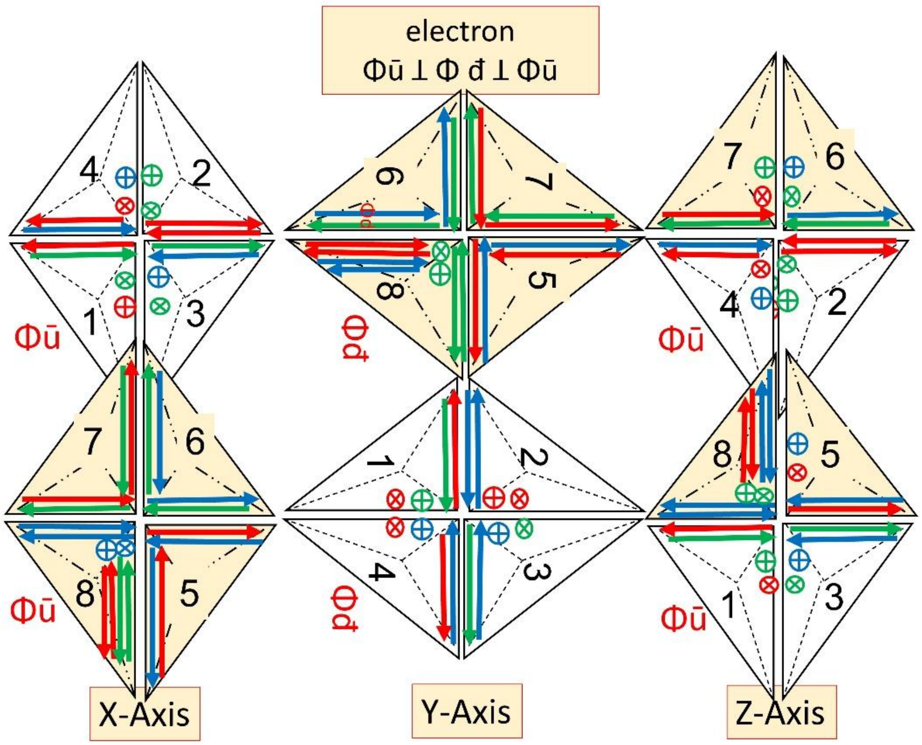


**Fig. 17 (electron): Vector diagram of the electron Triad** for the left-handed electron Triad. (a) X-axis view: momentum ↑, 16 color forces along X, top half into page, bottom half out of page. (b) Y-axis view: middle Octon flipped, momentum ← (left-handed). (c) Z-axis view: third Octon rotated along Z. All color ports are internally saturated; off-diagonal axions sum to -1.

The positron is the right-handed, charge-conjugate counterpart. Its vector diagrams (Fig. 18) follow the same projection conventions.

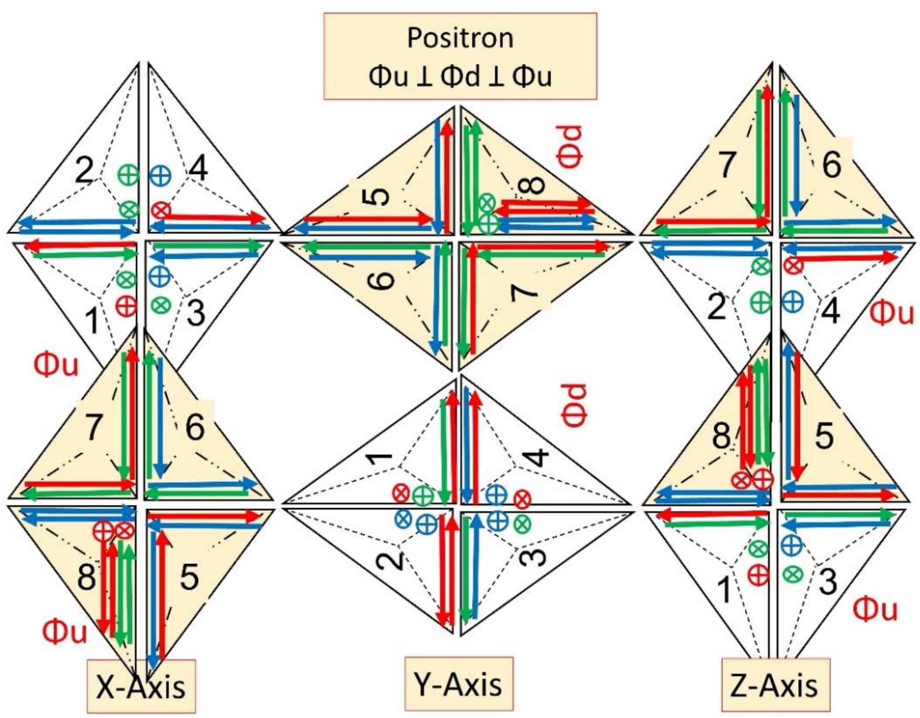


**Fig. 18 (positron): Vector diagram of the positron Triad** for the right-handed positron Triad. Conventions as in Fig. 17; note the central Octon's momentum → (right-handed). Same geometry and saturation; off-diagonal axions sum to +1.

## 6.3 Octonion Vector Diagrams of the e+ L-neutrino and e- R-anti-neutrino

Neutrinos in the Standard Model carry left-handed chirality; antineutrinos are right-handed. The positron can decay into the left-handed $V_e$ L-neutrino (Fig. 19), and the electron can decay into the right-handed $\overline{V}e$ R-anti-neutrino (Fig. 20). Both follow exactly the same projection method:

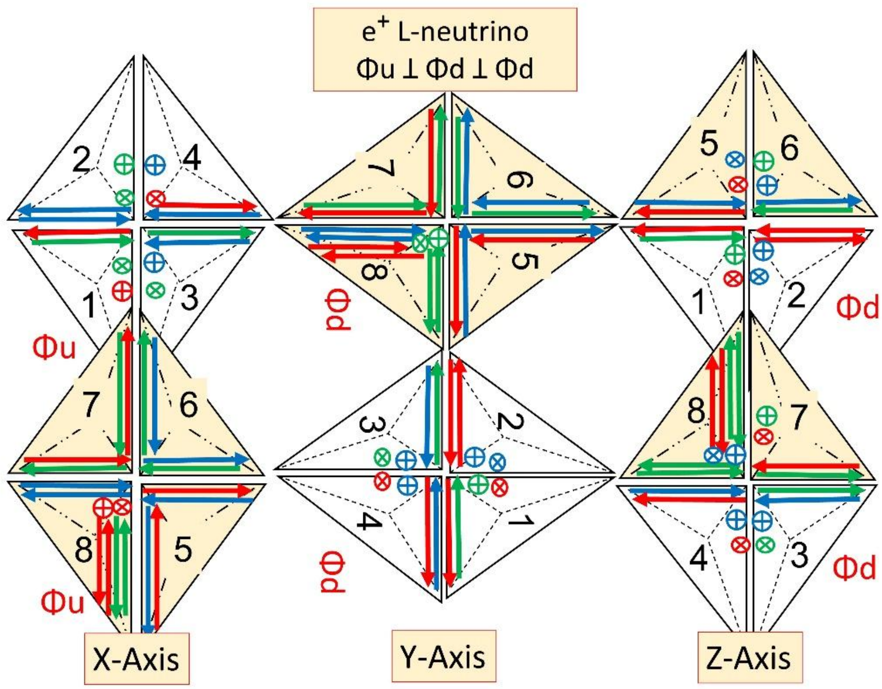


**Fig. 19. Left-handed Vector diagram of L-neutrino $V_e$:** (X, Y, Z views as in Fig. 17.) All ports locked internally; off-diagonal axions cancel to net charge 0.

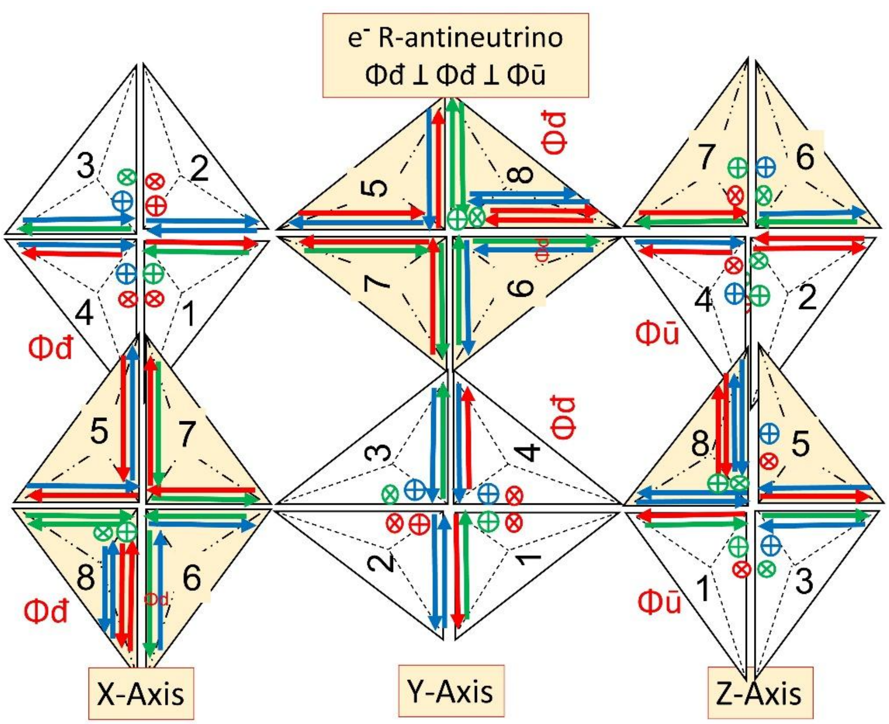


**Fig. 20. Right-handed e⁻ R-anti-neutrino $\overline{V}e$.** (X, Y, Z views as in Fig. 17.) Charge 0; weak-force decay product of the electron.

## 6.4 Neutrino Lagrangian and Hamiltonians

### Lattice Lagrangian (neutral Triad).

Let $S = A \cup B \cup C$ be the $3 \times 9$ sites for $A = \Phi_u$, $B = \Phi_q$, $C = \Phi_d$, with intra-Octon couplings $K_{st}$ and large port-locking $\kappa_{lock}$: The nonrelativistic 3D lattice Lagrangian is:

$$\mathcal{L}_{\nu}^{(3DLat)} = \sum_{s \in S} \left[\frac{1}{2}\dot{\phi}_s^{\,2} - \frac{1}{2}\omega_s^{\,2}\,\phi_s^2\right] - \frac{1}{2}\sum_{(s,t)\epsilon iO} K_{st}\,(\phi_s - \phi_t)^2$$

$$- V_{\text{lock}}(A, B, C) - V_{\text{flavor}}(\bar{q}) - V_{\text{drive}}(t)$$

With $q \in \{ d, s, b\} \}$, $(s,t)\epsilon iO = (s,t)\epsilon iintra - Octon$ and

$$V_{drive}(t) = -\frac{1}{\alpha} f\nu\,(t)\,\widehat{D}\nu(\{\phi_s\}).$$

### Flavor perturbations in the central Octon (operator level)

After quantization (see Hamiltonian below), the central Octon $B = \Phi_q$ carries the same weak-bond patterns used in §4.6–4.8:

$$\Delta\hat{H}^{(d)} = 0, \quad \Delta\hat{H}(s) = \varepsilon_s\,(\hat{N}_2^B - \hat{N}_5^B)^2, \quad \Delta\hat{H}(b) = \varepsilon_b\,(\hat{N}_3^B - \hat{N}_6^B)^2.$$

### Hamiltonian summary (after Legendre & quantization):

Canonical momenta: $\pi_s = \dot{\phi}_s$. The static lattice Hamiltonian is

$$\hat{H}_{\nu}^{\,static} = \sum_{s \in S} \left[\frac{1}{2}\hat{\pi}_s^{\,2} + \frac{1}{2}\omega_s^{\,2}\,\phi_s^2\right] + \frac{1}{2}\sum_{(s,t)\epsilon iO} K_{st}(\hat{\phi}_s - \hat{\phi}_t)^2 + \hat{H}_{\text{lock}} + \Delta\hat{H}(q)$$

which in a mode (number-operator) reduction is well-approximated by

$$\hat{H}_{\nu}^{\,static} \simeq \alpha\hbar\omega\,\Sigma_{\{s \in S\}}\,\hat{N}_s + \hat{H}_{\text{lock}} + \Delta\hat{H}(q),$$

The full time-dependent Hamiltonian is

$$\hat{H}_{\nu}(t) = \hat{H}_{\nu}^{\,Static} + \hat{H}_{drive}(t), \qquad \hat{H}_{drive}(t) = \frac{1}{\alpha} f_{\nu}(t)\,\widehat{D}_{\nu}$$

governing $i\hbar\,\partial_t\,\Psi(t) = \hat{H}_{\ell}(t)\,\Psi(t).$

## Methodological Note: Locking and mode selection (two-oscillator logic at each matched port)

Let $P_{AB}$ and $P_{BC}$ be the sets of matched port pairs ("tie-lines" in the vector diagrams). Use displacement and momentum locks.

**Displacement (configuration) lock:**

$$V_{lock}^{\phi} = \frac{\kappa}{2}\sum_{(p,q)\in P_{AB}\}} (\phi_p^A - s_{pq}\phi_q^B)^2 + \frac{\kappa}{2}\sum_{(p,q)\in P_{BC}} (\phi_p^B - s_{pq}\phi_q^C)^2$$

**Momentum (phase/velocity) lock:**

$$H_{lock}^{(\pi)} = \frac{\lambda}{2}\sum_{(p,q)\in P_{AB}\}} (\pi_p^A - s_{pq}\pi_q^B)^2 + \frac{\lambda}{2}\sum_{(p,q)\in P_{BC}} (\pi_p^B - s_{pq}\pi_q^C)^2$$

With $s_{pq} \in \{+1, -1\}$ choosing in-phase vs anti-phase locking per port, and $\kappa$, $\lambda > 0$ the lock stiffnesses. For *repeated components* (e.g., the two d's in $\nu_e$), set $s_{pq} = -1$ For a single matched pair, write $x_1 \equiv \phi_{A,p}$, $x_2 \equiv \phi_{B,q}$ and define normal modes

$$x_{\pm} = (x_1 \pm x_2)/\sqrt{2}\,, \quad p_{\pm} = (\pi_1 \pm \pi_2)/\sqrt{2}$$

Then

$$(\phi_{A,p} + \phi_{B,q})^2 = 2x^2_{+}, \quad (\phi_{A,p} - \phi_{B,q})^2 = 2x^2_{-}.$$

- With $s_{pq} = -1$, $V_{\text{lock}}^{(\phi)} \propto x^2_{+}$ **penalizes the sum mode** and $H_{\text{lock}}^{(\pi)} \propto p^2_{+}$ pushes it up in energy; the low-energy spectrum suppresses $X_+$ (destructive interference of diagonal amplitudes).
- The difference mode $X_-$ remains soft, providing a neutral, low-energy internal DoF — precisely what we want for neutrinos built from repeated components.

Thus, $H_{\text{lock}}^{(\pi)} = V_{\text{lock}}^{(\phi)} + H_{\text{lock}}^{(\pi)}$ kills the diagonal (sum) channel where duplicates would otherwise contribute, naturally yielding tiny neutrino energies.

## Mass hierarchy & smallness.

The locking term $\hat{H}_{lock} = V_{lock}^{\phi} + H_{lock}^{(\pi)}$ enforces destructive interference for repeated components (e.g., the two d's in $\nu_e$ ), strongly suppressing $E_{\nu_e}$. The single weak-bond term $\Delta\hat{H}(q)$ then lifts $\nu_\mu$ and $\nu_\tau$ relative to $\nu_e$ :

$$\Delta\hat{H}(\mathrm{s}) = \varepsilon_s\,(\hat{N}_{B,2} - \hat{N}_{B,5})^2,\;\; \Delta\hat{H}(b) = \varepsilon_b\,(\hat{N}_{B,3} - \hat{N}_{B,6})^2, \quad \varepsilon_s < \varepsilon_b,$$

yielding sub-eV scales with a mild hierarchy (consistent with data). Small port-phase choices $s_{pq}$ differing across (A,B) and (B,C) can seed PMNS-like flavor mixing without opening external color ports.

## 6.5 Observable Implications and Summary

- **Stability.** The electron has no observed decay mode (current limits exceed $10^{28}$ y for typical channels); in the Triad construction its internal color ports are fully saturated, and the same locking that suppresses neutrino energies yields a rigid $e^-$ Triad. Electron-flavor neutrinos are likewise ultra-long-lived.
- **Color blindness.** All charged- and neutral-lepton Triads saturate their internal color ports; no external Gluet (flux-tube) attachments are available. Leptons therefore do **not** carry QCD charge in this model, matching experimental observations.
- **Chirality selection.** Only one cyclic orientation of the three Octons has nonzero overlap with the $W\,/\,Z$ vertices; the opposite cyclic order is effectively sterile. This reproduces the SM's $V - A$ pattern (left-handed charged currents; no right-handed neutrino coupling).
- **Spectral substructure (testable in principle).** The displacement/phase locks introduce discrete internal normal modes (tiny gaps) rather than a continuum. In principle, such modes could imprint extremely small polarization-dependent asymmetries in high-precision production or scattering; candidate channels are listed in §8.
- **Unified scaling across families.** A single weak-bond penalty $\varepsilon_s\,(\hat{N}_{B,2} - \hat{N}_{B,5})^2$ for the strange-sector antiquark and $\varepsilon_b\,(\hat{N}_{B,3} - \hat{N}_{B,6})^2$ for the bottom-sector antiquark accounts simultaneously for the charged-lepton mass ratios ($\mu\,/\,e,\ \tau\,/\,e$) and the neutrino family ordering once the same locking is applied.
- **Neutrino oscillations.** The three neutrino Triads differ only by one swapped-bond pattern in the central Octon; mixing arises from small differences in port-phase choices $s_{pq}$ and lock strengths across the two interfaces $(A,\ B)$ and $(B,\ C)$. Mass-squared splittings are set chiefly by $\varepsilon_s,\ \varepsilon_b$; PMNS-like phases trace back to relative signs in the lock matrices.

**Summary.** From the same Octon building blocks that yield quarks and Gluets, the Triad Model constructs charged and neutral leptons that (i) are color-neutral and hence QCD-blind, (ii) couple chirally to the weak force in the SM pattern, and (iii) exhibit observed mass hierarchies via a minimal, index-matched weak-bond mechanism.

## 7.0 Dyad Octon Quarks and Photon Quantum Structures

Thus far, the Triad Model has shown how eight-gluon Octets self-assemble into:
• single quarks (Sections 3–4),
• Gluet flux tubes that bind quarks in mesons/baryons (Section 5), and
• three-Octon Triads that form leptons (Section 6).

A final self-assembled class is the **Dyad**: two Octon quarks interpenetrating orthogonally. In the Triad Model, the spin-1 bosons—**photons and the electroweak** $W^{\pm}$, $Z$ —are realized as **orthogonal Octon Dyads**. As with leptons, Dyads neutralize all Gluet ports, so they are blind to the strong force while carrying the right charges/helicities for QED and electroweak interactions.

## 7.1 Octon Dyads for the Photons

A systematic scan of orthogonal Octon pairings (via the vector-diagram coupling rules) yields **exactly two** Dyads that (i) achieve **full 3-color overlap at all eight addresses**, (ii) are **net neutral**, and (iii) **block** any Gluet attachment:

1. **L-Photon**

$$\Phi_{\gamma}^{L} = \Phi d \perp \Phi \bar{d} \text{, (net charge 0, left-helicity)} \tag{29}$$

2. **R-Photon**

$$\Phi_{\gamma}^{R} = \Phi u \perp \Phi \bar{u} \text{, (net charge 0, right-helicity)} \tag{30}$$

**Why only these two?** Among the four natural "same-flavor" Dyads ( $d \perp \bar{d}$ vs $u \perp \bar{u}$, each with the two possible orientation orders), only the pairings in Eqs. (29)–(30) realize **perfect three-color overlap** in all orthogonal projections (X–Y, Y–Z, X–Z). The orientation-reversed variants leave at least one address with only 2-color overlap (a weakened bond), rendering those configurations unstable**.**

**Properties.**

- **Maximal 3-color coupling.** Each of the eight addresses sees all three colors from the two interpenetrating Octons, yielding a strict singlet per site and high structural stability.
- **Orthogonality.** The right-angle interpenetration saturates all ports internally; **no Gluet** endpoint remains, explaining strong-force blindness.
- **Helicity.** The internal momentum-axis orientation of the second Octon fixes a handedness: $\Phi_{\gamma}^{L}$ and $\Phi_{\gamma}^{R}$ realize the two photon helicity states.

**Figure 21 (see below). Vector diagram for $\Phi_\gamma^L$ and $\Phi_\gamma^R$.** Both are neutral and Gluet-decoupled; their helicities differ by the orientation of the second Octon's momentum axis. All eight addresses are 3-color saturated. *It is important to note that the chiral nature of the L-photon and the R-antiphoton are unique.* For example, the R-photon ($\Phi$d ⊥ $\Phi\bar{d}$) is unstable with weak 2-color coupling at 3-6 and 7-1 in axis X-Y conformation and at 5-5, 2-4, and 1-1 in the Y-Z conformation, and at 6-6 and 7-1 in the X-Z conformation, while the L-Photon has perfect 3-color coupling at all 8 sites in both the X-Y and X-Z conformations. In contrast, the L-Photon (Φu ⊥ Φū) is unstable with weak 2-color coupling at 5-4 in axis X-Y conformation and at 6-6 and 1-1 in the Y-Z conformation and at 4-4 and 2-2 in the X-Z conformation, while the R-photon has perfect 3-color coupling at all 12 sites in both the X-Y and X-Z conformations. *Thus, the R-photon and L-antiphoton particles are the only stable Octon quark Dyads and each have predicted opposite helical chirality*. This pairing of quark–antiquark Octons into chiral, color-neutral Dyads provides a geometric and algebraic origin for photon helicity states, naturally reproducing the two polarization modes of the electromagnetic field.

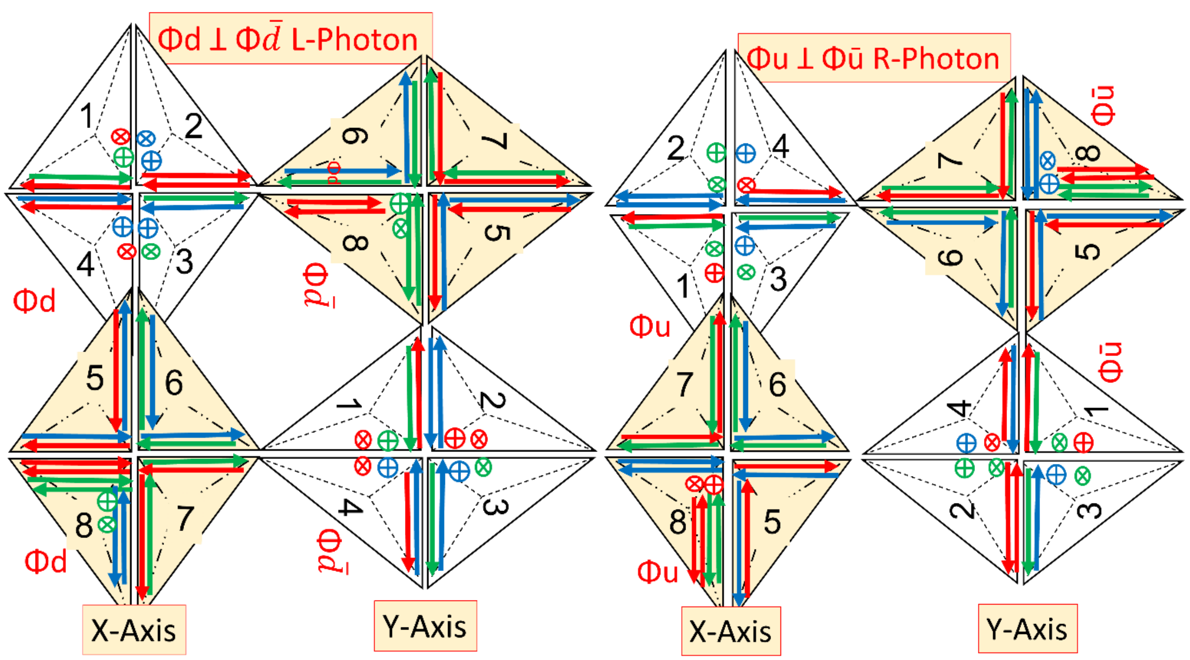


## 7.2 Photon Dyads & Phenomenology

**Neutral-Pion Decay** ($\pi^0 \longrightarrow 2\gamma$)

**The** $\pi^0$ is predominantly the flavor-singlet superposition $1/\sqrt{2}$ (uū −d$\bar{d}$). In the Dyad picture, its two components **reassemble** into the two helicity photons:

$$\Pi^0 \sim (1/\sqrt{2})\,(\mathrm{u}\bar{\mathrm{u}} - \mathrm{d}\bar{d}) \implies \Phi_\gamma^R + \Phi_\gamma^L = (\Phi\mathrm{u} \perp \Phi\bar{\mathrm{u}}) + (\Phi\mathrm{d}\text{---}\Phi\bar{d}) \qquad (31)$$

This schematic mapping explains why $\pi^0$ dominantly yields **two** photons and why the pair carries **opposite helicities**.

**Positron–electron annihilation.**
Back-to-back 511 keV photons from $e^+e^-$ annihilation naturally appear as the **two Dyads**:

$$e^+ + e^- \Rightarrow \Phi_\gamma^L + \Phi_\gamma^R = (\Phi\mathrm{d} \perp \Phi\bar{d}) + (\Phi\mathrm{u} \perp \Phi\bar{\mathrm{u}}) \qquad (32)$$

The Dyad composition accounts for the observed helicity anticorrelation in polarization-entanglement experiments while remaining fully consistent with standard quantum predictions.

**"Di-Photon Molecules".**
Recent experimental reports of bound or quasi-bound photon pairs under extreme conditions hint at residual interactions between photons [6]. Reports of bound or quasi-bound photon pairs in strongly interacting media (e.g., Rydberg-polaritonic regimes) can be viewed here as **medium-assisted** brief alignments of two Dyads: internal Octon structure provides transient color-overlap channels that mimic an effective attraction. (This is a **suggestive** mapping; the effect is highly medium-dependent and not required by the free-space theory.)

**Interference and duality.**
As a Dyad propagates through the Triad lattice, its 18 gluon sites exchange $\hbar$-axions coherently with the medium, providing a **single mechanism** for both wavefront formation (interference fringes) and localized detection (axion-exchange–driven collapse). This keeps standard optics intact while giving a concrete microstructure to "wave–particle duality."

## 7.3 Structural models for the W and Z weak force bosons

In the Triad Model, the $W^\pm$ and $Z^0$ are **orthogonal Octon Dyads** (two Octon quarks interpenetrating at right angles). As with photon Dyads, all color ports are saturated internally, so there are **no Gluet endpoints** (no strong-force coupling). Unlike photons, however, imperfect interpenetration (one or more 2-color overlaps) leaves **weak-bond defects**, which account for their **large, finite masses** and **short lifetimes**.

- **Weak-Force Range.** Dyads overlap only at "quantum-touching" distances $\lesssim 10^{-18}$ m, consistent with the weak interaction's short range.
- **Electroweak Continuity.** Building $W^\pm$ and $Z^0$ from the Dyad framework as photons mirrors the Glashow–Salam–Weinberg picture at the level of carriers (spin-1, no strong color), while encoding mass via Dyad geometry.

$W^{-}$ **(charge −1):** $$W^{-} = \Phi_d \perp \Phi_{\bar{u}} \tag{33}$$

Among the possible helicity/orientation pairings of $\Phi_d \perp \Phi_{\bar{u}}$, **only the left-helicity Dyad** achieves maximal three-color overlap at all addresses (Fig. 22). Besides weak-bond defects, locking penalties that enforce port-by-port mode selection between the two Octons are likely the major contribution to a large mass and short lifetime. Other orientations break multiple bonds and are unstable. These factors help explain the **large mass** $m_W \approx 80.4$ GeV and **short lifetime** $\tau_W \sim 10^{-25}$ s.

$W^{+}$ **(+1 charge):** $$W^{+} = \Phi_u \perp \Phi_{\bar{d}} \tag{34}$$

Of the four nominal orientations, the **right-helicity Dyad** preserves all strong three-color bonds (Fig. 23). Besides weak-bond defects, locking penalties that enforce port-by-port mode selection between the two Octons are likely the major contribution to a large mass and short lifetime. Other orientations have more defects and are disfavored.

## $Z^0$ (Charge 0)

$$Z^0 = \Phi_b \perp \Phi_{\bar{s}}$$

A neutral Dyad built from $\Phi_b \perp \Phi_{\bar{s}}$ is the most stable neutral pairing we find that preserves complete color saturation at most addresses while necessarily carrying **two** weak-bond defects (one per Octon block). Both weak bond defects and locking penalties naturally set a **heavier mass** $m_Z \approx 91.2$ GeV and a **lifetime** $\tau \sim 3 \times 10^{-25}$ s. (Small rotations within the neutral Dyad family leave quantum numbers unchanged but do not reduce the defect count.)

### Chirality and Weak Coupling

- Only the **left-helicity** $W^{-}$ and right-helicity $W^{+}$ Dyads are minimally defective; these are the states that couple in charged-current processes, matching the SM's $V - A$ selection rules.

- The opposite-helicity constructions exist kinematically but suffer **multiple** bond defects and are therefore dynamically suppressed—consistent with the **absence of right-handed charged currents**.

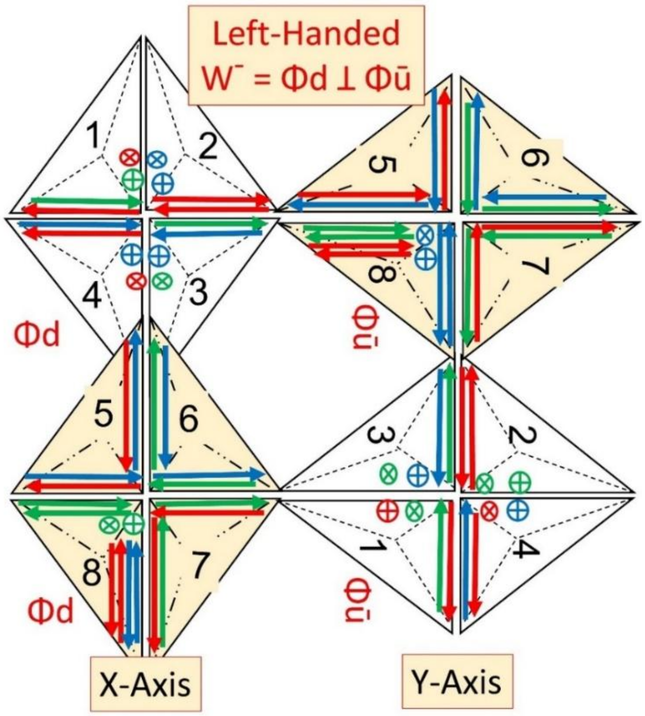


**Figure 22. The octonion vector diagrams for the left-handed $W^-$ Dyad ( $\Phi d \perp \Phi\bar{u}$).** $W^-$ has strong 3-color coupling at all coupling positions with left-handed helical movement and -1 charge. Besides weak-bond defects, locking penalties that enforce port-by-port mode selection between the two Octons is likely the major contribution to a large mass and short lifetime.

The putative structure of the right-handed quantum conformation of $W^+$ is shown in Fig. 23.

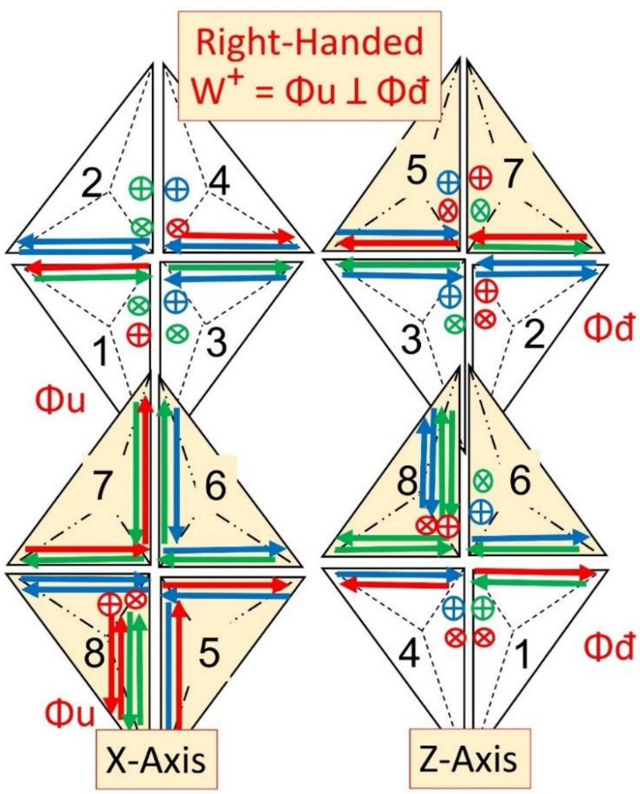


**Figure 23. The octonion vector diagrams of the right-handed $W^+$ ($\Phi u \perp \Phi\bar{d}$).** $W^+$ has strong 3-color coupling at all coupling positions with right-handed helical movement and +1 charge. Besides weak-bond defects, locking penalties that enforce port-by-port mode selection between the two Octons is likely the major contribution to a large mass and short lifetime. All the other left- and right-handed configurations of the up/anti-down Octons quarks have less stable coupling sites.

Both $W^{\pm}$ and $Z^0$ thus emerge as orthogonal Octon Dyads with one or more weak-bond defects—capturing their heavy masses, short lifetimes, and strict chirality in a unified octonionic framework.

## 7.4 Beta-minus neutron decay: $n \longrightarrow p + e^- + \bar{\nu}_e$

A viable model must reproduce dominant weak processes. In the Triad picture, **beta-minus decay** proceeds via two clean Dyad reassemblies:

1. **Dyad exchange that flips d →u inside the neutron:** $(\Phi d\text{---}\Phi\bar{d})$

$$\text{Neutron} + \Phi_\gamma^R \Rightarrow \text{Proton} + W^- \Leftrightarrow (u\ d\ d) + (\Phi u \perp \Phi\bar{u}) \rightarrow$$

$$(u\ d\ u) + (\Phi d \perp \Phi\bar{d}) \qquad (35)$$

2. **Leptonic vertex and photon emission:**

$$\mathbf{W^- + \bar{\nu}_e \Rightarrow} e^+ + \Phi_\gamma^L \Leftrightarrow (\Phi d \perp \boldsymbol{\Phi\bar{u}}) + (\boldsymbol{\Phi\bar{d}} \perp \Phi\bar{d} \perp \Phi\bar{u}) \rightarrow$$

$$(\boldsymbol{\Phi\bar{u}} \perp \Phi\bar{d} \perp \Phi\bar{u}) + (\Phi d \perp \boldsymbol{\Phi\bar{d}}) \qquad (36)$$

Step (35) is the **hadronic flavor change**; step (36) **creates the electron Triad** and an **L-helicity photon Dyad** as radiation. This mirrors the SM $n \longrightarrow p\, W^-$ followed by $W^- \rightarrow e^- \bar{\nu}_e$ with Dyad geometry standing in for the weak vertex.

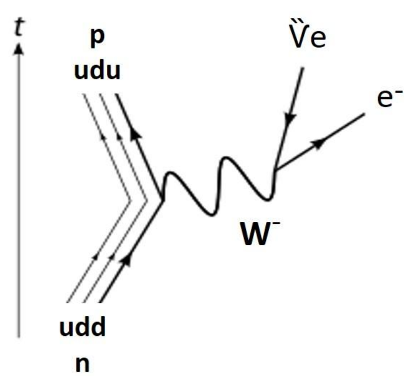


**Figure 24. Decay of a neutron (udd) into a proton (udu).** This occurs by the exchange of d quark for the u quark via a gamma R-antiphoton: (ud**d**) + (**Φu** ⊥ Φū)→ (ud**u**) + (**Φd** ⊥ Φū). This converts a neutron (udd) into proton (udu), while the photon is converted to the charged $W^-$ = (**Φd** ⊥ Φū). The $W^-$ is unstable and goes on to convert a V̄e antineutrino into e-electron by the reaction ($\boldsymbol{\Phi\bar{d}}$ ⊥ $\Phi\bar{d}$ ⊥ Φū)+ (Φd ⊥ **Φū**) → (**Φū** ⊥ $\Phi\bar{d}$ ⊥ Φū) + (Φd ⊥ $\boldsymbol{\Phi\bar{d}}$), which generates an e- L-electron and a gamma L-photon. Exchanged quarks are **bolded**. Feynman diagram for β− decay of a neutron as drawn by Joel Holdsworth (Joelholdsworth).

## 7.5 **Beta-plus decay:** proton (u d u) $\rightarrow$ Neutron (d d u) + e+ + $V_e$

Likewise, **beta-plus decay** is captured by the conjugate Dyad reassemblies: (Fig. 25):

1. **Dyad exchange that flips u → d inside the proton**

$$\text{Proton} + \Phi_\gamma^L \Rightarrow \text{Neutron } W^+ \Longleftrightarrow (\text{u d } \mathbf{u}) + (\boldsymbol{\Phi}\mathbf{d} \perp \Phi\bar{\boldsymbol{d}}) \rightarrow$$

$$(\mathbf{d} \text{ d u}) + (\boldsymbol{\Phi}\mathbf{u} \perp \Phi\bar{\boldsymbol{d}}) \qquad (37)$$

2. **Leptonic vertex and photon emission:** $W^+ + Ve \rightarrow$ e+ **+ L-Photon**

$$W^+ + V_e \Rightarrow e^+ + \Phi_\gamma^L \Longleftrightarrow (\boldsymbol{\Phi}\mathbf{u} \perp \Phi\bar{d}) + (\Phi\text{u} \perp \Phi\text{d} \perp \boldsymbol{\Phi}\mathbf{d}) \rightarrow$$

$$(\Phi\text{u} \perp \Phi\text{d} \perp \boldsymbol{\Phi}\mathbf{u}) + (\boldsymbol{\Phi}\mathbf{d} \perp \Phi\bar{d}) \qquad (38)$$

Again, flavor, charge, and **helicity flow** match the observed beta-plus channel (see Fig. 25).

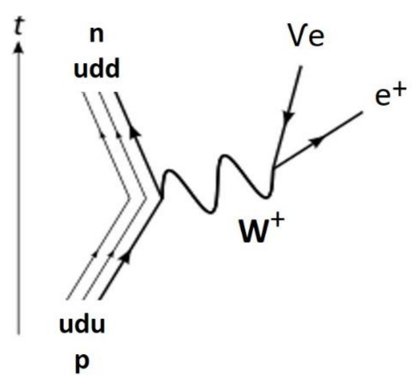


**Figure 25. Beta decay of a proton (p) into a neutron (n).** A up quark from proton is converted to a down quark to make a neutron. This occurs via the exchange of Φu in the proton for the Φd in a photon: (u d **u**) + (**Φd** ⊥ $\Phi\bar{\boldsymbol{d}}$) → (d d **u**) + (**Φu** ⊥ $\Phi\bar{\boldsymbol{d}}$). This converts a proton into a neutron, while the photon is converted to charged $W^+$. The $W^+$ is unstable and goes on to convert an e-neutrino into a positron by the reaction (Φu ⊥ Φd ⊥ **Φd**) + (**Φu** ⊥ $\Phi\bar{\boldsymbol{d}}$) → (Φu ⊥ Φd ⊥ **Φu**) + (**Φd** ⊥ $\Phi\bar{\boldsymbol{d}}$), which regenerates the photon. Exchanged quarks are bolded. Feynman diagram for β+ decay of a proton into a neutron (Pamputt).

*The decay of strange, charm, bottom, and top quarks and hadrons with variations of the above processes*. Once again, flavor, charge, and chirality exchange via Octon-Dyad reassembly is in perfect agreement with observed beta decays.

## 7.6 Z-Boson structure

The neutral current carrier (Fig. 26) should transfer momentum, spin, and energy **without changing flavor**. Within the Dyad framework, the most stable neutral Dyad (excluding any top-quark involvement, which introduces multiple defects) is

$$Z^0 = \Phi b \perp \Phi \bar{s} \quad \text{(Left-Helicity)}$$

**Why this Dyad?** A comprehensive scan of neutral Octon pairings that do **not** use u, d (to avoid coupling to residual charge patterns) identifies $\Phi b \perp \Phi\bar{s}$ as the unique configuration that (i) engages **all eight Dyad addresses** and (ii) maximizes three-color overlap while keeping the **number of weak-bond (2-color) defects minimal**.

**Defect accounting.**

- $\Phi b$ carries one unavoidable weak site (address **3–6**).
- $\Phi\bar{s}$ carries one unavoidable weak site (address **7–2**).
- The **Dyad overlap "repairs"** many other potential mismatches, so that **six** of the eight Dyad addresses are fully three-color saturated, while **two** remain 2-color (the minimal neutral configuration we found).

**Mass and lifetime.**
Two residual weak-bond defects naturally place $Z^0$ **heavier** than $W^{\pm}$ (which have only one defect), consistent with $m_Z \simeq 91.2$ GeV and $\tau_Z \sim 3\times10^{-25}$ s. In the Hamiltonian language from §3.6–3.7, this corresponds to a larger defect/locking energy $\Delta H_{defect} + H_{lock}$ for $Z^0$ than for $W^{\pm}$.

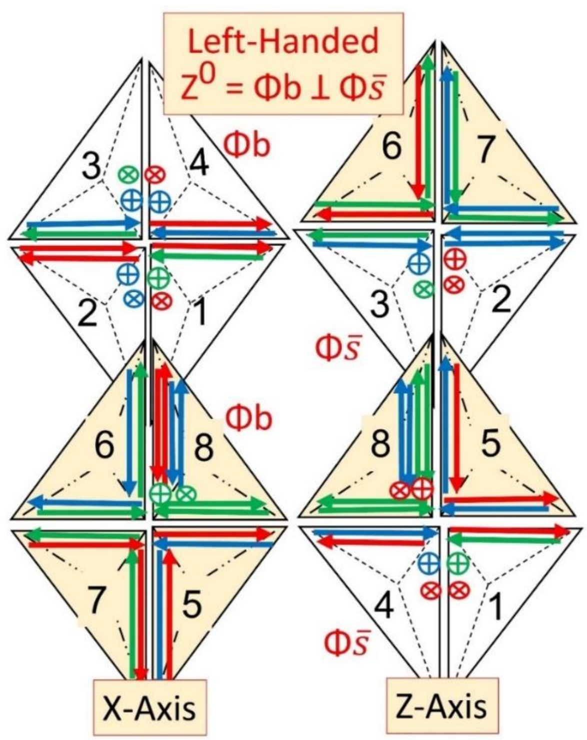


**Exclusions.**
Neutral Dyads built from u, $\bar{u}$ or d, $\bar{d}$ fail to maintain Dyad-wide three-color saturation at the required addresses; neutral Dyads involving t exhibit **multiple** defects and are dynamically unstable.

**Figure 26. Octonion vector projections for the left-handed $Z^0$ Dyad ($\Phi b \perp \Phi\bar{s}$).** Eight three-color bonds arise, with only minimal weak-bond defects, accounting for its high, but finite stability. Minor weak-bond defects within each Octon (sites 7–2 in $\Phi\bar{s}$ and 3–6 in $\Phi b$ ) are partially "repaired" by the Dyad overlap. All other addresses are three-color saturated.

## 7.7 Summary of Dyad Boson Structures

- **Unified carrier picture.** The electroweak carriers arise from the **same Dyad mechanism** as photons: two orthogonally interpenetrating Octons with **no Gluet ports**, hence no strong-force coupling.
- **Flavor and chirality selection.** Only **specific helicity orientations** achieve maximal Dyad saturation:

  $\Phi^{L}_{\gamma} = \Phi_{d} \perp \Phi_{\bar{d}}$ , $\Phi^{R}_{\gamma} = \Phi_{u} \perp \Phi_{\bar{u}}$

  $W^{-} = \Phi_{d} \perp \Phi_{\bar{u}}$ (left-helicity minimal-defect state);

  $W^{+} = \Phi_{u} \perp \Phi_{\bar{d}}$ (right-helicity minimal-defect state);

  $\mathbf{Z^{0}} = \Phi_{b} \perp \Phi_{\bar{s}}$ (left-helicity neutral minimal-defect state).

  Opposite-helicity constructions exist but carry multiple defects and are dynamically suppressed—matching the SM's V −A selection rules.

- **Mass ↔ defect count (qualitative ordering).**

  $$\gamma : 0 \text{ defects} \ll W : 1 \text{ defect} < Z^{0} : 2 \text{ defects}.$$

  This tracks $m_{\gamma} = 0$, $m_{W} \approx 80.4$ GeV, $m_{Z} \approx 91.2$ GeV, with widths set by Dyad reassembly matrix elements (large for W / Z).
- **Beta decays as Dyad exchanges.** Both $\beta^{-}$ and $\beta^{+}$ proceed via **sequential Dyad reassemblies** (Secs. 7.4–7.5), preserving charge, chirality, and color at every step.

Takeaway. Casting $W^{\pm}$ and $Z^{0}$ as **orthogonal Octon Dyads** with a small, quantized number of weak-bond defects yields a **geometric and algebraic** substructure for the electroweak sector that coherently explains strong-force blindness, helicity selection, and the observed $m_{Z} > m_{W}$ hierarchy.

## 8.0 H Boson and the Spacetime-Lattice Triad Subunit

We now return to the central question: *What is the microscopic substructure of spacetime?* In the Triad Model, every point of space is occupied by a **Stellated Rhombic Dodecahedron**—a "Triad" of three interpenetrating Octon quarks—which tessellates 3D space (Figs. 2-3). Each Octon is built from an independent octet of gluons, the same building blocks used throughout this framework for hadrons, leptons, and gauge bosons.

Within this model, **four** Triads—composed solely of the stable up/down Octon quarks and their antiquarks—are predicted to be *extremely long-lived* and are the only candidates for a repeating spacetime subunit:

1. $T^- = \Phi\bar{u} \perp \Phi\bar{d} \perp \Phi\bar{u}$, charge –1 (L-electron).
2. $T^+ = \Phi u \perp \Phi d \perp \Phi u$, charge +1 (R-positron). (39)
3. $T^0 = \Phi u \perp \Phi d \perp \Phi d$, charge 0 (L-neutrino).
4. $\widetilde{T}^0 = \Phi\bar{u} \perp \Phi\bar{d} \perp \Phi\bar{d}$, charge 0 (R-antineutrino).

A lattice of neutral Triads alone would break matter–antimatter symmetry, while mixed neutral/antineutral motifs fail to tessellate symmetrically. Even using all four flavors in one motif does not produce a uniform 3D tiling. We therefore seek a **charged** pair whose assembly properties naturally drive a symmetric lattice. In §8.1 we show that an **alternating $T^+$:$T^-$ dimer** appears uniquely capable of fulfilling this role. Sections 8.1–8.7 then explore the **$T^+$:$T^-$ dimer** generational variants, gravitational implications, and connection to the **Higgs boson** (interpreted as a collective scalar mode of the dimer lattice).

## 8.1 The $T^+$:$T^-$ Dimer as the Fundamental Spacetime Subunit

Simple modeling shows that positively charged $T^+$ and negatively charged $T^-$ Triads efficiently self-assemble into alternating layers throughout space. Instead of point like "atoms," the Triad Model proposes a **SU(3)³ lattice of charged Triad dimers**—alternating sheets of three-Octon molecules:

$$\text{Spacetime dimer} = T^+ : T^- = (\Phi u \perp \Phi d \perp \Phi u) : (\Phi\bar{u} \perp \Phi\bar{d} \perp \Phi\bar{u}) \qquad (40)$$

**Electrostatic Self-Assembly.** *Each $T^+$ (positron-type) layer alternates with a $T^-$ (electron-type) layer, forming stacked (+/–) sheets. A given $T^+$ bonds to eight neighboring $T^-$ (four above, four below) via Coulomb attraction—minimizing repulsion and optimizing packing*. Neutral Triads ($T^0$, $\widetilde{T}^0$) are disfavored by electrostatics and lattice symmetry.

**Strong-Force Isolation.** Each Triad internally saturates its eight tetrahedral addresses with three-color coupling, preventing any external **Gluet** flux tubes from attaching; leptons and photons do not "feel" the strong force. The 48 stellated faces project EM charge but carry no residual color.

**Mechanical Stability.** Like-charged layers repel (preventing lattice collapse); opposite-charged layers attract (providing rigidity against compression/tension)—analogous to ionic crystals.

**Field Propagation.** Axion/gluon perturbations propagate through this space lattice, transmitting EM waves and guiding particle trajectories—offering a microscopic mechanism for "fields" in a background-independent geometry.

Together, these features single out the alternating $T^+$:$T^-$ lattice as the only energetically self-assembling and symmetrically stable tiling of three-dimensional space.

## 8.2 Triad Model Predicts 3 Flavors/Generations of Dimer Spacetime Subunits

Just as there are three charged-lepton families, the Triad Model predicts three distinct charge-neutral lattice dimers (all neutral overall):

$$\text{Electron /positron dimer } (e- : e+) = (\Phi u \perp \Phi d \perp \Phi u) : (\Phi \bar{u} \perp \Phi \bar{d} \perp \Phi \bar{u}) \quad (41)$$

$$\text{Muon / antimuon dimer } (\mu- : \mu+) = (\Phi u \perp \Phi s \perp \Phi u) : (\Phi \bar{u} \perp \Phi \bar{s} \perp \Phi \bar{u}) \quad (42)$$

$$\text{Tau / antitau dimer } (\tau- : \tau+) = (\Phi u \perp \Phi b \perp \Phi u) : (\Phi \bar{u} \perp \Phi \bar{b} \perp \Phi \bar{u}) \quad (43)$$

- **Mass hierarchy:** Each successive dimer is heavier by approximately the same factors as its corresponding lepton family (roughly $\mu : e \approx 207$, $\tau : e \approx 17$).
- **Cosmological roles:** These three scalar (spin-0), charge-0 dimers define **three vacuum energy densities**, with potential implications for dark energy, neutron-star cores, and black-hole interiors. In §8.6–8.7 we relate the highest-energy dimer mode to a Higgs-like scalar excitation of the lattice.

## 8.3 Gravity as Lattice Distortion

In the Triad Model, **gravity** emerges as a local **conformal distortion** of the charged-dimer spacetime lattice driven by axion exchange with matter [18] and other potential effects [20, 21]:

- **Axion Exchange:** Quarks, leptons, and Dyads (photons, W / Z) continuously **emit and absorb** $\hbar\omega$-axions to/from the lattice (cf. the drive term $f(t)\widehat{D}$ in §3.6–3.7).
- **Contraction:** A Triad dimer that **uptakes** extra axions **shrinks** slightly (conformal rescaling of its internal length $L \to sL,\ s<1$), raising local energy density.
- **Curvature:** Spatial gradients of this rescaling act as an effective metric distortion. Writing a scalar "conformal field" $\sigma(x)$ for the local scale change, the **emergent metric** is

$$g_{\mu\nu}(x) \approx e^{2\sigma(x)}\, \eta^{\mu\nu}, \quad \boldsymbol{R} = -6e^{-2\sigma}(\Box\sigma + (\partial\sigma)^2), \quad \sigma(x) \simeq \Phi_N/c^2,$$

$$\nabla^2 \Phi_N \simeq 4\pi G\, (\rho_{\text{matter}} + \rho^{eff}_{axion}), \quad (\partial\sigma)^2 \equiv \eta^{\mu\nu}\, \partial_\mu\sigma\, \partial_\nu\sigma,$$

$\Box \equiv \eta^{\mu\nu}\, \partial_\mu \partial_\nu$ (mostly-+ signature) and $\boldsymbol{R}$ is the Ricci scalar curvature**.**

- **Mass Dependence:** Denser bodies exchange more axions with the lattice, producing a **deeper** σ(x) well and hence a stronger gravitational field.

- **Extreme Regime (phase change):** Near horizons, over dense dimers can **transition** to heavier **generational** dimers (μ- or τ-type), altering the local stiffness and permitting non-GR interior dynamics (relevant for ergospheres, lattice dragging, and black-hole cores).

**Methodological note**. In this picture, “gravity = geometry” is realized microscopically: axion-mediated changes of **local dimer scale** produce the conformal factor $e^{2\sigma(x)}$ that curves geodesics. The same $f(t)\widehat{D}$ drive/lock operators used for particle dynamics supply the source term for σ(x).

## 8.4 Spacetime Dimers as Higgs-Like Quanta

The Higgs field permeates space as a **spin-0, charge-0** condensate with a ∼125 GeV scalar excitation. In the Triad Model, the **charged $T^{+} : T^{-}$ dimer lattice** provides exactly such scalar, neutral building blocks:

- **Omnipresent Scalar:** Dimer units tile all of space; small **amplitude oscillations** of a dimer correspond to **Higgs-like** scalar modes of the lattice.
- **Mass Generation:** Effective masses arise from **axion-exchange coupling** between particles and the lattice (an analogue of Yukawa couplings), naturally enhancing couplings to heavier flavors.
- **Spin-0, Charge-0:** Each dimer is a scalar, neutral under electromagnetism.
- **Three Flavors:** Because the lattice admits **three** charged-dimer generations (Eqs. 41–43), the spectrum generically contains **three scalar modes**, with masses tracking the underlying dimer energies.

**Branching-ratio phenomenology.** The observed 125 GeV scalar decays predominantly to $b\bar{b}$ (∼58%) and $\tau^{+}\tau^{-}$ (∼6%), with sizable WW (∼21.5%) and ZZ (∼2.7%) channels and a very rare $\mu^{+}\mu^{-}$ mode (∼$2.2 \times 10^{-4}$). In our framework this pattern is expected: lattice-scalar couplings scale with effective mass/overlap, favoring third-generation final states. **A working identification is that the 125 GeV resonance corresponds to the lowest scalar normal mode of the τ-family dimer** (or a mixed mode with dominant third-generation overlap), while additional scalar modes associated with the e- and μ-dimers may be lighter/heavier and/or broader. Further experimental studies of rare channels (e.g.\ $\mu^{+}\mu^{-}$) can probe the existence of additional, lighter “Higgs-like” dimers.

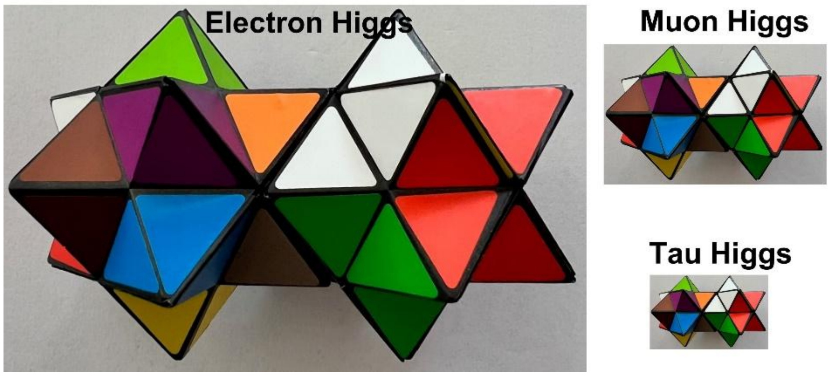


**Fig 27. The SU(3)³ spacetime dimers of Eqs 41-43** are three variations of the dimers. The **predicted muon Higgs** has $\sim 1.8 \text{ x } 10^9$ times the energy density of the e-Higgs while the tau Higgs has $\sim 1.6 \text{ x } 10^{14}$ times energy density of the e-Higgs.

**Energy-density scaling (model ansatz)**. If the lattice energy density ρ of a generational dimer scales as the **fourth power** of its characteristic mass scale, then $\rho = E \,/\, V$ and

$$\rho_\mu \,/\, \rho_e = (m_\mu \,/\, m_e)^4, \quad \rho_\tau / \,\rho_e = (m_\tau \,/\, m_e)^4$$

**Energy Density of muons vs electrons:** $\rho_\mu \,/\, \rho_e \approx (207)^4 \approx 1.83 \text{ x } 10^9$

**Energy Density of tau vs electrons:** $\rho_\tau / \,\rho_e \approx (3573)^4 \approx 1.46 \text{ x } 10^{14}$

Thus, μ- and τ-dimers would be **immensely** denser and more energetic than the e-dimer lattice. If realized in nature, such flavor-dependent stiffness could become relevant in **black-hole interiors**, **neutron-star cores**, and/or the **early Universe**.

## Lattice Implications

- **Gravity:** axion-driven **conformal contraction** bends geodesics and may avert classical singularities by phase-shifting to heavier and more powerful dimers at extreme density.
- **Electromagnetism:** axion currents across charged layers support EM wave propagation.
- **Higgs Field:** free **scalar excitations** of the same lattice reproduce Higgs-like phenomenology and suggest **generational** scalar structure.
- **Dark Energy:** inter-generational energy gaps provide a new handle on vacuum energy scales.

**Testing Triad Model**. We flag the $\rho \propto m^4$ scaling as a **model hypothesis** that can be stress-tested: (i) calibrate to the 125 GeV state; (ii) search for additional scalar modes with **enhanced** ττ and **suppressed** μμ couplings; (iii) look for environment-dependent Higgs-like shapes where lattice density is extreme.

## 8.5 Variable Cosmological "Constant" from Three Dimer Flavors

In General Relativity, the large-scale dynamics obey

$$R_{\mu\nu} - \frac{1}{2}\ R\, g_{\mu\nu} + \Lambda\, g_{\mu\nu} = \kappa\, T_{\mu\nu}\,,$$

where $R_{\mu\nu}$ is the Ricci curvature tensor, $R$ is the Ricci scalar curvature, $\Lambda$ is the cosmological constant, $\kappa = 8\pi\, G/c^4$, and $T_{\mu\nu}$ is the stress-energy tensor, describing distribution of matter and energy in spacetime.

In the Triad Model, the vacuum is a lattice of three charged-dimer species (Eqs 41–43), each contributing an **effective axion pressure** that can reinforce or oppose gravity. We therefore promote $\Lambda$ to a space- and time-dependent quantity:

$$\Lambda_{\mathrm{eff}} = \Lambda_0 + \sum_{i \in \{e,\mu,\tau\}} \lambda_i\, n_i(x)\quad ,$$

with $\Lambda_0$ is a bare vacuum term, $n_i\,(x)$ is the local number density of the *i*-th-generation dimer subunit $(e,\, \mu,\, \tau)$, and $\lambda_i$ parameters encoding that generation's compressional response.

The modified field equations are then

$$R_{\mu\nu} - \frac{1}{2}\ R\, g_{\mu\nu}\ + \Lambda_{\mathrm{eff}}\,(x) g_{\mu\nu} =\ \kappa\, T_{\mu\nu}\,. \tag{44}$$

**Interpretation:**

- In **late, low-density universe**, light electron-dimers ($n_e$) dominate, yielding a small positive $\Lambda_{\mathrm{eff}}$.
- In **high-density regimes (early universe, neutron-star cores, black-hole interiors):** heavier μ / τ dimers ($n_\mu$, $n_\tau$) accumulate, raising $\Lambda_{\mathrm{eff}}$ and mimicking a **variable dark-energy** component.
- **Our Hypothesis is:** The differing vacuum energies of the three dimer generations could imply a space- and time-variable effective cosmological constant.

---

## 8.6 Spinning Black Holes without Singularities

The discrete, torsional character of the Triad lattice **forbids true curvature singularities**. Incorporating intrinsic **spin density** of dimers in an Einstein–Cartan (EC) extension [16] gives

$$R_{\mu\nu} - \frac{1}{2}\, R\, g_{\mu\nu} + \Lambda_{eff}(x) g_{\mu\nu} = \kappa\, (T_{\mu\nu} + \nabla_a\, S^{a}{}_{\mu\nu}), \tag{45}$$

*where* $S^{a}{}_{\mu\nu}$ is the lattice **spin-density**. In an axisymmetric, rotating mass:

- **Frame Dragging:** Nonzero $\nabla S$ components generate Lense–Thirring like effects [17].
- **Core Regularization**: As curvature tries to diverge, the local lattice **torsion** increases and **prevents** $r \to 0$ blow-up, yielding a finite, torsion-supported core.

For a stationary, axisymmetric "black hole," one may adopt a modified Kerr-like metric with

$$\Lambda_{\text{eff}}(r,\theta) = \Lambda_0 + \lambda_e\, n_e\, (r,\, \theta) + \lambda_\mu n_\mu(r,\, \theta) + \lambda_\tau n_\tau(r,\, \theta),$$

with $n_i(\mathrm{r})$ increasing toward the center as heavier dimers accumulate. The same region develops enhanced $S^{\alpha}{}_{\mu\nu}$, jointly **regularizing** the core while preserving outer Kerr phenomenology.

---

Equations (44) and (45) describe gravity as a dynamically adaptive response of the lattice to local dimer composition, endowing rotating compact objects with an intrinsic torsion that regularizes their cores and thereby avoids singularities. Our present treatment remains at the **effective classical level**: how the underlying Triad microstructure might resolve the *quantum* aspects of black holes or generate **graviton-like excitations** is an open question. The Triad lattice should thus be viewed as one possible realization of a discrete spacetime framework. Future work will include **numerical simulations of the lattice dynamics** and **derivations of the full continuum and relativistic limits**.

## 8.7 Further Lattice Implications

**Dynamic Dark Energy**

$\Lambda_{\text{eff}}$ varies with the local mix $(\mathrm{n_e},\, \mathrm{n_\mu},\, \mathrm{n_\tau})$. As the universe expands and cools, $\mathrm{n_e}$-dimers dominate, leaving a small positive $\Lambda_{\text{eff}}$. In high-density environments (early universe, galaxy clusters), heavier muon/tau dimers boost $\Lambda_{\text{eff}}$, offering a lattice-based handle on **structure formation** without extra fields.

**Singularity Avoidance and observables**

EC torsion sourced by lattice spin density replaces central singularities with **finite cores**. Inhomogeneous spin–torsion distributions naturally produce **frame dragging** and ergospheres [16, 17]. The model predicts **modified ringdown** systematics and potentially **asymmetric black-hole shadows**—concrete targets for LIGO–Virgo–KAGRA and EHT–ngEHT analyses.

**Electroweak Unification via Octon Dyads**

Photons, $\mathrm{W}^{\pm}$, and $\mathrm{Z}^{0}$ arise from **orthogonal Octon Dyads** built from the same gluon subunits as quarks/leptons. Chirality selection and boson masses map to the **count of weak-bond defects** (Sec. 7), mirroring SM patterns.

**Higgs Field as Dimer Excitations**

The observed ~125 GeV scalar's leading decays - $b\bar{b}$(~ 58%), WW* (~21%), ZZ* (~2.6%), $\tau^{+}\tau^{-}$ (6%), $\mu^{+}\mu^{-}$ (~0.022 %) - fits the **mass-weighted coupling** expectation of the lattice-scalar picture.

**Unified Substructure for Forces**

- **Strong force:** Octon quarks and Gluet flux tubes (§ 4–5).
- **Electroweak:** Triads/Dyads for leptons and gauge bosons (§ 6–7).
- **Gravity & Electromagnetism:** Axion exchange and **lattice distortions** mediate geometry and wave propagation (§ 8).

**In summary**. By extending Einstein's equations with a **composition-dependent** $\Lambda_{\mathrm{eff}}$ and a **spin-torsion** source, and by identifying the Higgs as a **lattice scalar**, the Triad Model advances from a particle substructure to a **coherent framework for matter, forces, and spacetime geometry**, with multiple observational touchpoints.

## 8.8 Theoretical Cyclic Ergosphere Cosmos: Black Hole–Driven Big Bang

In the Triad Model, the discrete, torsion-regularized spacetime lattice **forbids true singularities**. Cosmic expansion can instead originate in the **outer ergosphere** of a spinning (Kerr) black hole. Classical **frame dragging** is reinterpreted microscopically as **lattice dragging**: the rotating mass couples to the axion–dimer lattice and drags it azimuthally.

**Kerr geometry: definitions** (for clarity)

Let the *dimensionless* spin be χ in place of $a\backslash*$

$$\chi \equiv [(cJ)\,/\,(G M^{2})] \in [0,1], \qquad J = (\chi\, \mathrm{G}\, \mathrm{M}^{2})\,/\,\mathrm{c}\ .$$

Then the event-horizon and static-limit (ergosurface) radii are

$$r_+ = (GM/c^2)\,[1+\sqrt{1-\chi^2}\,],\;\; r_s(\theta) = (GM/c^2)\,\left[\sqrt{(1-\chi^2 cos^2\theta)}\right],$$

and the **ergosphere** is the shell $r_+ \leq \mathrm{r} \leq r_s(\theta)$.
($At\ \chi = 0$ one recovers Schwarzschild radius: $r_s = r_+ = 2\ GM/c^2$.)

## Proposed Cyclic Ergosphere Cosmos (CEC):

### (i) Pre–Bang spin-down ( $\chi\downarrow$ )

Infalling matter and radiation exchange $\hbar$-axions with the lattice, and the ergosphere gradually **shrinks** as $\chi$ decreases. Near the horizon, axion pressure and density can drive a **phase shift** of local dimers into heavier μ- and τ-generations (the "μ-Higgs / τ-Higgs" phases), stiffening the interior and avoiding a curvature singularity.

### (ii) Bang-like ejection at ( $\chi = 0$ )

When $\chi \to 0$, the static limit meets the horizon ($r_s \longrightarrow r_+$). The rapidly circulating ergospheric flow impinges on a now **non-rotating** horizon and its dense heavy-dimer layer, **disrupting the lattice** and launching a hot, dense ejecta shell from (effectively) all azimuths just outside $r_+$. The outward shock **converts** heavy dimers toward the lighter e-dimer lattice, seeding an expanding spacetime domain as the ergosphere explodes outward from the horizon.

### (iii) Spin rebuilds and then repeats decline ( $\chi\uparrow\rightarrow\downarrow$ )

As accretion continues, inward angular momentum **re-spins** the hole ($\chi\uparrow$), enlarging the ergosphere. Lattice-drag torques, axion currents, and outflows then **conserves** spin energy, causing $\chi$ to decline again; heavy dimers re-accumulate, closing the cycle.

## Toy evolution laws (bookkeeping)

Use $J(t) = \chi(t)\, G\, M^2(t) / c$. A minimal angular-momentum/mass budget is

$$\frac{dJ}{dt} = \dot{M}_{in}\,\ell_{in} - \dot{M}_{ej}\,\ell_{\mathrm{out}} - \tau_{drag}\,,\quad \frac{dJ}{dt} = \dot{M}_{in}\,\ell_{in} - \dot{M}_{ej}\,\ell_{\mathrm{out}} - L_{rad}/c^2\,,$$

with **order-of-magnitude** specific angular momenta

$$\ell_{\mathrm{in}} \sim \sqrt{GM\,r_s}\,,\qquad \ell_{\mathrm{out}} \sim \sqrt{GM\,r_+}$$

and $\tau_{drag}$ the lattice-drag (frame-drag) torque; $L_{rad}$ aggregates radiative losses (gravitational/EM/neutrino). These equations generate cyclic $\chi(t)$ and $r_s(t)$ behavior consistent with the qualitative CEC picture. *(They are intended as phenomenological closures; detailed transport is addressed by the lattice field equations.)*

## Observable handles (qualitative)

- **Spin demographics & ringdowns.** A preference for high-spin states punctuated by spin-down episodes; possible **modulations** in post-merger ringdowns if interior torsion/lattice phases are excited.
- **Jet energetics/variability.** Episodic angular-momentum extraction by lattice-drag can imprint quasi-cyclic patterns in Poynting-dominated outflows.
- **Large-scale alignments.** A spin-seeded expansion can accommodate reported axis/handedness alignments on cosmic scales (to be tested against survey systematics).

---

## Why lattice dragging matters here

Classical frame dragging explains the kinematics; **lattice dragging** supplies a **microphysical sink/source** for angular momentum and energy via axion-mediated stresses and generational dimer phase changes. Near $r_+$, the lattice's ability to shift between e, μ, and τ dimers provides the **pressure/stiffness** needed to (i) avoid a singularity, (ii) store and release rotational free energy, and (iii) power a Bang-like ejecta when $\chi = 0$.

**Units & conventions.** All Kerr expressions above use SI factors explicitly; when G = c = 1 the standard textbook forms are recovered with

$$r_+ = M(1+\sqrt{1-\chi^2}\,) \text{ and } r_s(\theta) = M\left[1+\sqrt{(1-\chi^2 cos^2\theta)}\right]$$

We consistently use the *dimensionless* spin $\chi$ (not the length-parameter $a$) to avoid ambiguity.

**Bridge to §8.9.** The CEC picture above supplies the *mechanism*—lattice dragging in a Kerr ergosphere that cyclically excites and relaxes heavy dimer phases, avoiding singularities and releasing spin energy into an expanding spacetime domain. To test this scenario against data, we now translate its background effect into a minimal, **localized pre-recombination energy component** $f_{\text{extra}}(z)$ that briefly elevates $H(z)$near matter–radiation equality and then decays. In §8.9 we quantify its impact on the **CMB sound horizon** $r_s$and show how a modest peak fraction (order 10–15%) **reduces $r_s$ by** $\sim 9\%$—precisely the shift needed to reconcile the early-time (CMB) and late-time (ladder) values of $H_0$ at fixed $\theta_{\backslash *}$, while remaining consistent with BBN, the CMB damping tail, and late-universe distances.

## 8.9 Reconciling the $H_0$ Tension via an Ergosphere-Origin Early Component

**Motivation.** The Hubble constant inferred from early-time CMB anisotropies (≈ 67 km s⁻¹ Mpc⁻¹) and the late-time distance ladder (≈ 73 km s⁻¹ Mpc⁻¹) differ at the few-σ level. In ΛCDM, the CMB determination is set primarily by the **acoustic angular scale**

$$\theta_{\backslash *} \equiv \frac{r_s(z_{\backslash *})}{D_A(z_{\backslash *})},$$

where $r_s$is the sound horizon and $D_A$ the angular-diameter distance to last scattering at $z_{\backslash *} \approx 1090$. Any **pre-recombination enhancement of the expansion rate $\boldsymbol{H}(z)$**reduces $r_s$ and, at fixed $\theta_{\backslash *}$, **raises the CMB-inferred** $H_0$—without altering late-time distance-ladder measurements.

**Ergosphere-origin parameterization**. In the Triad/ergosphere picture, a brief reservoir of rotational/drag energy is excited near matter–radiation equality and then redshifts away. At the background level we model this as a **localized early component with fractional density**

$$f_{\text{extra}}(z) \;\equiv\; \frac{\rho_{\text{extra}}(z)}{\rho_{\text{tot}}(z)},$$

peaked at $z_c \sim 3000$ and negligible both at BBN and after recombination. A convenient, agnostic profile is

$$f_{\text{extra}}(z) \;=\; f_0 \,\exp\left[-\frac{\ln^2((1+z)/(1+z_c))}{2\sigma^2}\right] \,\Xi(z; z_c, m),$$

with a smooth cap $\Xi = \frac{1}{1+[(1+z)/(1+z_c)]^m+[(1+z_c)/(1+z)]^m}$ (we use $m \gtrsim 4$, $\sigma \approx 0.4-0.6$) to guarantee rapid decay away from the peak. The expansion history becomes

$$H^2(z) \;=\; H_0^2[\Omega_r(1+z)^4 + \Omega_m(1+z)^3 + \Omega_\Lambda]\;(1+f_{\text{extra}}(z)).$$

**Effect on the sound horizon.** The sound horizon is

$$r_s = \int_{z_{\backslash *}}^{\infty} \frac{c_s(z)}{H(z)}\,dz, \quad c_s(z) \simeq \frac{c}{\sqrt{3(1+R)}}, \quad R \equiv \frac{3\rho_b}{4\rho_\gamma}.$$

For a modest, localized $f_{\text{extra}}$ one finds to first order

$$\frac{\Delta r_s}{r_s} \;\simeq\; -\frac{1}{2}\,\langle f_{\rm extra}\rangle_w, \qquad \langle f_{\rm extra}\rangle_w \equiv \frac{\int_{z_{\backslash *}}^{\infty} \quad f_{\rm extra}(z)\,\frac{c_s}{H}\,dz}{\int_{z_{\backslash *}}^{\infty} \quad \frac{c_s}{H}\,dz}.$$

Thus, a **weighted early fraction** $\langle f_{\rm extra}\rangle_w \approx 0.18$ produces $\Delta r_s/r_s \approx -9\%$. This is **precisely** the shift needed to move the CMB-inferred $H_0$ from ≈ 67 to ≈ 73 km s⁻¹ Mpc⁻¹ at fixed $\theta_{\backslash *}$. In practice, for $\sigma \approx 0.5$ and $m \gtrsim 4$, a **peak** value $f_0 \sim 10 - 15\%$ localized near $z_c \sim 3000$ achieves an $8 - 10\%$ reduction of $r_s$.

**Consistency conditions.**
**(i) BBN**: $f_{\rm extra}(z)$ must be negligible at $z \sim 10^9$ so as not to upset light-element yields (equivalently, $\Delta N_{\rm eff}$ consistent with bounds).
(ii) **CMB damping tail / polarization:** the component should decay by the end of recombination to leave Silk damping and EE/TE spectra within current uncertainties.
(iii**) Isotropy:** the component is homogeneous/isotropic at background level (Triad's ergosphere excitation is treated as an **effective fluid**; any anisotropy is higher-order and suppressed).
(iv) **Late-time distances:** by construction $f_{\rm extra} \to 0$ for $z \ll z_{\backslash *}$ ; SN/BAO distances remain ΛCDM.

**Interpretation within Triad.** In our framework the early component corresponds to a **transient excitation** of lattice degrees of freedom associated with the **outer ergosphere initial condition** (spin-drag energy). Microscopically, this appears as enhanced local exchange between matter and the lattice dimers, increasing $H(z)$ over a narrow redshift window. Macroscopically it is fully captured by the background $f_{\rm extra}(z)$ above.

**Empirical pass/fail.** The scenario is **falsifiable**: CMB fits that allow a localized pre-recombination term should recover (i) $\sim$9% smaller $r_s$, (ii) a higher CMB-inferred $H_0$ consistent with the ladder, and (iii) **no** degradation in BBN or high-$\ell$ CMB fits. Conversely, a high-S/N null for such a component (once jointly fitting Planck + ACT/SPT + BAO) would disfavor the ergosphere-origin interpretation.

**Practical recipe for data analysis**. When inferring $H_0$ from the CMB under this hypothesis, include $f_{\rm extra}(z)$ in $H(z)$ at the parameter-estimation stage; do not modify late-time distance-ladder data or fits. One may sample $(f_0, z_c, \sigma, m)$ with priors enforcing the consistency conditions above.

**Summary.** A short-lived early component—motivated here by an ergosphere-origin initial condition—can be encoded by a localized fractional density $f_{\rm extra}(z)$ peaking near matter–radiation equality. For conservative profiles ($z_c \sim 3000$, width $\sigma \approx 0.4 - 0.6$, cap $m \gtrsim 4$) a modest peak fraction $f_0 \sim 10$–$15\%$ yields $r_s'/r_s \approx 0.91$ (a $\sim 9\%$ reduction), which raises the CMB-inferred $H_0$ to the distance-ladder value at fixed $\theta_{\backslash *}$ while leaving late-time distances essentially ΛCDM. Consistency is maintained provided the component is negligible at BBN, decays by the end of recombination (preserving the damping tail and polarization), and remains homogeneous at background level; BAO/SN fits are unaffected because $f_{\text{extra}} \to 0$ for $z \ll z_{\backslash *}$. Operationally, this invites a standard CMB re-analysis in which $(f_0, z_c, \sigma, m)$ are sampled with priors enforcing these conditions; success is defined by a smaller $r_s$, a higher CMB-inferred $H_0$consistent with the ladder, and no degradation of BBN or high-$\ell$ CMB likelihoods.

## 9.0 Discussion - Background Independence Via a Dynamical Lattice

In contrast to field theories placed on a fixed background, the Triad Model treats spacetime as a **dynamical lattice** built from charged Triad dimers. In this picture:

- **Geometry is emergent.** Local axion exchange changes the effective size/stiffness of lattice subunits, producing curvature **phenomenology** without positing an external metric a priori (§8.3–8.6).
- **Forces share substructure.** The same eight-gluon building blocks form Octons (quarks), Dyads (bosons), Triads (leptons), and the spacetime lattice.
- **Symmetry is organizing, not absolute.** O(4) (binary octahedral) and $\mathrm{SU}(3) \times \mathrm{SU}(3) \times \mathrm{SU}(3)$ symmetries act as structural guides for the lattice units; we do **not** claim an exact microscopic isometry group of the full lattice.
- **The axion–dimer lattice is introduced as a phenomenological regulator of spacetime at sub-Planckian scales.** This is analogous to how QED is treated as a low-energy effective theory valid below a Landau-pole scale, or how lattice QCD is employed without full derivation from a UV-complete model. In this spirit, the Triad lattice not only encodes substructure but regularizes curvature and torsion dynamically. A natural next step is to derive Einstein–Cartan equations as the long-wavelength coarse-grained limit of lattice dynamics—mapping discrete torsion and curvature onto continuum fields. Such derivations would mirror the emergence of hydrodynamics from microscopic models and are well-suited for both analytical and numerical exploration in future work.

## 9.1 Twelve Low-Mass Axions as Dark-Matter Candidates

**Content.** The model posits twelve light axionlike modes ($\hbar\omega$ quanta) that also underlie gluons/quarks/bosons and the lattice.

**Behavior.** If sufficiently light and weakly coupled, these modes are cold/ultracold, non-radiative, and long-lived—consistent with **dark-matter phenomenology**.

**Galaxy dynamics (hypothesis).** Halo-scale axion over-densities [19] deepen the potential and can flatten rotation curves.

**Constraints and consistency.** Any viable parameter space must respect bounds from stellar cooling, direct axion searches, CMB/BAO/LSS, and strong/weak lensing. We take this as a target to be tested, not as established.

**Observational handles**.

Small departures in strong-lens substructure relative to baryon-only models;

Core–cusp behavior and halo shapes;

If axions are ultralight, wave interference (soliton-like cores) on kpc scales.

*Conservatism check.* We do not assert a replacement of ΛCDM; rather, we outline how the Triad axions could **embed within** or **deform it**, subject to standard cosmological tests.

## 9.2 Higgs-Flavor Dimers as Dark-Energy Agents

- **Three neutral scalar dimers**. Electron-, muon-, and tau-dimers are spin-0, charge-0 lattice excitations with **different energy densities** (§8.1–8.4).
- Effective vacuum term (ansatz).

$$\Lambda_{\mathrm{eff}} = \Lambda_0 + \sum_{i \in \{e,\mu,\tau\}} \lambda_i \, n_i(x) \quad ,$$

  where $n_i$ are local dimer densities and $\lambda_i$ encode their (repulsive) axion pressure.

- **Cosmic history (qualitative).** Heavy ($\mu$, $\tau$) dimers could dominate in early/high-density phases (inflation-like push), while the late universe is e-dimer dominated with a small residual $\Lambda_{\mathrm{eff}}$.
- **Tests and bounds**. Any variability in $\Lambda_{\mathrm{eff}}$ must respect tight limits on the dark-energy equation of state $w(z)$ ($w \approx -1$ with $|1 + w| \lesssim$ a few percent for $z \lesssim 1$). Signatures may include ISW correlations, mild anisotropy, or redshift-dependent $w(z)$.

*Conservatism check.* We present $\Lambda_{\mathrm{eff}}$ as an **effective parameterization**; detailed fits to CMB/BAO/SNe are future work.

---

## 9.3 Black Holes without Singularities

- **Mechanism.** We borrow the spirit of **Einstein–Cartan**: intrinsic spin density of the lattice (from dimer chirality) sources torsion-like terms that oppose infinite compression, yielding a **finite, ultra-dense core** instead of a curvature singularity (§8.6).
- **Phase layering (hypothesis).** Radius-dependent dimer composition (outer e, mid μ, inner τ) alters stiffness and effective $\Lambda_{\mathrm{eff}}$.

- **Observables (must respect current bounds).**
  - Ringdown spectra: small shifts in quasinormal-mode frequencies/phases;
  - Photon-ring morphology: modest, spin-dependent asymmetries (within current EHT tolerances);
  - No-hair deviations parameterizable and constrained by LIGO/Virgo/KAGRA.

*Conservatism check.* We do **not** claim present detections of torsion; we outline a phenomenology that can be bounded or supported by upcoming GW and VLBI data.

---

## 9.4 Wave–Particle Duality and Vacuum Activity (Heuristic Map)

- **Axion exchanges as the wave substrate.** Dyads and Triads continuously exchange $\hbar$-axions with the lattice, providing a microscopic picture for **coherent wave propagation** and interference.
- **Vacuum fluctuations (mapping).** Local constructive interference of axion fields can seed short-lived excitations, while destructive interference reabsorbs them—**heuristically paralleling** virtual pairs in QFT.
- **Uncertainty relations**. The canonical $[\hat{x}, \hat{p}] = i\hbar$ of each oscillator chain underwrites the usual $\Delta x \ \Delta p \geq \hbar/2$.

*Conservatism check.* This section offers an **interpretive bridge** to standard QFT phenomena; it does not replace renormalized QFT calculations.

---

## 9.5 Quantum Entanglement and Chirality Pairing

- **Production structure.** In this model, photon pairs are naturally produced **as opposite-helicity Dyads** $(\Phi d \perp \Phi\bar{d})$ and $(\Phi u \perp \Phi\bar{u})$, giving robust polarization anticorrelations.
- **Compatibility with quantum tests.** The model is intended to be **consistent with Bell-test violations** and no-signalling. We do **not** introduce a local-hidden-variable mechanism; instead, the internal chirality label provides a **state-preparation handle** that reproduces standard quantum correlations.
- **Possible refinements/tests.** Look for tiny, helicity-conditioned dispersion/birefringence or phase-memory effects that remain within existing astrophysical bounds; absence of such effects constrains coupling parameters.

*Conservatism check.* We avoid claims of "restored local realism." Entanglement remains nonclassical; any additional structure must reduce to standard QM statistics in tested regimes.

## 9.6 Summary of Key Discussion Points

**Unified substructure (hypothesis).** Twelve light axion modes underlie eight-gluon Octons; Octons assemble into Dyads (bosons) and Triads (leptons). Charged Triad dimers tile space as a dynamical lattice (§3–8).

**Background independence (effective)**. Curvature phenomenology arises from lattice responses to axion exchange (§8.3–8.6). We treat GR as the coarse-grained limit of this discrete medium, not as an externally imposed metric.

**Dark sectors (to be tested).**

• Dark matter: light axion modes provide halo mass without radiative losses (§9.1).

• Dark energy: three "Higgs-flavor" dimers modulate an effective $\Lambda_{eff}$ via their local densities (§9.2).

**Compact objects (model feature).** Lattice spin density (torsion-like response) and high-density dimer phases can regularize black-hole cores within the model (§9.3), subject to gravitational-wave and VLBI constraints.

**Quantum phenomena (interpretive map).** Wave–particle duality, vacuum activity, and entanglement are described through axion-lattice interactions and Octon substructure (§9.4–9.5), while remaining consistent with standard QM phenomenology.

*Positioning statement.* We present a cohesive effective framework with falsifiable signatures, not a replacement of established theory where it already fits data**.**

## 9.7 Symmetry Groups in the Triad Model

We use familiar groups as **organizing symmetries** of the proposed assemblies; they need not be exact microscopic symmetries of the full dynamics.

**Notation fix.** To avoid confusion with the 4D orthogonal group O(4), we refer to the **octahedral point group** as **O_h** (order 48). Where a spin double cover is implied, we use the **binary octahedral group 2O** (order 48).

**Table 3. Summary table (organizing symmetries).**

| Quantum structure | Assembly | Symmetry content (organizing) |
|---|---|---|
| Pauli spinors | 2 × 2 Pauli matrices | SU(2) (spin) |
| Axion "color" tetrahedron | 1 × (axion quaternion) | SU(3) (color-like) |
| Gluon tetrahedron | 1 × (gluon from ≥137 axions) | $O_h$ (geometry), SU(3) |
| Quark Octon (octahedron) | 8 × gluons → 1 × Octon | $O_h$ (geometry), SU(3) |
| Photon / W / Z Dyad | Octon ⊥ Octon | $O_h$ SU(3) × SU(3) (two color sets) |
| Lepton Triad | Octon ⊥ Octon ⊥ Octon | $O_h$ SU(3) × SU(3) × SU(3) |

| Quantum structure | Assembly | Symmetry content (organizing) |
|---|---|---|
| Spacetime lattice (charged dimers) | $T^+ : T^-$ tiling | $O_h$ (tiling), U(1) (net charge order), $SU(3)^3$ (subunit content) |

**Context notes.**
• SU(2) governs nonrelativistic spinors (Pauli matrices).
• SU(3) here plays a structural role inherited from the axion/gluon construction; it is not claimed to be identical to QCD color at all scales.
• SU(3) × SU(3) and SU(3)^3 label orthogonal intersections (Dyads, Triads) as bookkeeping symmetries for independent Octon subspaces.
• Possible embeddings in larger groups (e.g., trinification-like SU(3)^3, or exceptional groups) are speculative and deferred to future work.

---

## 9.8 Key Experimental and Observational Tests of the Triad Model

Below are focused avenues to **validate or falsify** the model's central claims. Each item states (i) what to measure, (ii) how it differs from alternatives, and (iii) a practical pass/fail criterion.

### A. Near-term astrophysical probes

1. **Black-hole ringdowns (GW "echoes")**
   • What: Search LIGO/Virgo/KAGRA catalogs for **late-time, low-amplitude echoes** after the primary quasinormal modes in BBH mergers.
   • Triad signature: Echo delay scales with the remnant mass/spin as expected for a **torsion-supported inner core** (not horizonless ECOs). Delays should cluster when rescaled by M and χ.
   • Pass: A stacked excess consistent with a mass- and spin-scaled delay model. Fail: Tight null bounds across many events that disfavor any universal echo component.
2. **EHT shadow asymmetries**
   • What: Measure **deviations from Kerr shadow circularity** and brightness asymmetry in M87* and Sgr A*.
   • Triad signature: Small but **correlated, spin-aligned asymmetries** consistent with lattice-drag–induced photon-orbit shifts, not explainable by flow parameters alone.
   • Pass: Persistent non-Kerr residuals after controlling for accretion and scattering systematics. Fail: Kerr fits with no systematic residuals at improved resolution.
3. **Strong-lens "axion sea" granularity**
   • What: In strongly lensed quasars, test for **extra small-scale lensing power** (anomalous flux ratios, time-delay perturbations, wave-optics fringes).
   • Triad signature: Excess microstructure **beyond CDM sub-halo expectations**, with a mild frequency dependence indicative of wave-like axions.

• Pass: Population-level excess inconsistent with sub-halo-only models. Fail: Data fully explained by standard substructure plus microlensing.

## B. Collider- and intensity-frontier tests

4. Higgs–dimer mapping (branching patterns)
   • What: Re-examine $h \to b\bar{b}$}, $\tau^+\tau^-$, WW, ZZ, $\mu^+\mu^-$ couplings for **coherent shifts** consistent with a **τ-dimer interpretation** of the 125 GeV scalar.
   • Triad signature: Patterned deviations within current uncertainties (no single dramatic anomaly), consistent across production modes.
   • Pass: A global-fit preference for the predicted pattern over SM-only by O(2–3)σ. Fail: Fits converge to SM with shrinking errors.
5. Higgs-dimer mapping scalar X at ~0.35 GeV to ~7 GeV
   • Channels: $B \to K\,X$, $X \to \mu^+\mu^-$ (Belle II, LHCb).
   • Triad benchmark: Two spin-0 states (electron- and muon-dimer excitations) with Br(B→KX).
   • Pass: Resolving one or both peaks with consistent production/decay systematics. Fail: Experimental Limits exclude this window, forcing revised dimer-mass mapping.
6. Rare decays: $\pi^0$, $\eta \to \gamma\,X$, $X \to e^+e^-$ (NA62/REDTOP/KOTO)
   • Triad signature: **Bump-hunt** in $e^+e^-$ with possible displaced vertices for sub-GeV X.
   • Pass/Fail: Standard; exclusion contours directly test the light-dimer hypothesis.
7. Light-shining-through-walls (axion regeneration)
   • What: Laser-magnet setups testing **γ** ↔ **a** ↔ **γ**.
   • Triad benchmark: $g_{a\gamma\gamma} \sim \alpha/(2\pi\, f_a)$ with $f_a \sim 10^7$–$10^9$ GeV ⇒ $g_{a\gamma\gamma} \sim 10^{-12}$ –$10^{-10}$ GeV$^{-1}$.
   • Pass: Rates within this window. Fail: Exclusions push $f_a$ higher or require weaker couplings than the benchmark.

## C. Precision photon & lepton tests

8. Vacuum birefringence beyond QED (PVLAS/OVAL class)
   • Triad signature: An extra rotation $\Delta\psi \lesssim 10^{-10}$ rad/m atop the QED signal, scaling with magnetic-field region and wavelength.
   • Pass: Statistically significant residual consistent across apparatus changes. Fail: Residuals vanish with improved systematics.
9. Table-top interferometry (Holometer-style)
   • What: Long-integration searches for **stochastic path-length noise**.
   • Triad signature: $\delta L / L \sim 10^{-20}$ with a broad, stationary spectrum characteristic of discrete lattice steps rather than instrument noise.
   • Pass/Fail: Either a reproducible excess with the predicted stationarity, or null bounds constraining lattice discreteness.

## D. Neutrino sector (locking/mode-selection imprint)

10. Long-baseline oscillation phase offsets

• What: Fit $\nu_\mu \to \nu_e$ appearance/disappearance data for an **energy-independent phase offset** $\varphi_{lock}$ added to standard PMNS phases ($\nu$ and $\bar{\nu}$ separately).
• Triad signature: A tiny, common offset attributable to H/V locking in the central Octon of neutrino Triads (see §6.4).
• Pass: $\varphi_{lock} \neq 0$ preferred across baselines with consistent sign. Fail: Global fits constrain $\varphi_{lock} \to 0$.

## E. Key predictions (testable now)

- **Higgs coupling pattern:** mild, coherent tilt toward **τ/b** vs **W/Z** within current HL-LHC bounds.
- **Axion sector:** $g_{\{a\gamma\gamma\}}$ in **$10^{-12}$ – $10^{-11}$ GeV$^{-1}$** window (LSW/helioscope reach); tiny vacuum birefringence beyond QED.
- **BH strong-gravity:** stacked **ringdown echoes** and subtle **non-Kerr shadow asymmetry** correlated with spin.
- **Planck-scale discreteness:** stationary, direction-independent interferometric position noise at **$\delta L/L \sim 10^{-20}$.**

## How these tests separate Triad from alternatives

• **GW echoes + EHT asymmetries** probe the **torsion/lattice** core directly (vs horizonless ECOs or pure Kerr).
• **Higgs/dimer patterns + light scalars** provide **collider handles** tied to the compositional mapping.
• **Axion-sea lensing + LSW/birefringence** jointly test the **light axion sector** with orthogonal systematics.
• **Neutrino phase** touches the **locking mechanism** that also underpins charged-lepton Triads.

## Closing perspective

We have presented the Triad Model as a compact, testable framework: a **physical** discrete lattice of charged Triad-dimers underlies spacetime, while the same eight-gluon subunits assemble quarks, leptons, photons, and the weak bosons via Octon Dyads and Triads. Where the proposals are unconventional (e.g., an effective cosmological term varying with dimer flavors, torsion-regularized black holes, and an ultralight axion sea), we state them as falsifiable hypotheses tied to concrete signatures (see §9.8). The 3D Lagrangian/Hamiltonian formulations (§3.6–§3.7) anchor the construction in standard field-theoretic practice, and the neutrino/lepton locking terms make the mode-selection assumptions explicit. Our intent is not to supplant established theory by assertion, but to enable decisive tests across collider, astrophysical, and precision arenas. If the predicted patterns fail to appear, key parameters of the model will be sharply bound; if they do appear, the Triad lattice offers a unified microscopic origin for matter, forces, and geometry.

It is useful to situate Triad among **geometry-first programs [23-25]**. In **lattice QCD**, the lattice is a *regulator* for non-perturbative QCD on Euclidean spacetime, removed in the continuum limit; in **positive geometry**, scattering amplitudes are encoded as canonical forms on polytopes, with locality/unitarity emerging from geometric structure. Triad differs in assigning **ontic status to an internal lattice**: the discreteness is physical and lives in internal space rather than in spacetime as a calculational device. We view these approaches as complementary cross-checks—lattice QCD benchmarks hadronic spectra/splittings relevant to Triad's substructure, while positive-geometry tools may eventually provide an efficient language for Triad scattering factorization—without overlap in ontology.


## Acknowledgements

The Triad Model represented here has been developed intermittently over a period of 21 years. I am grateful to Drs. Sat Kirpal Khalsa and Ali Massih who have made helpful comments and suggestions on drafts over the long developmental process. I also thank Dr. Mirianas Chachisvilis and my son Kyle Villeponteau, who have helped with more recent drafts.

## Competing Interests

No competing interests.

## Funding Source and History

This research did not receive any grant funding from agencies in the public, commercial, or non-profit sectors. The search for the potential quantum substructure of spacetime started as a "thought" project in early 2004. An incomplete early version of the Triad Model was published in June of 2023 [7].


# References


1. Harari, *A Schematic Model of Quarks and Leptons*, Phys. Lett. B 86 (1979) 83-86.
2. Shupe, M.A., *Composite model of leptons and quarks*, Phys. Lett. B, 86 (1979) 87-92.
3. Baez, J.C., Huerta, J., *The Algebra of Grand Unified Theories*, arXiv:0904.1556v2 (2010).
4. Furey, C., *Standard model physics from an algebra?*, arXiv:1611.09182v1, (2016).
5. Wen, X.-G. *Emergent anomalous higher symmetries from topological order and from dynamical electromagnetic field in condensed matter systems*, Phys. Rev. B **99**, 205139 7 (2019) DOI: https://doi.org/10.1103/PhysRevB.99.205139.
6. Liang, Q.-Y., Venkatramani, A.V., Cantu, S.H., Nicholson, T.L. , Gullans, M.J. , Gorshkov, A.V., Thompson, J.D., Chin, C., Lukin , M.D., Vuletić, I., *Observation of three-photon bound states in a quantum nonlinear medium*, Science, 359 (2018) 783-786.

7. Villeponteau, B. *Unified Quantum Substructures for Spacetime, Quarks, Leptons, and Bosons*, SSRN (2023) https://ssrn.com/abstract=4480645.
8. Visinelli, L. *Axion-Electromagnetic Waves*, Mod. Phys Letters A (2014) https://arxiv.org/pdf/1401.0709v1401.pdf.
9. Evans, E. Schützhold, R. *Search for axion resonances in vacuum birefringence with three-beam collisions*, arXiv arXiv:2307.08345v3 (2023).
10. Patel, T.P. Singh, *CKM matrix parameters from the exceptional Jordan algebra,* arXiv:2305.00668v2 (2023).
11. Pauli, W. *General Principles of Quantum Mechanics* (Springer, 1980 reprint).
12. Gell-Mann, M. "A Schematic Model of Baryons and Mesons," *Phys. Lett.* **8**, 214 (1964).
13. Fritzsch, H. Gell-Mann, M. and Leutwyler, H. "Advantages of the color octet gluon picture," *Phys. Lett. B* **47**, 365 (1973).
14. Gell-Mann, M. "The Eightfold Way: A Theory of Strong Interaction Symmetry" (Caltech Synchrotron Laboratory Report CTSL-20, 1961).
15. Georgi, H. *Lie Algebras in Particle Physics* (CRC Press, 1999).
16. Hehl, F. W., von der Heyde, P. , Kerlick, G. D. and Nester, J. M. "General relativity with spin and torsion: Foundations and prospects," *Rev. Mod. Phys.* **48**, 393 (1976).
17. Everitt, C. W. F., et al. (Gravity Probe B Collaboration), "Gravity Probe B: Final Results of a Space Experiment to Test General Relativity," *Phys. Rev. Lett.* **106**, 221101 (2011).
18. Peccei, R. D., and Quinn, H. R. "CP Conservation in the Presence of Instantons," *Phys. Rev. Lett.* **38**, 1440 (1977).
19. Sikivie, P. "Experimental Tests of the 'Invisible' Axion," *Phys. Rev. Lett.* **51**, 1415 (1983).
20. Benabou, N., Fraser, K. Reig, M., Safdi, B.R. String Theory and Grand Unification Suggest a Sub-Microelectronvolt QCD Axion, arXiv (2025) https://doi.org/10.48550/arXiv.2505.15884.
21. Kondo, D., Murayama, H. Multiple Axions Save High-Scale Inflation, arXiv (2025) https://doi.org/10.48550/arXiv.2507.07973.
22. Baxter, R. J. *Exactly Solved Models in Statistical Mechanics* (1982) — eight-vertex & transfer matrices.
23. Hashimoto, S. and Sharpe, S. R. "Lattice Quantum Chromodynamics." *in* Review of Particle Physics (S. Navas *et al.*; Particle Data Group), *Phys. Rev. D* **110**, 030001 (2024Arkani-Hamed, N. and Trnka, J. *The Amplituhedron*, JHEP (2014).
24. Arkani-Hamed, N. and Trnka, J. "The Amplituhedron." *J. High Energy Phys.* **10** (2014) 030. doi:10.1007/JHEP10(2014)030. arXiv:1312.2007 [hep-th].
25. Arkani-Hamed, N., Bai, Y., and Lam, T. "Positive Geometries and Canonical Forms." *J. High Energy Phys.* **11** (2017) 039. doi:10.1007/JHEP11(2017)039. arXiv:1703.04541 [hep-th]